GEORGIA INSTITUTE OF TECHNOLOGY
OFFICE OF CONTRACT ADMINISTRATION
SPONSORED PROJECT INITIATION

4015

Date: February 17, 1977

Project Title: Cylindrical Wave Expansion Study

Project No: E-21-607

Project Director: Dr. W. Marshall Leach, Jr.

Sponsor: NASA, Goddard Space Flight Center

Agreement Period: From 2/8/77 Until 2/7/78 (performance period)

Type Agreement: Contract No. NAS5-23886

Amount: $25,000

Reports Required:

Monthly Progress Reports; Final Report ~~Vol I Record 10/27/78~~

Sponsor Contact Person (s):

Technical Matters

R. F. Schmidt
Code 811
NASA
Goddard Space Flight Center
Greenbelt Road
Greenbelt, Maryland 20771

CC Sam Brucker

Contractual Matters
(thru OCA)

J. C. Arena
Code 268.2
NASA
Goddard Space Flight Center
Greenbelt Road
Greenbelt, MD. 20771

Defense Priority Rating: none

Assigned to: Electrical Engineering (School/Laboratory)

COPIES TO:

- Project Director
- Division Chief (EES)
- School/Laboratory Director
- Dean/Director—EES
- Accounting Office
- Procurement Office
- Security Coordinator (OCA)
- Reports Coordinator (OCA) ✓
- Library, Technical Reports Section
- Office of Computing Services
- Director, Physical Plant
- EES Information Office
- Project File (OCA)
- Project Code (GTRI)
- Other _____

CA—3 (3/76)

GEORGIA INSTITUTE OF TECHNOLOGY
OFFICE OF CONTRACT ADMINISTRATION

SPONSORED PROJECT TERMINATION

Date: 8/11/78

Project Title: Cylindrical Wave Expansion Study

Project No: E-21-607

Project Director: Dr. W. Marshall Leach, Jr.

Sponsor: NASA, Goddard Space Flight Center

Effective Termination Date: 4/7/78 (R&D Period)

Clearance of Accounting Charges: 6/24/78 (Approved Final Report to Sponsor)

Grant/Contract Closeout Actions Remaining:

- X Final Invoice and Closing Documents
- _ Final Fiscal Report
- X Final Report of Inventions
- X Govt. Property Inventory & Related Certificate
- _ Classified Material Certificate
- _ Other _____

Assigned to: Electrical Engineering (School/Laboratory)

COPIES TO:

Project Director
Division Chief (EES)
School/Laboratory Director
Dean/Director—EES
Accounting Office
Procurement Office
Security Coordinator (OCA)
✓Reports Coordinator (OCA)
Library, Technical Reports Section
Office of Computing Services
Director, Physical Plant
EES Information Office
Project File (OCA)
Project Code (GTRI)
Other _____

CA—4 (3/76)

E-21-607

GEORGIA INSTITUTE OF TECHNOLOGY
SCHOOL OF ELECTRICAL ENGINEERING
ATLANTA, GEORGIA 30332

EPHONE: (404) 894-2901

March 31, 1977

National Aeronautics and Space Administration
Goddard Space Flight Center
Greenbelt, Maryland 20771

Attention: Contract Management Branch
Code 242.1

Subject: Monthly Progress Report on Contract NAS5-23886

The starting date on the subject contract was modified with the approval of Mr. Richard F. Schmidt, NASA Technical Monitor, to coincide with the beginning date of the spring academic quarter at Georgia Tech. This date was March 29, 1977. Two items have been initiated in the brief period since then. First, an approximation to the cylindrical wave coupling equations is being developed which will allow pattern calculations without the need for computing the cylindrical Hankel functions. This approximation is valid when the near-field measuring probe is not too close to the antenna under test. Second, development of a computer program to simulate the near field radiated by a parabolic reflector has been initiated. The simulated data will be used in phase two of the program in the effort to identify a near-field signature of focused antennas.

W. Marshall Leach
Assistant Professor

E-21-607

GEORGIA INSTITUTE OF TECHNOLOGY
SCHOOL OF ELECTRICAL ENGINEERING
ATLANTA, GEORGIA 30332

PHONE: (404) 894-2901

May 3, 1977

National Aeronautics and Space Administration
Goddard Space Flight Center
Greenbelt, Maryland 20771

Attention: Contract Management Branch
Code 242.1

Subject: Monthly Progress Report on Contract NAS5-23886

The probe coupled cylindrical wave theory has been greatly simplified by writing the Hankel functions in the equations in terms of their integral definitions. A stationery phase approximation to these integrals can then be made which eliminates the need for calculating the Hankel functions. The approximations are valid when the radius of the measurement cylinder is not too large.

Attempts have been made to modify the FFT algorithm in order to achieve better resolution of antenna far fields calculated with it. However, the approach has not been successful. Although this effort has not been abandoned, it appears that it may not be possible to modify the FFT so that its output can be wavenumber or frequency scaled. The limitation seems to be inherent in the matrix factorization scheme that is the basis of the FFT.

W. Marshall Leach
Assistant Professor

E-21-607

GEORGIA INSTITUTE OF TECHNOLOGY
SCHOOL OF ELECTRICAL ENGINEERING
ATLANTA, GEORGIA 30332

EPHONE: (404) 894-2901

June 20, 1977

National Aeronautics and Space Administration
Goddard Space Flight Center
Greenbelt, Maryland 20771

Attention: Contract Management Branch
Code 242.1

Subject: Monthly Progress Report on Contract NAS5-23886

This report covers the period from 5/1/77 to 5/31/77. A method has been formulated to test the focus of planar antennas from near-field measurements on a cylinder. The method involves the determination of the cylindrical wave coefficients in the field radiated by the antenna from the near-field measurements, the computation of the plane wave spectrum of the field from the cylindrical wave coefficients, and the translation of the plane wave spectrum into the aperture field of the antenna. The phase and amplitude distribution of the aperture field are then examined and compared to the correct distributions to indicate defocus. Computer programs are presently being written to test the method on simulated near-field data.

The sponsor has been supplied a report on 12 questions concerning near-field antenna theory which had been requested by letter.

The attempts to modify the FFT algorithm which were described in the letter report of May 3 have been unsuccessful. This effort will not be pursued further.

W. Marshall Leach
Assistant Professor

E-21-607

GEORGIA INSTITUTE OF TECHNOLOGY
SCHOOL OF ELECTRICAL ENGINEERING
ATLANTA, GEORGIA 30332

LEPHONE: (404) 894-2901

July 1, 1977

National Aeronautics and Space Administration
Goddard Space Flight Center
Greenbelt, Maryland 20771

Attention: Contract Management Branch
Code 242.1

Subject: Monthly Progress Report on Contract NAS5-23886

This report covers the period from 6/1/77 to 6/30/77. The computer simulation of the method to test the focus of planar antennas from near-field measurements on a cylinder is now being implemented. The near fields on a cylinder which result in a focused beam at infinity are being used to compute the cylindrical wave coefficients of the field. The plane wave spectrum of the field is then computed and translated back to the reference plane aperture where the test for focus is determined.

Preparation of a document on near-field measurements is now being prepared as part of the contract agreement. The document will cover the planar, cylindrical, and spherical measurement surfaces with emphasis on the cylindrical surface.

W. Marshall Leach
Assistant Professor

E-21-607

GEORGIA INSTITUTE OF TECHNOLOGY
SCHOOL OF ELECTRICAL ENGINEERING
ATLANTA, GEORGIA 30332

LEPHONE: (404) 894-2901

August 1, 1977

National Aeronautics and Space Administration
Goddard Space Flight Center
Greenbelt, Maryland 20771

Attention: Contract Management Branch
Code 242.1

Subject: Monthly Letter Report on Contract NAS5-23886

This letter report covers the period from 7/1/77 to 7/31/77. A continuation of the work reported in the previous letter report has been performed during this period. Computer programs for the computation of the cylindrical wave harmonics from the near field on a cylinder have been written, "de-bugged", and tested. The programs are also capable of computing the far-field pattern from these harmonics.

The computer program for the calculation of the plane wave spectrum from the computed cylindrical wave expansion has been written. It is presently being "de-bugged" and will be made operational during the next reporting period. Attempts to perform this spectral transformation with the FFT algorithm have not been successful since the cylindrical wave expansion varies linearly with the azithmul coordinate, while the plane wave spectrum expansion varies linearly with wavenumbers. Conventional Fourier transform techniques are therefore being used.

W. Marshall Leach
Assistant Professor

E-21-607

GEORGIA INSTITUTE OF TECHNOLOGY
SCHOOL OF ELECTRICAL ENGINEERING
ATLANTA, GEORGIA 30332

.EPHONE: (404) 894-2901

September 1, 1977

National Aeronautics and Space Administration
Goddard Space Flight Center
Greenbelt, MD 20771

Attention: Contract Management Branch
Code 242.1

Subject: Monthly Letter Report on Contrace NAS5-23886

This letter report covers the period from 8/1/77 to 8/31/77. During this period, the sponsor has been supplied a report on 13 questions concerning near-field measurement theory which had been requested by letter.

The computer programs for the calculation of aperture amplitude and phase distributions from near-field measurements on a cylinder have been virtually completed and run successfully for the case of a one-dimensional aperture. Attached are sample outputs from this program which give the calculated aperture amplitude and phase distributions over a 2λ aperture from the near field on a cylinder containing that aperture whose wavenumber/radius product is $kr = 12$. The assumed vertically polarized electric field over the cylinder was of the form $E_z = \exp(-jkr\cos\phi)$ for $-30^o < \phi < 30^o$ and 0 otherwise.

W. Marshall Leach
Assistant Professor

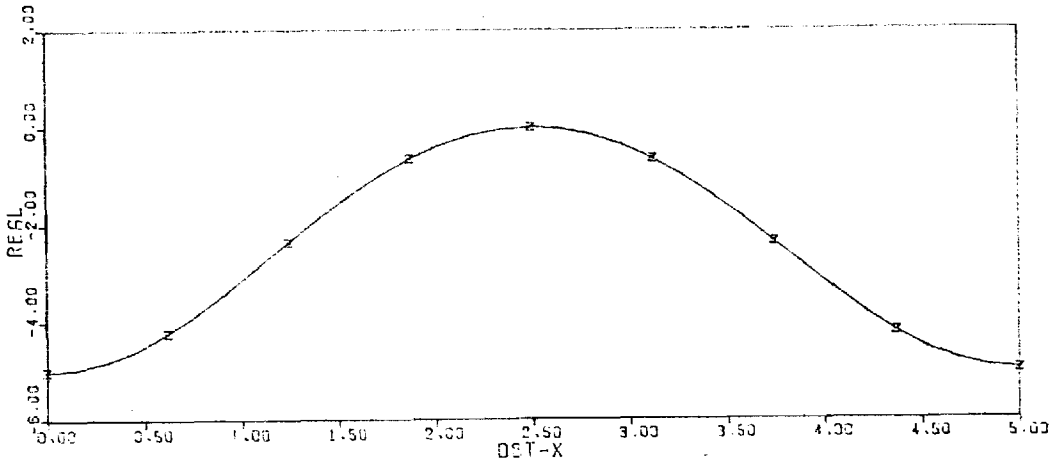

Amplitude distribution in dB versus normalized distance across the aperture.

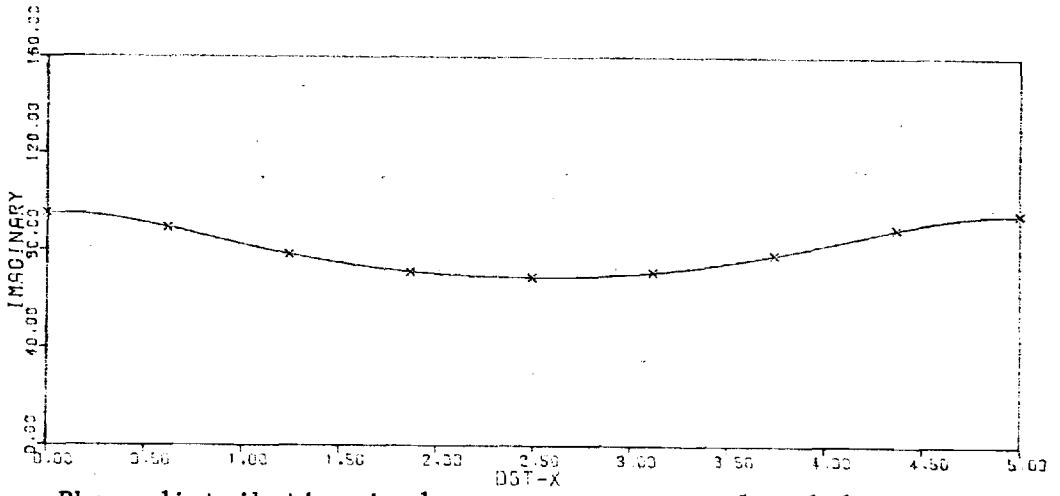

Phase distribution in degrees versus normalized distance across aperture.

E-21-607

GEORGIA INSTITUTE OF TECHNOLOGY
SCHOOL OF ELECTRICAL ENGINEERING
ATLANTA, GEORGIA 30332

TELEPHONE: (404) 894-2901

October 1, 1977

National Aeronautics and Space Administration
Goddard Space Flight Center
Greenbelt, MD 20771

Attention: Contract Management Branch Code 242.1

Subject: Monthly Letter Report on Contract NAS5-23886,
"Cylindrical Wave Study"

This letter report covers the period from 9/1/77 to 9/30/77.

An error has been found and corrected in the computer simulated data presented in the letter report of September 1. The corrected calculations are attached. These plots give the amplitude and phase distribution across a 2 λ aperture calculated from the near-field on a cylinder containing that aperture whose wavenumber-radius product is kr=12. The assumed vertically polarized electric field intensity over the cylinder was $Ez=\exp(-jkr\cos\varphi)$ for $-30^{\circ} < \varphi < 30^{\circ}$ and zero otherwise.

Since the aperture phase distribution is the most sensitive indicator of the focus of a parabolic reflector, it is this distribution which is being used to calculate the position of the feed of a defocused paraboloid. The technique which has been developed uses a least squares curve fit of the theoretical aperture phase function to the actual phase function to calculate the position of the feed. Computer programs are presently being written to test the technique by simulation.

W. Marshall Leach
Assistant Professor

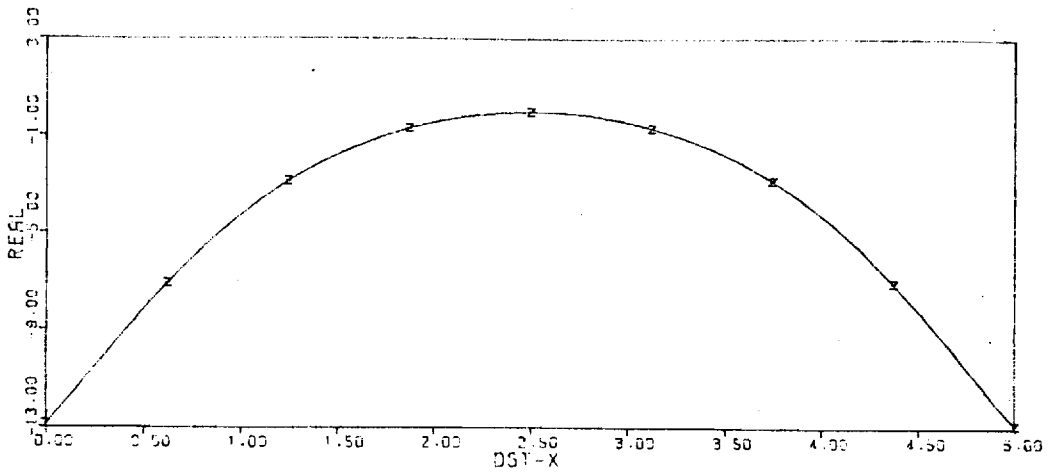

Amplitude Pattern

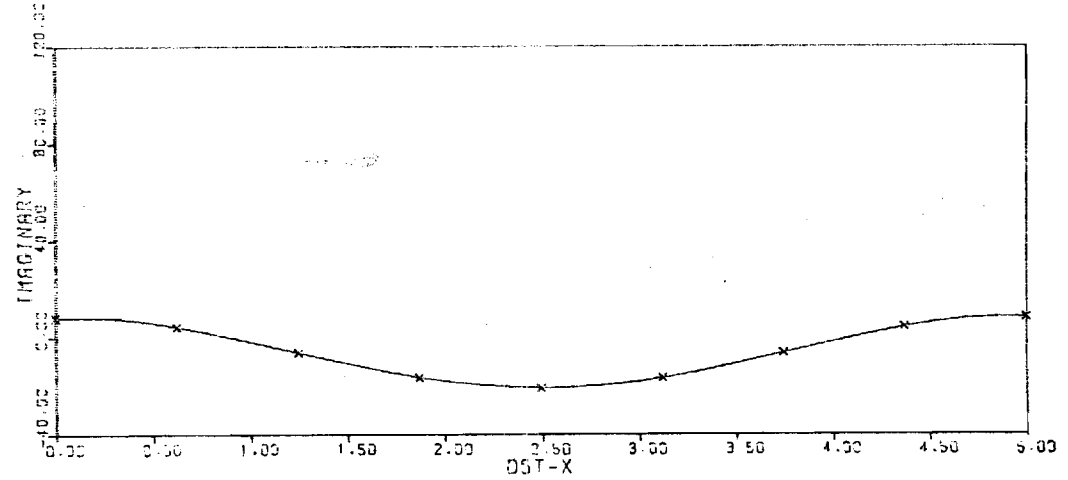

Phase Pattern

IE-21-607

GEORGIA INSTITUTE OF TECHNOLOGY
SCHOOL OF ELECTRICAL ENGINEERING
ATLANTA, GEORGIA 30332

LEPHONE: (404) 894-2901

November 1, 1977

National Aeronautics and Space Administration
Goddard Space Flight Center
Greenbelt, Md. 20771

Attention: Contract Management Branch
Code 242.1

Subject: Monthly Letter Report on Contract NAS5-23886,
"Cylindrical Wave Study"

This letter report covers the period from 10/1/77 to 11/1/77.

A study has been conducted to show that the position of the feed for a defocused parabolic reflector can be calculated from the known phase distribution across the aperture. The study was performed using simulated phase data calculated by a method described by Kelleher. A least squares technique was then used to calculate the position of the defocused feed from the simulated data. Random noise was added to the data to simulate measurement data.

Figure 1 shows the simulated phase data for equal defocus errors in the x, y, and z positions of the feed given by $kg = 0.1$, where $k = 2\pi/\lambda$, and g is the defocused feed position in the x, y, and z directions. In both cases $kR = 10$, where R is the radius of the reflector aperture. The least squares defocus computation on the data in Figure 1 predicted the exact defocus positions which were assumed in calculating the distribution of Figure 1. Figure 2 shows the same distribution of Figure 1 after the addition of gaussian random noise to simulate a 10 dB signal to noise ratio, a figure that is considered to be a worse case condition for any measurement system. The least squares defocus computation on the data in this figure predicted the normalized defocused positions of the feed to be 0.091, 0.117, and 0.099 for the x, y, and z directions, respectively. These figures are in error by 9%, 17%, and 1%, respectively, from the initially assumed positions before addition of the random noise. These percentage errors become much smaller with increasing signal to noise ratios.

Respectfully submitted,

W. Marshall Leach
Assistant Professor

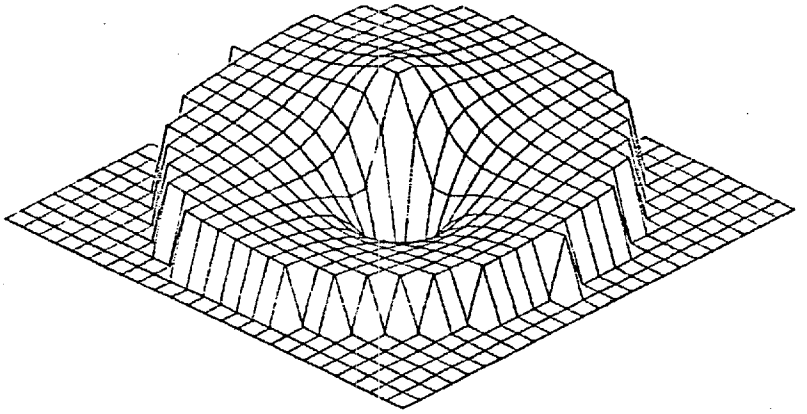

Figure 1.

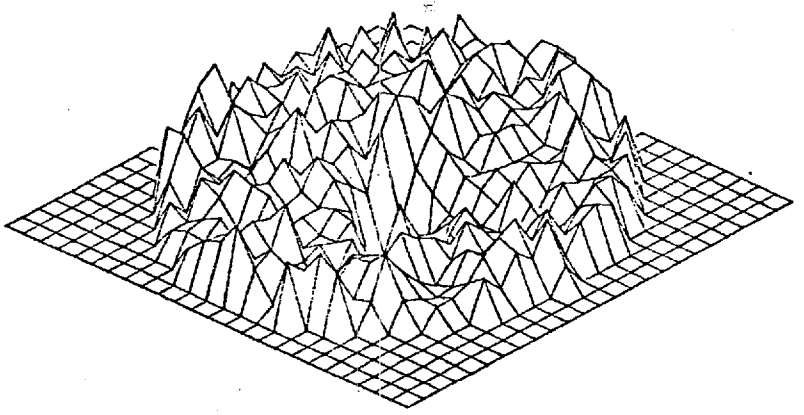

Figure 2.

E-21-607

GEORGIA INSTITUTE OF TECHNOLOGY
SCHOOL OF ELECTRICAL ENGINEERING
ATLANTA, GEORGIA 30332

TELEPHONE: (404) 894-2901

December 1, 1977

National Aeronautics and Space Administration
Goddard Space Flight Center
Greenbelt, MD 20771

Attention: Contract Management Branch
Code 242.1

Subject: Monthly Letter Report on Contract NAS5-23886,
"Cylindrical Wave Study"

This letter report covers the period from 11/1/77 to 12/1/77.

The computer programs for calculation of planar aperture fields from near-fields on a cylinder containing that aperture are being extended from a two-dimensional field formulation to a three-dimensional one. These programs are presently being "debugged".

A tentative outline for the final report on this project is attached.

Respectfully submitted,

W. Marshall Leach
Assistant Professor

WML/clj

E-21607

GEORGIA INSTITUTE OF TECHNOLOGY
SCHOOL OF ELECTRICAL ENGINEERING
ATLANTA, GEORGIA 30332

.EPHONE: (404) 894-2901

January 1, 1978

National Aeronautics and Space Administration
Goddard Space Flight Center
Greenbelt, Maryland 20771

Attention: Contract Management Branch
Code 242.1

Subject: Monthly Letter Report on Contract NAS5-23886,
"Cylindrical Wave Study"

This letter report covers the period from 12/1/77 to 1/1/78.

The computer programs for calculation of planar aperture fields from the near field on a cylinder are only partially operational. Attached is a copy of a sample output from this program which shows the problems being encountered. The problems are caused by an error in the computer programs which has not been found.

The first draft of Chapter I for the final report has been completed.

Respectively submitted,

W. Marshall Leach, Jr.
Assistant Professor

WML/clj

ENC

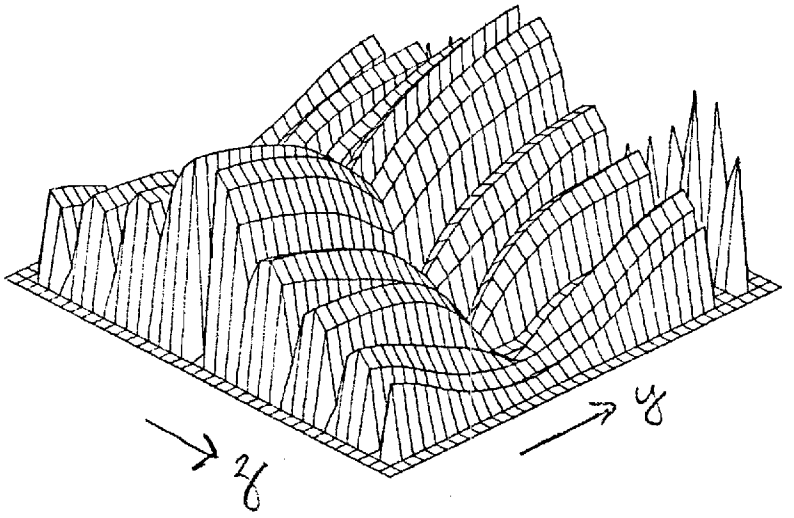
x
y

E-21-607

GEORGIA INSTITUTE OF TECHNOLOGY
SCHOOL OF ELECTRICAL ENGINEERING
ATLANTA, GEORGIA 30332

EPHONE: (404) 894-2901

January 31, 1978

National Aeronautics and Space Administration
Goddard Space Flight Center
Greenbelt, Maryland 20771

Attention: Contract Management Branch
Code 242.1

Subject: Monthly letter Report on Contract NAS5-23886,
"Cylindrical Wave Study"

This letter report covers the period from 1/1/78 to 2/1/78.

The problems mentioned in the last letter report with the computer program to compute antenna aperture fields from the near field on a surrounding cylinder have been almost completely solved. In the attached figure, a plot of the computed aperture fields for a rectangelar aperture are shown. With the exception of the "dropped" points through the center of this plot, the results agree with the two-dimensional data presented in the letter report of October 1, 1977. The cause of the "dropped" points is not known at this time.

The program for calculation of parabolic reflector feed position from aperture phase distribution has been re-run for an aperture diameter to wave length ratio of 20 and a focal length to diameter ratio of 0.375. The attached figures show the calculated aperture phase before and after the addition of random gaussian noise for a defocus distance of one-eight a wavelength in the x,y, and z distances from the focal point. After random gaussian noise was added corresponding to a signal-to-noise ratio of 20 dB, the feed position was calculated from the corrupted data by the minimim mean squared error program which has been previously developed. The feed position calculations were correct to within 0.1%.

Respectfully submitted,

W. Marshall Leach, Jr.
Assistant Professor

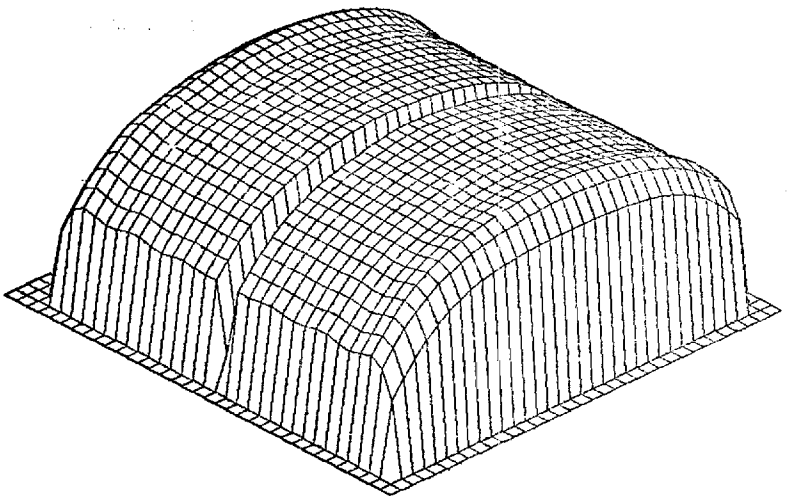

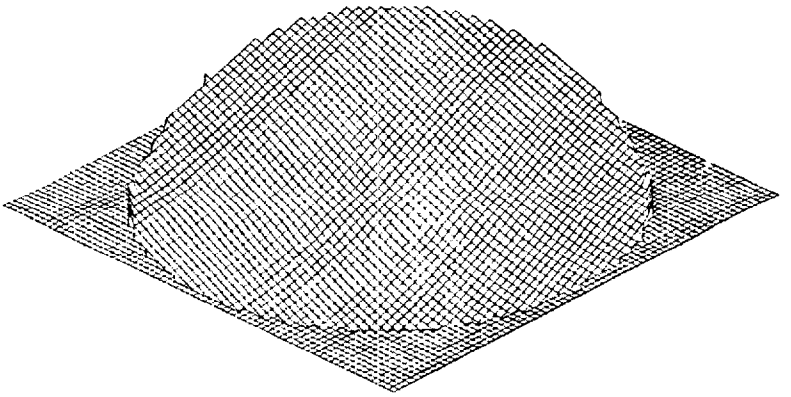

PRINTED IN U.S.A.

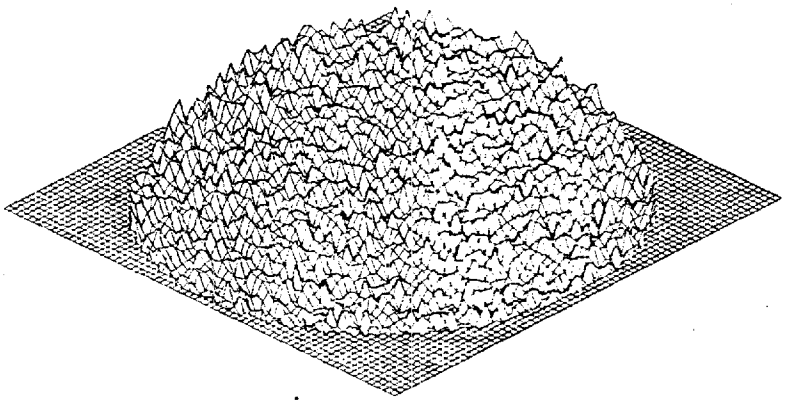

E 21-607

GEORGIA INSTITUTE OF TECHNOLOGY
SCHOOL OF ELECTRICAL ENGINEERING
ATLANTA, GEORGIA 30332

EPHONE: (404) 894-2901

March 6, 1978

National Aeronautics & Space Administration
Goddard Space Flight Center
Greenbelt, Maryland 20771

Attention: Contract Management Branch
Code 242.1

Subject: Monthly Letter Report on Contract NAS5-23886
"Cylindrical Wave Study"

This letter report covers the period from February 1, 1978 to March 1, 1978.

The attached graph shows the far-field pattern radiated by a rectangular aperture computer from cylindrical wave harmonics. The computer program for calculating the far-field pattern from near fields on a cylinder which is being developed under this study was used to calculate this pattern. The program is only semi-operational at this time, however, for it has given erroneous results for the far-field radiated by a quarter wave slot on a cylinder. Because some of the subroutines used in the program are used in the program to compute aperture fields from near fields on a cylinder, it is felt that the problem in both programs is the same. A detailed study of the program is being made to find the error.

The report being prepared under this study will follow the format of the Goddard Space Flight Center "X-Documents" with the exception that it will be organized into chapters and sections rather than sections only.

Respectfully submitted,

W. Marshall Leach, Jr.
Assistant Professor

WML/em
Attachment

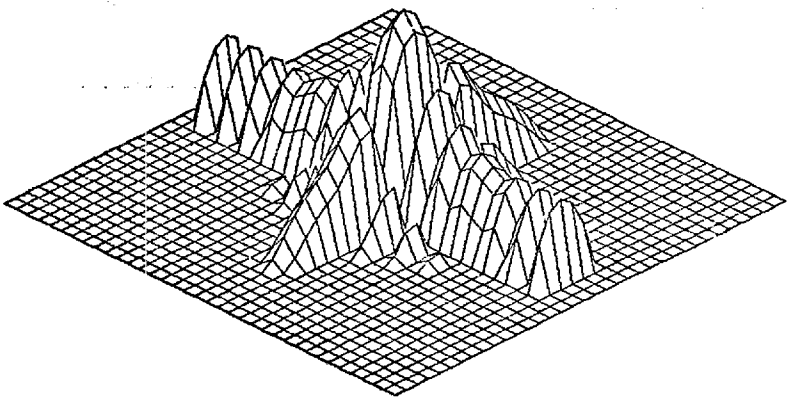

F 21-607

GEORGIA INSTITUTE OF TECHNOLOGY
SCHOOL OF ELECTRICAL ENGINEERING
ATLANTA, GEORGIA 30332

EPHONE: (404) 894-2901

April 2, 1978

National Aeronautics & Space Administration
Goddard Space Flight Center
Greenbelt, Maryland 20771

Attention: Contract Management Branch
Code 242.1

Subject: Monthly Letter Report on Contract NAS5-23886
"Cylindrical Wave Study"

This letter report covers the period from March 1, 1978, to April 1, 1978. The final report for this project has been written and delivered to the typist. Upon completion of typing and printing, nine bound copies plus one reproducible copy will be forwarded to the NASA.

Respectfully submitted,

W. Marshall Leach, Jr.
Assistant Professor

WML/apg

FINAL RESEARCH REPORT
Contract NAS5–23886
April 8, 1977 to April 7, 1978

CYLINDRICAL WAVE STUDY

By
W. Marshall Leach, Jr., and
Lam Nhat An

Prepared for
NATIONAL AERONAUTICS AND SPACE ADMINISTRATION
Goddard Space Flight Center
Greenbelt, Maryland 20771

GEORGIA INSTITUTE OF TECHNOLOGY
SCHOOL OF ELECTRICAL ENGINEERING
ATLANTA, GEORGIA 30332

1978

CYLINDRICAL WAVE EXPANSION STUDY

by

W. Marshall Leach, Jr.

and

Lam Nhat An

GEORGIA INSTITUTE OF TECHNOLOGY
School of Electrical Engineering
Atlanta, Georgia 30332

Final Research Report
Contract NAS5-23886
April 8, 1977 to April 7, 1978

Prepared for
NATIONAL AERONAUTICS AND SPACE ADMINISTRATION
Goddard Space Flight Center
Greenbelt, Maryland 20771

TABLE OF CONTENTS

FOREWARD

This final report was prepared by the Georgia Institute of Technology, School of Electrical Engineering, Atlanta, Georgia 30332 in fulfillment of the requirements of Contract NAS5-23886 for the National Aeronautics and Space Administration, Goddard Space Flight Center, Greenbelt, Maryland 20771. The period of performance covered by this report is April 8, 1977 to April 7, 1978. The report authors are W. Marshall Leach, Jr., Associate Professor of Electrical Engineering, and Lam Nhat An, Graduate Research Assistant.

The authors acknowledge the assistance and guidance of Mr. Richard F. Schmidt of the Goddard Space Flight Center in defining the problems addressed by this report and for his direction and concern.

ABSTRACT

This document summarizes the basic relevant theory of probe corrected near-field measurements on a cylinder. It presents the basic theory of cylindrical wave solutions to the time harmonic wave equation and the application of these solutions to cylindrical near-field measurement systems. An application of the theory to the determination of correct focus of planar aperture parabolic reflector antennas is given. The technique is based on calculating the feed position of the reflector by statistically comparing the measured or calculated aperture phase distribution to the theoretical phase distribution. The theoretical phase distribution is obtained by wavefront image techniques.

Several numerical simulations of the theory are presented. The programs written for these simulations are listed in the Appendix. The numerical examples include both far-field pattern calculations and defocused reflector feed position calculations.

GLOSSARY OF SYMBOLS

∇	del operator of vector analysis
ω	angular frequency
μ	permeability
ε	permittivity
k	free-space wavenumber
$\hat{}$	carat symbol used over coordinate variable to indicate a unit vector directed along that coordinate
$\rightarrow$	arrow symbol used over variables to indicate vector quantities
(x,y,z)	rectangular coordinates of a point
(r,ϕ,z)	cylindrical coordinates of a point
(R,θ,ϕ)	spherical coordinates of a point
$\vec{r}$	general position vector in any coordinate system
ψ	scalar solution to the time harmonic wave equation or aperture phase function
h or η	wavenumber in cylindrical wave expansions
Λ,λ	$\sqrt{k^2-h^2}$ and $\sqrt{k^2-\eta}$, respectively
Z_n^i	any one of four cylindrical Bessel functions ($i=1,2,3,4$) $Z_n^1 = J_n$, $Z_n^2 = Y_n$, $Z_n^3 = H_n^{(1)}$, $Z_n^4 = H_n^{(2)}$
$\vec{L}$, $\vec{M}$, and $\vec{N}$	independent vector solutions to the time harmonic wave equation
$\vec{E}$, $\vec{H}$	electric and magnetic field intensities
$\vec{A}$	magnetic vector potential

$a_n(h)$, $b_n(h)$, $c_n(h)$, $d_n(h)$	cylindrical wave amplitude functions
η	intrinsic impedance of medium
$\vec{J}$	current density
Σ	closed surface or summation symbol
Δ	determinant
C	integration contour in the complex plane
j	$\sqrt{-1}$ in complex variable theory
m,n,ℓ,i	integer subscripts and superscripts
λ	free space wavelength
$\vec{A}(\vec{k})$	plane wave spectrum function
$\vec{k}$	vector wavenumber with components k_x, k_y, k_z
p	focal length of parabola

LIST OF ILLUSTRATIONS

CHAPTER I

INTRODUCTION

Near-field techniques have been shown to be a potentially powerful method for the determination of the far-field patterns of antennas. Although the planar measurement surface has received the most attention, experimental and theoretical work have been performed in cylindrical and spherical systems also. The advantages of near-field techniques for far-field pattern determination are many. They include time and cost effectiveness, accuracy that is comparable to or better than that for the far-field range, and none of the size limitations for large antennas that are associated with conventional far-field ranges. There are disadvantages to near-field techniques. These include the requirement for a more complicated and expensive measurement system, the requirement for a more extensive procedure to calibrate the near-field probes as compared to far-field probes, the patterns are not obtained in real time, and computer software plays an important role in calculating the patterns.

There has been little or no work done on the application of near-field techniques to antenna diagnostics other than far-field pattern determination. The techniques are applicable, however, to antenna diagnostics such as the determination and location of defective elements in phased array antennas, on site tests of aircraft radar antennas by means of portable near-field probe positioners, and the determination of correct focus for large reflector antennas. Part of this report is addressed to the latter application.

This report concerns near-field techniques in cylindrical coordinates. It is organized into four major parts plus relevant appendices. Chapter II presents a review of solutions to the time harmonic wave equation is cylindrical coordinates. Solutions are developed for both scalar and vector waves. The approximations which are valid in the far-field region of a source are then developed. In Chapter III, the basic theory of probe corrected near-field measurements on a cylinder is developed. It is shown that the response of a probe which requires no correction is that of the short dipole. Finally spatial sampling of near fields on a cylinder is discussed. Chapter IV presents a technique for the determination of correct focus of planar aperture parabolic reflector antennas from near-field measurements on a cylinder. The technique involves both cylindrical wave and plane wave modal expansions of the near field radiated by the antenna. Finally, Chapter V presents the basic numerical considerations that are required to implement the theory. In addition, numerical simulations of the theory are presented. All computer programs used in the simulations are included in the Appendix.

CHAPTER II

CYLINDRICAL WAVE EXPANSIONS

2.1 Introduction

The cylindrical wave expansion is the most general solution to the Helmholtz wave equation in the cylindrical coordinate system. This chapter presents a mathematical development of the cylindrical wave expansion for a region of space containing no free-charge density such as the region external to a radiating antenna. Both the scalar and vector cylindrical wave expansions are presented. The scalar wave expansion is the simplest and is presented first. The scalar expansion is useful as a representation of the acoustic pressure field in cylindrical coordinates. It can also be used to represent any rectangular component of the electromagnetic field vectors in a simple medium. The vector cylindrical wave expansion is the most general solution to the vector Helmholtz wave equation in cylindrical coordinates. Thus it can be used to represent the total vector field of any one of the electromagnetic field vectors. The chapter is concluded with a development of the far-field approximations to both the scalar and vector cylindrical wave expansions.

2.2 The Scalar Cylindrical Wave Expansion

Although modal expansions of time varying scalar fields are not of interest in most electromagnetic field problems, solutions to the scalar wave equation are much simpler to obtain. Thus the scalar case makes an appropriate introduction to the vector case. In addition,

the technique used in the following section to generate the vector cylindrical wave expansion first requires the solution to the scalar wave equation in cylindrical coordinates.

In a linear, homogeneous, isotropic medium, i.e., a simple medium, which contains no sources the electromagnetic field vectors $\vec{E}$, $\vec{H}$, $\vec{D}$, and $\vec{B}$ and the magnetic vector potential $\vec{A}$ all satisfy the same differential equation. For time variation of the form $e^{j\omega t}$, this equation is

$$\vec{\nabla}^2 \vec{C} + k^2 \vec{C} = 0 \tag{2-1}$$

where $\vec{C}$ denotes any one of these field vectors and $k = \omega\sqrt{\mu\epsilon}$. This equation is commonly referred to as the vector Helmholtz wave equation. Because it is a vector equation, it can be replaced by a system of three simultaneous scalar equations to obtain a solution. Unfortunately, this is impractical in most cases, for the equations are coupled and difficult to solve simultaneously. There is one exception, however. If $\vec{C}$ is written in its rectangular form $\vec{C} = \hat{x}C_x + \hat{y}C_y + \hat{z}C_z$, three independent equations are obtained and in this case

$$\nabla^2 C_i + k^2 C_i = 0 \tag{2-2}$$

where the subscript i can be either x, y, or z.

Although the C_i in Equation (2-2) are rectangular components of the vector $\vec{C}$, there is no restriction on the coordinate system in which the differential equation is solved. Let C_i be expressed in cylindrical coordinates as a function of r, ϕ, and z as defined in Figure 1. In

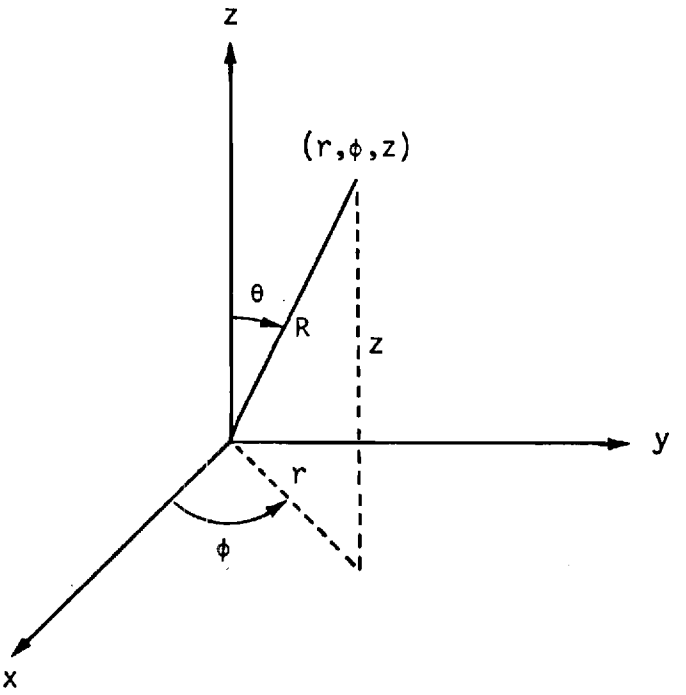

Figure 1. Coordinate System Definitions.

addition, let C_i be replaced by the scalar function $\psi(r,\phi,z)$ in order to eliminate notational difficulties casued by the subscript. In cylindrical coordinates, Equation (2-2) then becomes

$$\frac{1}{r}\frac{\partial}{\partial r}\left(r\frac{\partial\psi}{\partial r}\right) + \frac{1}{r^2}\frac{\partial^2\psi}{\partial\phi^2} + \frac{\partial^2\psi}{\partial z^2} + k^2\psi = 0 \qquad (2\text{-}3)$$

The normal procedure for obtaining a solution to a partial differential equation such as Equation (2-3) is to use the method of separation of variables in which ψ is written as a product of three functions of the form

$$\psi(r,\phi,z) = \psi_1(r)\psi_2(\phi)\psi_3(z) \qquad (2\text{-}4)$$

Substitution of this into Equation (2-3) then yields an equation which can be separated into three independent ordinary differential equations that can be solved by standard techniques. However, the resulting product solution for ψ must be summed over a set of mode indices to form the total solution. By varying the amplitude of each mode in the sum, the solution can be made to represent any function which satisfies Equation (2-3).

Substitution of Equation (2-4) into Equation (2-3) and division by ψ yields

$$\frac{1}{r\psi_1}\frac{d}{dr}\left(r\frac{d\psi_1}{dr}\right) + \frac{1}{r^2\psi_2}\frac{d^2\psi_2}{d\phi^2} + \frac{1}{\psi_3}\frac{d^2\psi_3}{dz^2} + k^2 = 0 \qquad (2\text{-}5)$$

To separate this into three ordinary differential equations, let

$$\frac{1}{\psi_2}\frac{d^2\psi_2}{d_\phi{}^2} = -p^2 \tag{2-6}$$

$$\frac{1}{\psi_3}\frac{d^2\psi_3}{dz^2} = -h^2 \tag{2-7}$$

for which case Equation (2-5) reduces to

$$\frac{1}{r\psi_1}\frac{d}{dr}\left(r\frac{d\psi_1}{dr}\right) - \frac{p^2}{r^2} - h^2 + k^2 = 0 \tag{2-8}$$

Multiplication of this equation by $r^2\psi_1$ yields the familiar Bessel equation

$$r\frac{d}{dr}\left(r\frac{d\psi_1}{dr}\right) + \left[(k^2-h^2)r^2 - p^2\right]\psi_1 = 0 \tag{2-9}$$

The solutions for ψ_2 and ψ_3 are the familiar complex exponential. That for ψ_1 is any one of the four cylindrical Bessel functions. These solutions will be written

$$\psi_1 = Z_p^i(\Lambda r),\ i=1,2,3,4 \tag{2-10}$$

$$\psi_2 = e^{jp\phi} \tag{2-11}$$

$$\psi_3 = e^{-jhz} \tag{2-12}$$

where h and p are yet to be specified from boundary conditions. The choice of the algebraic sign in the exponent of the solutions for ψ_2 and ψ_3 is arbitrary. These have been chosen to agree with the convention used in [1] and [2]. The functions $Z_p^i(\Lambda r)$ are the four cylindrical

Bessel functions

$$Z_p^1(\Lambda r) = J_p(\Lambda r) \tag{2-13}$$

$$Z_p^2(\Lambda r) = Y_p(\Lambda r) \tag{2-14}$$

$$Z_p^3(\Lambda r) = H_p^{(1)}(\Lambda r) = J_p(\Lambda r) + j\, Y(\Lambda r) \tag{2-15}$$

$$Z_p^4(\Lambda r) = H_p^{(2)}(\Lambda r) = J_p(\Lambda r) - j\, Y_p(\Lambda r) \tag{2-16}$$

where Λ must satisfy the relation

$$\Lambda^2 = k^2 - h^2 \tag{2-17}$$

The function $J_p(\Lambda r)$ is the Bessel function of the first kind, $Y_p(\Lambda r)$ is the Bessel function of the second kind, $H_p^{(1)}(\Lambda r)$ is the Hankel function of the first kind, and $H_p^{(2)}(\Lambda r)$ is the Hankel function of the second kind.

In the present case, a solution for ψ is sought which represents waves in free space propagating outward from some finite size source located at or near the origin of the coordinate system. This is a sufficient and necessary constraint on the solution to specify the parameter p and the Bessel function which appears in the solution. Because the solution must be periodic in ϕ in order to be single valued, it follows that p must be an integer. This will be denoted by n. The proper choice of the Bessel function can be made by examining their large argument asymptotic expansions. These are

$$J_n(\Lambda r) \sim \sqrt{\frac{2}{\pi\Lambda r}} \cos\left(\Lambda r - \frac{2n+1}{4}\pi\right) \tag{2-18}$$

$$Y_n(\Lambda r) \sim \sqrt{\frac{2}{\pi\Lambda r}} \sin\left(\Lambda r - \frac{2n+1}{4}\pi\right) \tag{2-19}$$

$$H_n^{(1)}(\Lambda r) \sim \sqrt{\frac{2}{\pi\Lambda r}}\, e^{j\left(\Lambda r - \frac{2n+1}{4}\pi\right)} \tag{2-20}$$

$$H_n^{(2)}(\Lambda r) \sim \sqrt{\frac{2}{\pi\Lambda r}}\, e^{-j\left(\Lambda r - \frac{2n+1}{4}\pi\right)} \tag{2-21}$$

Of these four functions, it can be seen that only $H_n^{(2)}(\Lambda r)$, i.e., the Hankel function of the second kind, represents waves diverging from the origin. This follows because its phase varies as $e^{-j\Lambda r}$. Thus the product solution for ψ becomes

$$\psi(r,\phi,z) = H_n^{(2)}(\Lambda r)\, e^{jn\phi} e^{-jhz} \tag{2-22}$$

This solution for ψ is called a mode because it is not only a function of position but also of the two mode parameters n and h. To construct a total solution, a linear combination of all modes must be formed. Because n is an integer, the linear combination in n must be a summation similar to a Fourier series. The linear combination in h must be an integral over some contour in the complex plane. This is similar to the representation of a time function by the inverse Laplace transform. In the present case, a finite power constraint on the total field requires that the integral

$$\int_{-\infty}^{\infty}\int_{-\pi}^{\pi} \psi\psi^*\, \rho\, d\phi\, dz \tag{2-23}$$

be finite. This is a sufficient condition for the integral in h to be over real values only of h. Thus the field expansion is mathematically complete in the sense that it is in the form of a Fourier integral representation [3].

The total solution for ψ is formed by multiplying each mode by an amplitude function and combining all elementary mode solutions into a modal expansion. This is given by

$$\psi(r,\phi,z) = \sum_{n=-\infty}^{\infty} \int_{-\infty}^{\infty} c_n(h)\, H_n^{(2)}(\Lambda r)\, e^{jn\phi}\, e^{-jhz}\, dh \qquad (2\text{-}24)$$

where $c_n(h)$ is the complex amplitude of each mode in the solution. The mode amplitude is a function of the mode parameters n and h. Examination of Equation (2-24) shows that if r is a constant, the solution is in the form of a Fourier series in ϕ and a Fourier integral in h. This suggests a convenient procedure for determining the mode amplitude function $c_n(h)$ if ψ is known on a given cylinder. Let r_1 be the radius of that cylinder. It follows from Fourier inversion of Equation (2-24) that $c_n(h)$ is given by

$$c_n(h) = \frac{1}{4\pi^2 H_n^{(2)}(\Lambda r_1)} \int_{-\infty}^{\infty} \int_{\pi}^{\pi} \psi(r_1,\phi,z)\, e^{-jn\phi} e^{jhz} d\phi dz \qquad (2\text{-}25)$$

Thus it is possible to solve for $\psi(r,\phi,z)$ at any point in space external to a given cylinder on which ψ is known by first evaluating Equation (2-25) and then Equation (2-24). Equation (2-25) is a straightforward two-dimensional Fourier integral with well known techniques for

numerical solutions. However, Equation (2-24) is not so simple. Fortunately, it is the far-field approximation to ψ that is of interest in most applications. This approximation will be developed in Section 2.4 for the vector field solution to the wave equation.

The mode solution of Equation (2-24) can be used to represent any one of the three rectangular components of the electromagnetic field vectors. A total vector solution can then be written as the vector sum of the x, y, and z components. Each component in the vector sum would have a different amplitude function $C_n^i(h)$, where i can be either x, y, or z. Although these amplitude functions are different for each component, they are not independent, for the total solution must satisfy Maxwell's equations. Thus a tedious procedure would be required to obtain a vector modal expansion which must then be converted from three rectangular components to three cylindrical components. Fortunately, this procedure can be circumvented by use of the method described in the following section.

2.3 Vector Cylindrical Waves

In a series of interesting papers published in 1935 through 1937, Hansen [4] described a useful technique for generating a complete set of vector solutions to the Helmholtz equation. The technique requires only that the scalar wave equation be solved by the conventional technique described in the preceding section. The vector solution is then obtained from appropriate operations on the scalar solution. The technique has been used extensively in spherical coordinates, but the literature shows little or no application to other coordinate systems. However, it is

applicable to any coordinate system in which the scalar wave equation can be solved by the method of separation of variables. It leads to rapid solutions to the vector wave equation in the more familiar rectangular, cylindrical, and spherical coordinate systems. Its application to cylindrical systems will be described in this section. A useful reference to this technique is Section 7.1 of [5].

The scalar function ψ of Equation (2-22) is a solution to the scalar Helmholtz equation in the cylindrical coordinate system. Let $\hat{a}$ be any constant unit vector (i.e., the direction and magnitude of $\hat{a}$ must, in general, be a constant, although in spherical systems, a solution can be obtained with $\hat{a} = \hat{r}$). Three independent vector solutions to Equation (2-1) can then be formed as follows:

$$\vec{L}^i = \nabla\psi^i \tag{2-26}$$

$$\vec{M}^i = \nabla x \hat{a}\psi^i \tag{2-27}$$

$$\vec{N}^i = \frac{1}{k}\nabla x\vec{M}^i \tag{2-28}$$

where the superscript i has been introduced to indicate which of the four cylindrical Bessel functions is used in the product solution for ψ. It follows that these three vectors do indeed satisfy Equation (2-1) by direct substitution. This is shown as follows:

$$\begin{aligned}\nabla^2\vec{L} + k^2\vec{L} &= \nabla^2(\nabla\psi) + k^2\nabla\psi \\ &= \nabla\,[\nabla^2\psi + k^2\psi] \\ &= 0\end{aligned} \tag{2-29}$$

$$\nabla^2\vec{M} + k^2\vec{M} = \nabla^2(\nabla x\hat{a}\psi) + k^2\nabla x\hat{a}\psi$$
$$= \nabla x\hat{a}[\nabla^2\psi + k^2\psi]$$
$$= 0 \qquad (2\text{-}30)$$

$$\nabla^2\vec{N} + k^2\vec{N} = \nabla^2\left(\frac{1}{k}\nabla x\vec{M}\right) + k\nabla x\vec{M}$$
$$= \frac{1}{k}\nabla x[\nabla^2\vec{M} + k^2\vec{M}]$$
$$= 0 \qquad (2\text{-}31)$$

These follow directly from the useful identities

$$\nabla^2(\nabla\phi) = \nabla(\nabla^2\phi) \qquad (2\text{-}32)$$

$$\nabla^2(\nabla x\vec{C}) = \nabla x(\nabla^2\vec{C}) \qquad (2\text{-}33)$$

The vectors $\vec{L}$, $\vec{M}$, and $\vec{N}$ are functions of the coordinates r,ϕ, and z and of the cylindrical wave parameters n and h. Any general solution for a vector field must be written as a linear combination of the three vectors for all values of n and h similar to the general scalar solution of Equation (2-24). It is convenient at this point to write a general solution for the vector magnetic potential function $\vec{A}(r,\phi,z)$. The corresponding solutions for the magnetic field intensities can then be obtained from the familiar relations

$$\vec{H} = \frac{1}{\mu}\nabla x\vec{A} \qquad (2\text{-}34)$$

$$\vec{E} = \frac{1}{j\omega\varepsilon}\nabla x\vec{H} \qquad (2\text{-}35)$$

The vector $\vec{A}$ satisfies Equation (2-1) as do both $\vec{E}$ and $\vec{H}$. The reason for first writing the solution for $\vec{A}$ is that this is the most direct approach to show that the vector $\vec{L}$ cannot appear in the general solution for $\vec{E}$ or $\vec{H}$.

The most general solution for $\vec{A}$ is obtained in a way similar to the way that the most general solution for the scalar ψ was written in Equation (2-24). However, in this case, three complex amplitude functions must be introduced because there are three independent vector functions in the solution. The solution for $\vec{A}$ will be written as

$$\vec{A}(r,\phi,z) = \frac{-1}{j\omega} \sum_{n=-\infty}^{\infty} \int_{-\infty}^{\infty} \left[a_n(h) \vec{M}^i_{nh}(r,\phi,z) + b_n(h) \vec{N}^i_{nh}(r,\phi,z) + c_n(h) \vec{L}^i_{nh}(r,\phi,z) \right] dh \qquad (2\text{-}36)$$

where $a_n(h)$, $b_n(h)$, and $c_n(h)$ are scalar amplitude functions of the three vectors. The superscript i, that indicates which of the four Bessel functions is used in the field expansion, must be chosen to satisfy the boundary conditions of the region in which the expansion is made. The factor $\frac{-1}{j\omega}$ has been added to simplify the resulting expression for the electric field intensity $\vec{E}$.

In the present case, a solution is desired for the region of space external to some cylinder enclosing all sources. Thus the choice $i = 4$ must be made in Equation (2-36) as has been discussed in the preceding section. Solutions for the electric and magnetic field intensities follow from Equations (2-34) and (2-35) and the useful relations

$$\nabla \times \vec{L} = 0 \tag{2-37}$$

$$\vec{M} = \frac{1}{k} \nabla \times \vec{N} \tag{2-38}$$

These solutions are

$$\vec{E} = \sum_{n=-\infty}^{\infty} \int_{-\infty}^{\infty} \left[a_n(h) \vec{M}^4_{nh} + b_n(h) \vec{N}^4_{nh} \right] dh \tag{2-39}$$

$$\vec{H} = \frac{-k}{j\omega\mu} \sum_{n=-\infty}^{\infty} \int_{-\infty}^{\infty} \left[a_n(h) \vec{N}^4_{nh} + b_n(h) \vec{M}^4_{nh} \right] dh \tag{2-40}$$

where the coordinate dependence has been omitted for simplicity. The absence of the vector $\vec{L}$ in the solution results from the fact that $\vec{H}$ is obtained as the curl of $\vec{A}$ and the curl of $\vec{L}$ is identically zero.

The constant unit vector $\hat{a}$ in Equation (2-27) can be chosen arbitrarily. However, it is convenient to choose this so that $\vec{M}$ has no z component. The choice $\hat{a} = \hat{z}$ does this. For this case, the solution for $\vec{M}$ and $\vec{N}$ yields

$$\vec{M}^i_{nh} = \vec{m}^i_{nh} \, e^{jn\phi} e^{-jhz} \tag{2-41}$$

$$\vec{N}^i_{nh} = \vec{n}^i_{nh} \, e^{jn\phi} e^{-jhz} \tag{2-42}$$

where

$$\vec{m}^i_{nh} = \hat{r} \frac{jn}{r} Z^i_n(\Lambda r) - \hat{\phi} \frac{\partial Z^i_n}{\partial r} \tag{2-43}$$

$$\vec{n}^i_{nh} = -\hat{r} \frac{jh}{k} \frac{\partial Z^i_n}{\partial r} + \hat{\phi} \frac{nh}{kr} Z^i_n(\Lambda r) + \hat{z} \frac{\Lambda^2}{k} Z^i_n(\Lambda r) \tag{2-44}$$

With the introduction of these solutions into Equation (2-39), the solution for the electric field intensity becomes

$$\vec{E} = \sum_{n=-\infty}^{\infty} e^{jn\phi} \int_{-\infty}^{\infty} \left[a_n(h) \vec{m}^{4}_{nh} + b_n(h) \vec{n}^{4}_{nh} \right] e^{-jhz} dz \qquad (2\text{-}45)$$

It can be seen from this that $\vec{E}$ is written as the sum of two solutions. Because the $\vec{m}$ vector contains no z component, this part of the solution is tranverse electric to the z direction, or $(TE)_z$. Similarly, it follows that the $\vec{n}$ vector is transverse magnetic to the z direction, or $(TM)_z$.

On any cylinder for which r is a constant, each scalar component of Equation (2-45) is in the form of a Fourier series in ϕ and a Fourier transform integral in z. Thus it follows that the inverse relationship

$$a_n(h) \vec{m}^{4}_{nh} + b_n(h) \vec{n}^{4}_{nh} = \frac{1}{4\pi^2} \int_{-\infty}^{\infty} \int_{-\pi}^{\pi} \vec{E}(r_1, \phi, z) e^{-jn\phi} e^{jhz} \, d\phi dz \qquad (2\text{-}46)$$

must exist, where r_1 is the radius of the cylinder. Examination of this shows that it is sufficient to know only two vector components of $\vec{E}$ on the cylinder in order to determine both $a_n(h)$ and $b_n(h)$ for any given n or h. Normally, it is the tangential components E_ϕ and E_z that are used to do this. When Equation (2-46) is separated into its scalar components and solved for $a_n(h)$ and $b_n(h)$ as functions of E_ϕ and E_z, the result is

$$a_n(h) = \frac{-I_\phi(n,h)}{\frac{\partial}{\partial r_1}\left[H_n^{(2)}(\Lambda r_1)\right]} + \frac{nhI_z(n,h)}{\Lambda^2 r_1 \frac{\partial}{\partial r_1}\left[H_n^{(2)}(\Lambda r_1)\right]} \qquad (2\text{-}48)$$

$$b_n(h) = \frac{I_z(n,h)}{\frac{\Lambda^2}{k} H_n^{(2)}(\Lambda r_1)} \tag{2-49}$$

where the functions $I_\phi(n,h)$ and $I_z(n,h)$ are given by

$$I_\phi(n,h) = \frac{1}{4\pi^2} \int_{-\infty}^{\infty} \int_{-\pi}^{\pi} E_\phi(r_1,\phi,z) e^{-jn\phi} e^{jhz} d\phi dz \tag{2-50}$$

$$I_z(n,h) = \frac{1}{4\pi^2} \int_{-\infty}^{\infty} \int_{-\pi}^{\pi} E_z(r_1,\phi,z) e^{-jn\phi} e^{jhz} d\phi dz \tag{2-51}$$

Both of these integrals are Fourier transform integrals which can be solved numerically with the efficient fast Fourier transform (FFT) algorithm.

In order to use the above equations, it is necessary to know the exact tangential fields on the cylinder of radius r_1. If these fields are measured, it follows that the measuring probe must be ideal or the measured data must be corrected for its directional response characteristics. A method for doing this will be described in the following chapter. Once $a_n(h)$ and $b_n(h)$ have been determined, Equation (2-45) can be used to evaluate the electric field intensity at any point external to the cylinder of radius r_1. The far-field approximation to Equation (2-45) is developed in the next section.

2.4 The Far-Field Approximation to the Cylindrical Wave Expansion

In the previous section, a general expression for the electric field intensity external to a closed surface containing all sources was developed. In general, the evaluation of this expression is a formidable task. However, a considerable simplification results if the field

is to be evaluated in the far-field region of the source. In this section, the far-field approximation to the cylindrical wave expansion given by Equation (2-45) is developed. First, the Hankel functions which appear in the cylindrical wave vectors $\vec{m}^{4}_{nh}$ and $\vec{n}^{4}_{nh}$ are replaced by their large argument asymptotic expansions. The integral in Equation (2-45) is then evaluated by the method of steepest descent. The far field is then shown to be a spherical transverse electromagnetic field.

For large r, the cylindrical wave vectors $\vec{m}^{4}_{nh}$ and $\vec{n}^{4}_{nh}$ which are defined in Equations (2-43) and (2-44), can be simplified considerably if the Hankel function $H^{(2)}_{n}(\Lambda r)$ and its partial derivative with respect to r are replaced by their large argument asymptotic expansions. The large argument asymptotic expansion for $H^{(2)}_{n}(\Lambda r)$ has been given in Equation (2-21). The corresponding expansion for $\frac{\partial H^{(2)}_{n}}{\partial r}$ can be obtained by taking the partial derivative of this equation with respect to r to yield

$$\frac{\partial H^{(2)}_{n}}{\partial r} \sim j^{n-\frac{1}{2}} \sqrt{\frac{2\Lambda}{\pi r}}\ e^{-j\Lambda r} \tag{2-52}$$

where the term involving $r^{-3/2}$ has been neglected for large r. The resulting expressions for the cylindrical wave vectors $\vec{m}^{4}_{nh}$ and $\vec{n}^{4}_{nm}$ are

$$\vec{m}^{4}_{nh} = -\hat{\phi} j^{n-\frac{1}{2}} \sqrt{\frac{2\Lambda}{\pi r}}\ e^{-j\Lambda r} \tag{2-53}$$

$$\vec{n}^{4}_{nh} = -(\hat{r}h - \hat{z}\Lambda)\ \frac{j^{n+\frac{1}{2}}}{k} \sqrt{\frac{2\Lambda}{\pi r}}\ e^{-j\Lambda r} \tag{2-54}$$

Substitution of these expressions into the equation for the general solution for $\vec{E}$ yields

$$\vec{E} = j^{\frac{1}{2}}\sqrt{\frac{2}{\pi r}} \sum_{n=-\infty}^{\infty} j^n e^{jn\phi} \int_{-\infty}^{\infty} \Lambda^{\frac{1}{2}} [\hat{\phi} j a_n(h) \tag{2-55}$$

$$- \frac{1}{k} (\hat{r}h - \hat{z}\Lambda) b_n(h)] e^{-j\Lambda r} e^{-jhz} dh$$

where $\Lambda = \sqrt{k^2-h^2}$. This equation will be transformed into one more suitable for application of the method of steepest descent by making the change in variables

$$h = k\sin\alpha \tag{2-56}$$

and by converting the far-field point to spherical coordinates with the transformations

$$r = R\sin\theta \tag{2-57}$$

$$z = R\cos\theta \tag{2-58}$$

The result is

$$\vec{E} = j^{1/2} k^{3/2} \frac{2}{\pi R\sin\theta} \sum_{n=-\infty}^{\infty} j^n e^{jn\phi} \int_C [\hat{\phi} j a_n(k\sin\theta) \tag{2-59}$$

$$- (\hat{r}\sin\alpha - \hat{z}\cos\alpha) b_n(k\sin\alpha)] \cos^{3/2}\alpha \; e^{-jkR\sin(\alpha+\theta)} d\alpha$$

where C is the contour illustrated in Figure 2.

The integral in the above expression is evaluated in Appendix A using the method of steepest descent. The resulting expression for the electric field intensity is shown to be

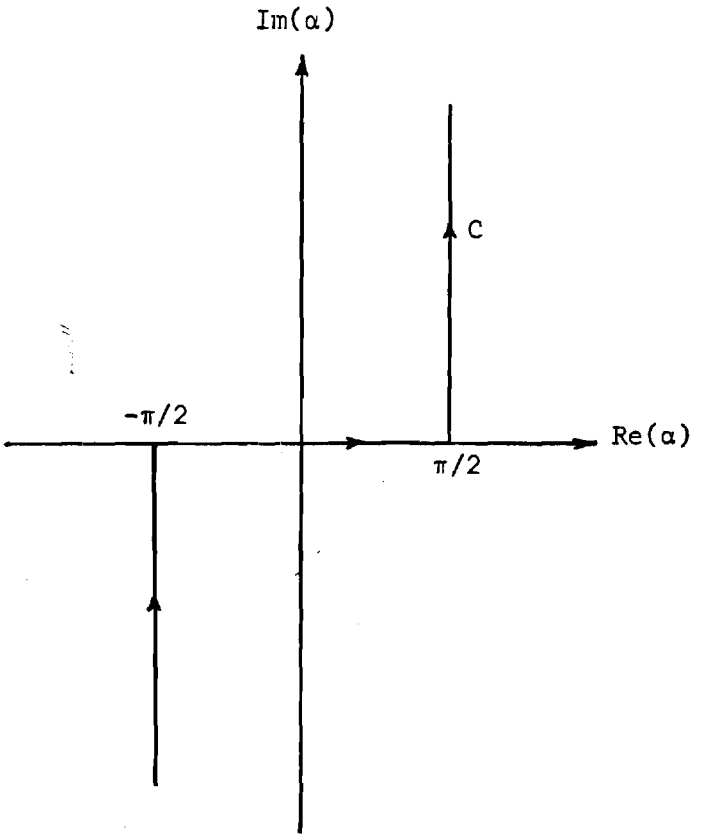

Figure 2. The Contour of Integration C

$$\vec{E} = \frac{-2k\sin\theta}{R} e^{-jkR} \sum_{n=-\infty}^{\infty} j^n e^{jn\phi} [\hat{\phi} a_n(k\cos\theta) + j(\hat{r}\cos\theta - \hat{z}\sin\theta) b_n(k\cos\theta)] \tag{2-60}$$

Because $\hat{\theta} = \hat{r}\cos\theta - \hat{z}\sin\theta$, this equation can be separated into the spherical components

$$E_R = 0 \tag{2-61}$$

$$E_\theta = \frac{-j2k\sin\theta}{R} e^{-jkR} \sum_{n=-\infty}^{\infty} j^n b_n(k\cos\theta) e^{jn\phi} \tag{2-62}$$

$$E_\phi = \frac{-2k\sin}{R} e^{-jkR} \sum_{n=-\infty}^{\infty} j^n a_n(k\cos\theta) e^{jn\phi} \tag{2-63}$$

Thus the far-field electric field intensity is transverse to the radial direction, as would be expected.

Comparison of Equations (2-39) and (2-40) reveals that the far-field magnetic field intensity can be obtained from the solution for the electric field intensity by simply interchanging the amplitude weighting functions $a_n(h)$ and $b_n(h)$ and by including the multiplicative factor $-k/j\omega\mu$. The resulting expressions are

$$H_R = 0 \tag{2-64}$$

$$H_\theta = -\frac{E_\phi}{\eta} \tag{2-65}$$

$$H_\phi = \frac{E_\theta}{\eta} \tag{2-66}$$

where $\eta = \sqrt{\mu/\varepsilon}$. Thus the far-field magnetic field intensity is also transverse to the radial direction and is related to the solution for E by the vector equation

$$\vec{H} = \frac{\hat{R}\times\vec{E}}{\eta} \tag{2-67}$$

Because both $\vec{E}$ and $\vec{H}$ have no radial components and are mutually perpendicular, the far field comprises a spherical transverse electromagnetic field.

Examination of the foregoing solutions shows that the far field is determined only by those values of $a_n(h)$ and $b_n(h)$ for which $-k \leq h \leq k$ because $|k\cos\theta| \leq k$. Thus it can be concluded that the part of the near field for which $|h| > k$ represents evanescent waves in the vicinity of the antenna. These waves represent reactive energy storage which in no way influences the far-field structure except to the extent that they are necessary to support a particular current distribution on the antenna. In Section 3.6 a spatial sampling criterion is discussed for the near field on the surface of a cylinder enclosing an antenna. In that section, it will be assumed that the reactive energy stored outside the cylinder is negligible. This assumption will be shown to be true for any antenna which is not a high-Q or supergain structure.

CHAPTER III

ANTENNA PATTERN DETERMINATION FROM NEAR-FIELD MEASUREMENTS ON A CYLINDER

3.1 Introduction

In the preceding chapter, a method has been described which allows one to determine the far-field pattern of an antenna if the tangential components of the near field electric field intensity are known over a cylinder enclosing the antenna. The method requires that the exact near field be known and does not account for the directional response effects of a measuring probe. In this chapter, the problem will be reformulated so that these effects can be corrected for. It will be shown that the cylindrical wave harmonics for the field radiated by an antenna can be determined independently of the measuring probe provided the cylindrical wave harmonics for the field radiated by the probe when it is used as a transmitter are known. The basic assumption is that the probe is a reciprocal measuring device so that its transmitting and receiving characteristics are the same.

3.2 Lorentz Reciprocity Applied to the Coupling Between Two Antennas

Because it can be used to deduce a number of fundamental properties, the Lorentz reciprocity theorem is one of the most useful theorems in applied electromagnetics. This theorem is the key to the derivation of the probe correction of near-field measurements and can be applied

to any coordinate system. Because of its basic role in the derivations of this chapter, this section will be devoted to a tutorial review of the development of this theorem.

Figure 3 shows a closed surface Σ containing two current source distributions $\vec{J}_1$ and $\vec{J}_2$. Let $\vec{E}_1$ and $\vec{H}_1$ be the fields radiated by $\vec{J}_1$. Similarly, define $\vec{E}_2$ and $\vec{H}_2$ as the fields radiated by $\vec{J}_2$. Because each set of fields must independently satisfy Maxwell's equations, it follows that

$$\begin{aligned} \nabla \times \vec{E}_1 &= -j\omega\mu\vec{H}_1 \\ \nabla \times \vec{H}_1 &= j\omega\varepsilon\vec{E}_1 + \vec{J}_1 \end{aligned} \tag{3-1}$$

$$\begin{aligned} \nabla \times \vec{E}_2 &= -j\omega\mu\vec{H}_2 \\ \nabla \times \vec{H}_2 &= j\omega\varepsilon\vec{E}_2 + \vec{J}_2 \end{aligned} \tag{3-2}$$

To obtain the Lorentz theorem, the relation $\nabla \cdot (\vec{E}_1 \times \vec{H}_2 - \vec{E}_2 \times \vec{H}_1)$ is first expanded and then Equations (3-1) and (3-2) are substituted for each curl term in the expansion. The result is

$$\nabla \cdot (\vec{E}_1 \times \vec{H}_2 - \vec{E}_2 \times \vec{H}_1) = (\nabla \times \vec{E}_1) \cdot \vec{H}_2 - (\nabla \times \vec{H}_2) \cdot \vec{E}_1 - (\nabla \times \vec{E}_2) \cdot \vec{H}_1$$

$$+ (\nabla \times \vec{H}_1) \cdot \vec{E}_2 = -\vec{J}_2 \cdot \vec{E}_1 + \vec{J}_1 \cdot \vec{E}_2 \tag{3-3}$$

By integrating this over the volume V and applying the divergence theorem to the left side of the equation, the Lorentz theorem is obtained. It is

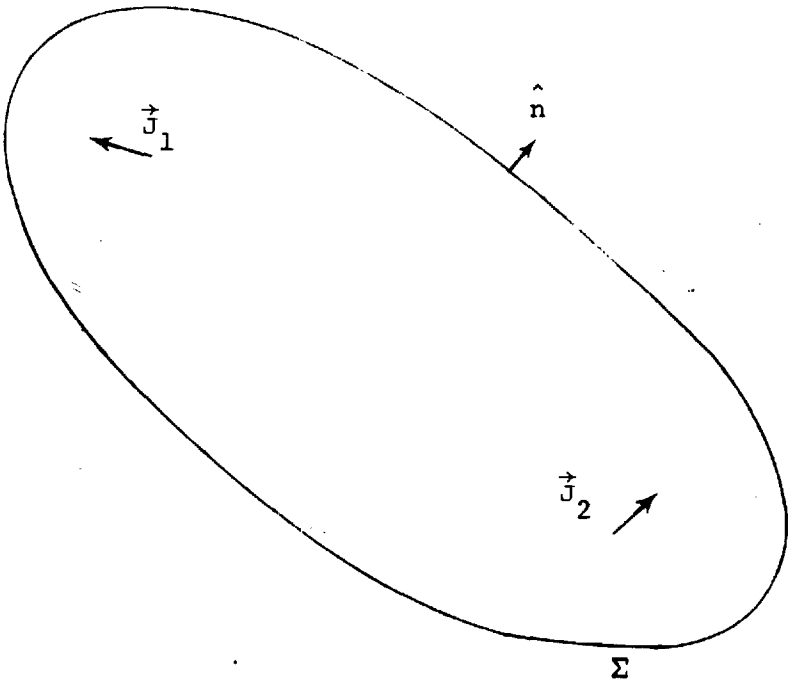

Figure 3. Illustration for the Lorentz Reciprocity Theorem.

$$\oint_{\Sigma} (\vec{E}_1 x \vec{H}_2 - \vec{E}_2 x \vec{H}_1) \cdot \hat{n} \, da$$

$$= \int_{V} (\vec{E}_2 \cdot \vec{J}_1 - \vec{E}_1 \cdot \vec{J}_2) dv \qquad (3\text{-}4)$$

In a source free region, the right hand side of Equation (3-4) is zero because $\vec{J}_1 = \vec{J}_2 = 0$. In the present case, it is desired to apply the theorem to the region external to Σ which contains no sources, i.e., the sources are inside Σ. It follows that if Σ contains all sources and the spherical surface at infinity Σ_∞ contains Σ, then the volume integral on the right side of Equation (3-4) is the same for the region inside Σ_∞ as it is for the region inside Σ. Subtraction of the two equations for the two different regions yields

$$\int_{\Sigma} (\vec{E}_1 x \vec{H}_2 - \vec{E}_2 x \vec{H}_1) \cdot \hat{n} \, da$$

$$= - \int_{\Sigma_\infty} (\vec{E}_1 x \vec{H}_2 - \vec{E}_2 x \vec{H}_1) \cdot \hat{R} \, da \qquad (3\text{-}5)$$

To obtain the desired result, it is necessary to use the fact that the fields over an infinite sphere produced by any finite source near the origin are in the form of a spherical TEM wave for which $\vec{E}$ and $\vec{H}$ have the relation given by Equation (2-67). Substitution of this for both $\vec{H}_1$ and $\vec{H}_2$ in the integrand of Equation (3-5) yields

$$(\vec{E}_1 x \vec{H}_2 - \vec{E}_2 x \vec{H}_1)$$

$$= \frac{1}{\eta}\left[\vec{E}_1 x (\hat{R} x \vec{E}_2) - \vec{E}_2 x (\hat{R} x \vec{E}_1)\right]$$

$$= \frac{1}{\eta}\left[(\vec{E}_1 \cdot \vec{E}_2)\hat{R} - (\vec{E}_1 \cdot \hat{R})\vec{E}_2 - (\vec{E}_2 \cdot \vec{E}_1)\hat{R} + (\vec{E}_2 \cdot \hat{R})\vec{E}_1\right]$$

$$= 0 \qquad (3\text{-}6)$$

where the fact that $\vec{E}_1 \cdot \hat{R} = \vec{E}_2 \cdot \hat{R} = 0$ on Σ_∞ has been used. Thus it follows that if there are no sources external to Σ, the Lorentz theorem reduces to

$$\oint_\Sigma (\vec{E}_1 x \vec{H}_2 - \vec{E}_2 x \vec{H}_1) \cdot \hat{n}\, da = 0 \qquad (3\text{-}7)$$

This is the form of the theorem which will be applied in the following section.

3.3 Probe Correction of Near-Field Measurements on a Cylinder

In this section, a method will be presented to obtain the cylindrical wave amplitude functions for the field radiated by an antenna from probe corrected near-field measurements over the surface of a cylinder containing the antenna. The method has as its basis the Lorentz reciprocity theorem which was summarized in the preceding section. It will be shown that the solution for the cylindrical wave amplitude functions requires the knowledge of the cylindrical wave amplitude functions for the field radiated by the measuring probe when it is used as a transmitter. A

method for obtaining this information is discussed in Chapter V.

In Figure 4, let Σ_a be a cylinder of radius r_a that contains an arbitrary test antenna connected to signal generator A. Denote the field radiated by the test antenna by $\vec{E}_a(\vec{r})$ and $\vec{H}_a(\vec{r})$. Let this field be incident on a probe antenna whose reference origin 0' is located at the point (r_o, ϕ_o, z_o). Let the probe be connected via a waveguide or transmission line feeder to generator B. Denote the field radiated by the probe when generator B is activated by $\vec{E}_b(\vec{r}')$ and $\vec{H}_b(\vec{r}')$, where $\vec{r}'$ is measured with respect to 0'. Let the field scattered by the test antenna when generator B is activated be denoted by $\vec{E}_{as}(\vec{r})$ and $\vec{H}_{as}(\vec{r})$ and the field scattered by the probe when generator A is activated by $\vec{E}_{bs}(\vec{r}')$ and $\vec{H}_{bs}(\vec{r}')$. In the following analysis, it will be assumed that there are no multiply scattered fields between the test antenna and the probe so that the total scattered field is given by these terms.

It is desired to solve for the signal induced across the terminals of generator B when only generator A is activated. If generator B is then replaced by a linear detector having an input impedance equal to the output impedance of generator B, it will be shown that the cylindrical wave amplitudes for the field radiated by the test antenna can be calculated from the detector output voltage if its amplitude and phase are known as functions of ϕ_o and z_o over the cylinder of radius r_o. It will be assumed that the cylindrical wave amplitudes for the field radiated by the probe when generator B is activated are known. Without loss of generality, it will be assumed that both generators A and B are matched to their respective line feeders. Otherwise the theory holds with only slight modifications.

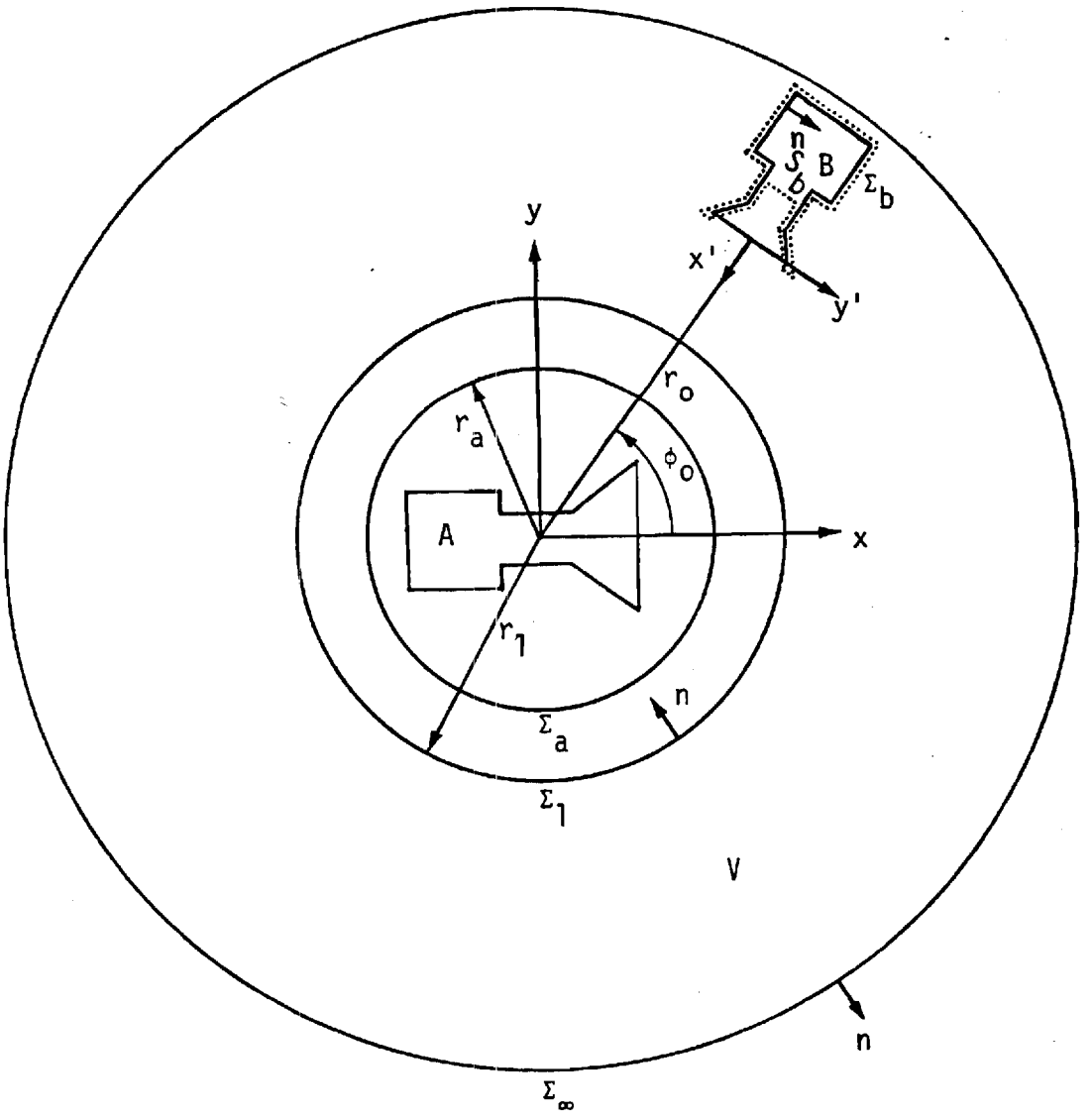

Figure 4. Geometry for the Probe Correction Derivation.

In Figure 4, let V be the volume bounded by the surfaces Σ_1, Σ_b, and Σ_∞, where Σ_1 is the cylinder of radius r_1, Σ_b is the closed surface lying just outside the probe antenna and shield enclosing generator B which cuts the feeder for the probe at S_b, and Σ_∞ is the sphere of infinite radius. Because V contains no sources, it follows from the Lorentz reciprocity theorem that

$$\oint_{\Sigma_1+\Sigma_b+\Sigma_\infty} \left[(\vec{E}_a + \vec{E}_{bs}) \times (\vec{H}_b + \vec{H}_{as}) - (\vec{E}_b + \vec{E}_{as}) \times (\vec{H}_a + \vec{H}_{bs}) \right] \cdot n\,da = 0 \tag{3-8}$$

where all multiply scattered terms have been neglected. The integrand of this expression vanishes identically over Σ_∞ as shown in the preceding section. The integrand also vanishes over Σ_b except for the area S_b because the tangential components of E vanish at the surface of a good conductor. Also, $\vec{E}_{bs} = 0$ and $\vec{H}_{bs} = 0$ over S_b by virtue of their definition. Thus it follows that Equation (3-8) reduces to

$$\begin{aligned} &\oint_{\Sigma_1} (\vec{E}_a \times \vec{H}_b - \vec{E}_b \times \vec{H}_a) \cdot (-\hat{r})\,da + \oint_{\Sigma_1} (\vec{E}_a \times \vec{H}_{as} - \vec{E}_{as} \times \vec{H}_a) \cdot (-\hat{r})\,da \\ &+ \oint_{\Sigma_1} (\vec{E}_{bs} \times \vec{H}_b - \vec{E}_b \times \vec{H}_{bs}) \cdot (-\hat{r})\,da + \int_{S_b} (\vec{E}_a \times \vec{H}_b - \vec{E}_b \times \vec{H}_a) \cdot (-\hat{x}')\,da = 0 \end{aligned} \tag{3-9}$$

where the terms involving products of the scattered fields have been neglected and where it has been assumed that $\vec{E}_b + \vec{E}_{as} \simeq \vec{E}_b$ and $\vec{H}_{as} \simeq \vec{H}_b$ over S_b. These assumptions are valid if the scattered fields over Σ_1 and S_b are small compared to the incident fields. Without them, the desired solution to Equation (3-8) would be impossible.

Let the four integrals in Equation (3-9) be denoted by I_1, I_2, I_3, and I_4, respectively. It can be shown [6] that the integral I_4 is proportional to the negative of the open circuit received voltage of the probe antenna. From network theory, it is known that the received voltage into any load impedance is proportional to this open-circuit voltage for a fixed frequency. Thus the integral over S_b will be replaced by $-Kv(r_o, \phi_o, z_o)$, where K is a constant which can change with frequency and $v(r_o, \phi_o, z_o)$ is the received voltage by the probe which is a function of probe position (r_o, ϕ_o, z_o).

To evaluate the integral for I_1 in Equation (3-9), the cylindrical wave expansions of the fields over Σ_1 will be written initially in the forms

$$\vec{E}_a(\vec{r}) = a_n(h)\, \vec{M}^4_{nh}(\vec{r}) + b_n(h)\vec{N}_{nh}(\vec{r}) \tag{3-10}$$

$$\vec{H}_a(\vec{r}) = \frac{-k}{j\omega\mu}\left[b_n(h)\vec{M}^4_{nh}(\vec{r}) + a_n(h)\vec{N}^4_{nh}(\vec{r})\right] \tag{3-11}$$

$$\vec{E}_b(\vec{r}') = c_m(\eta)\vec{M}^4_{m\eta}(\vec{r}') + d_m(\eta)\vec{N}^4_{m\eta}(\vec{r}') \tag{3-12}$$

$$\vec{H}_b(\vec{r}') = \frac{-k}{j\omega\mu}\left[d_m(\eta)\vec{M}^4_{m\eta}(\vec{r}') + c_m(\eta)\vec{N}^4_{m\eta}(\vec{r}')\right] \tag{3-13}$$

After I_1 is evaluated for these fields, the result must be summed in m and n and integrated in η and h to obtain the final value of the integral.

With the vector addition theorems developed in Appendix B, the origin for $\vec{E}_b$ and $\vec{H}_b$ is first changed from 0' to 0. The result is

$$\vec{E}_b(\vec{r}) = \sum_{\ell=-\infty}^{\infty} (-1)^{\ell} H^{(2)}_{m+\ell}(\lambda r_o)\, e^{j\ell\phi_o} e^{j\eta z_o}\left[c_m(\eta)\, \vec{M}^{1}_{-\ell\eta}(\vec{r}) + d_m(\eta)\vec{N}^{1}_{-\ell\eta}(\vec{r})\right] \tag{3-14}$$

$$\vec{H}_b(\vec{r}) = \frac{-k}{j\omega\mu} \sum_{\ell=-\infty}^{\infty} (-1)^{\ell} H^{(2)}_{m+\ell}(\lambda r_o) e^{j\ell\phi_o} e^{j\eta z_o} \times \left[d_m(\eta)\vec{M}^{1}_{-\ell\eta}(\vec{r}) + c_m(\eta)\vec{N}^{1}_{-\ell\eta}(\vec{r})\right] \tag{3-15}$$

where $\lambda = \sqrt{k^2-\eta^2}$. Substitution of these expressions and those for $\vec{E}_a$ and $\vec{H}_a$ into the integrand for I_1 gives

$$I_1 = \frac{k}{j\omega\mu} \sum_{\ell=-\infty}^{\infty} (-1)^{\ell} H^{(2)}_{m+\ell}(\lambda r_o)\, e^{j\ell\phi_o} e^{j\eta z_o} \int_{-\infty}^{\infty}\int_{-\pi}^{\pi} \Big[\Big(a_n(h)d_m(\eta) + b_n(h)c_m(\eta)\Big)\Big(\vec{M}^{4}_{nh}\times\vec{M}^{1}_{-\ell\eta} + \vec{N}^{4}_{nh}\times\vec{N}^{1}_{-\ell\eta}\Big) + \Big(a_n(h)c_m(\eta) + b_n(h)d_m(\eta)\Big) \times \Big(\vec{M}^{4}_{nh}\times\vec{N}^{1}_{-\ell\eta} + \vec{N}^{4}_{nh}\times\vec{M}^{1}_{-\ell\eta}\Big)\Big] \cdot \hat{r}\, r_1\, d\phi dz \tag{3-16}$$

where the vectors $\vec{M}$ and $\vec{N}$ are functions of the coordinates (r,ϕ,z).

From the orthogonality properties of the cylindrical wave vectors developed in Appendix C, it follows that the terms involving the products $\vec{M}^{4}_{nh} \times M^{1}_{-\ell\eta} \cdot \hat{r}$ and $\vec{N}^{4}_{nh} \times \vec{N}^{1}_{-\ell\eta} \cdot \hat{r}$ have zero contribution to Equation (3-16). The remaining terms can be evaluated with the aid of Equation (C-3). Thus I_1 becomes

$$I_1 = \frac{kr_1}{j\omega\mu} \sum_{\ell=-\infty}^{\infty} (-1)^{\ell} H^{(2)}_{m+\ell}(\lambda r_o)\, e^{j\ell\phi_o} e^{j\eta z_o}\Big(a_n(h)c_m(\eta) + b_n(h)\, d_m(\eta)\Big) \left[\frac{4\pi^2\Lambda^3}{k}\, \delta_{n\ell}\delta(\eta+h)\, \Big(J'_{-n}(\Lambda r_1)\, H^{(2)}_n(\Lambda r_1) - J_{-n}(\Lambda r_1)\, H^{(2)\prime}_n(\Lambda r_1)\Big)\right] \tag{3-17}$$

where $\delta_{n\ell}$ is the Kronecker delta and $\delta(\eta+h)$ is the Dirac delta function. This expression can be simplified with the aid of the identity

$$J'_{-n}(\Lambda r_1)\, H_n^{(2)}(\Lambda r_1) - J_{-n}(\Lambda r_1)\, H_n^{(2)'}(\Lambda r_1) = \frac{j2(-1)^n}{\pi \Lambda r_1} \tag{3-18}$$

Thus I_1 reduces to

$$I_1 = \frac{8\pi\Lambda^2}{\omega\mu} H_{n+m}^{(2)}(\Lambda r_o)\, e^{jn\phi_o} e^{j\eta z_o} \delta(\eta+h) \left[a_n(h) c_m(\eta) + b_n(h) d_m(\eta)\right] \tag{3-19}$$

which is independent of r_1. When this expression is summed over all m and n and integrated in η and h, the result is

$$I_1 = \frac{8\pi}{\omega\mu} \sum_{n=-\infty}^{\infty} e^{jn\phi_o} \int_{-\infty}^{\infty} \Lambda^2 \Big[a_n(h) \sum_{m=-\infty}^{\infty} c_m(-h) H_{n+m}^{(2)}(\Lambda r_o)$$

$$+ b_n(h) \sum_{m=-\infty}^{\infty} d_m(-h)\, H_{n+m}^{(2)}(\Lambda r_o) \Big] e^{-jhz_o}\, dh \tag{3-20}$$

Because multiple scattering is neglected, $\vec{E}_a$, $\vec{H}_a$, $\vec{E}_{as}$, and $\vec{H}_{as}$ satisfy the homogeneous wave equation outside of Σ_a. Thus by the Lorentz reciprocity theorem it follows that I_2 is identically zero. Similarly, I_3 is also zero. Thus it follows that Equation (3-9) reduces to

$$v(r_o,\phi_o,z_o) = \frac{1}{4\pi^2 k^2} \sum_{n=-\infty}^{\infty} e^{jn\phi_o} \int_{-\infty}^{\infty} \Lambda^2 \Big[a_n(h) \sum_{m=-\infty}^{\infty} c_m(-h)\, H_{n+m}^{(2)}(\Lambda r_o)$$

$$+ b_n(h) \sum_{m=-\infty}^{\infty} d_m(-h)\, H_{n+m}^{(2)}(\Lambda r_o) \Big] e^{-jhz_o}\, dh \tag{3-21}$$

where $v(r_o,\phi_o,z_o)$ has been normalized by choosing the constant of proportionality defined in the preceding to be $32\pi^3k^2/\omega\mu$.

Examination of this equation reveals that $v(r_o,\phi_o,z_o)$ is in the form of a Fourier series in ϕ_o and a Fourier integral in z_o. Thus the equation has an inverse which is given by

$$a_n(h) \sum_{m=-\infty}^{\infty} c_m(-h)\, H_{n+m}^{(2)}(\Lambda r_o) + b_n(h) \sum_{m=-\infty}^{\infty} d_m(-h)\, H_{n+m}^{(2)}(\Lambda r_o) = \frac{k^2}{\Lambda^2} \int_{-\infty}^{\infty} \int_{-\pi}^{\pi} v(r_o,\phi_o,z_o)\, e^{-jn\phi_o} e^{jhz_o} d\phi_o dz_o \tag{3-22}$$

This is the desired result. It relates the cylindrical wave amplitude functions $a_n(h)$ and $b_n(h)$ of an arbitrary test antenna to the two-dimensional Fourier transform of the output voltage of a probe antenna when the measurement surface is a cylinder of radius r_o. If the cylindrical wave amplitude functions for the probe antenna are known, it follows that Equation (3-22) can be solved for $a_n(h)$ and $b_n(h)$ provided two independent measurements of $v(r_o,\phi_o,z_o)$ are made.

Let $v'(r_o,\phi_o,z_o)$ represent the voltage output of the probe antenna when it is rotated 90^o about its longitudinal axis. An equation identical to Equation (3-22) can be written which realtes $a_n(h)$ and $b_n(h)$ to $v'(r_o,\phi_o,z_o)$ with the exception that $c_m(-h)$ and $d_m(-h)$ must be replaced by the amplitude functions for the rotated probe. If these are denoted by $c'_m(-h)$ and $d'_m(-h)$, then this equation and Equation (3-22) can be solved simultaneously for $a_n(h)$ and $b_n(h)$ to obtain

$$a_n(h) = \frac{k^2}{\Lambda^2 \Delta_n(h)} \left[I_n(h) \sum_{m=-\infty}^{\infty} d'_m(-h)\, H_{n+m}^{(2)}(\Lambda r_o) - I'_n(h) \sum_{m=-\infty}^{\infty} d_m(-h)\, H_{n+m}^{(2)}(\Lambda r_o) \right] \tag{3-23}$$

$$b_n(h) = \frac{k^2}{\Lambda 2\Delta_n(h)} \left[I_n'(h) \sum_{m=-\infty}^{\infty} c_m(-h)\, H_{n+m}^{(2)}(\Lambda r_o) + I_n(h) \sum_{m=-\infty}^{\infty} c_m'(-h)\, H_{n+m}^{(2)}(\Lambda r_o) \right] \tag{3-24}$$

where

$$I_n(h) = \int_{-\infty}^{\infty} \int_{-\pi}^{\pi} v(r_o,\phi_o,z_o)\, e^{-jn\phi_o} e^{jhz_o}\, d\phi_o\, dz_o \tag{3-25}$$

$$I_n'(h) = \int_{-\infty}^{\infty} \int_{-\pi}^{\pi} v'(r_o,\phi_o,z_o) e^{-jn\phi_o} e^{jhz_o} d\phi_o\, dz_o \tag{3-26}$$

$$\Delta_n(h) = \left[\sum_{m=-\infty}^{\infty} c_m(-h) H_{n+m}^{(2)}(\Lambda r_o) \right] \left[\sum_{m=-\infty}^{\infty} d_m'(-h) H_{n+m}^{(2)}(\Lambda r_o) \right] - \left[\sum_{m=-\infty}^{\infty} c_m'(-h) H_{n+m}^{(2)}(\Lambda r_o) \right] \left[\sum_{m=-\infty}^{\infty} d_m(-h) H_{n+m}^{(2)}(\Lambda r_o) \right] \tag{3-27}$$

It is assumed that the probe responds predominantly to one polarization component so that a solution for $a_n(h)$ and $b_n(h)$ exists, i.e., $\Delta_n(h)$ must not be zero.

Equations (3-23) through (3-27) form the basis of the method for the determination of the cylindrical wave functions for the field radiated by an arbitrary antenna from measurements made with a probe on a cylinder containing the antenna. By using these equations to determine the cylindrical wave amplitude functions $a_n(h)$ and $b_n(h)$, the far field of the antenna can be determined from Equations (2-62) and (2-63). Because the far field is determined from only those values of $a_n(h)$ and $b_n(h)$ for which $-k \leq h \leq k$, it follows that the cylindrical wave amplitude functions for the probe need be known only for arguments inside this interval. In the next chapter, a method will be developed

for calculating the aperture field distribution for antenna A from these cylindrical wave amplitude functions under the assumption that antenna A has a planar aperture.

3.4 Probe Correction in the Quasi Near Field

A simplification in the probe correction can be obtained if the radius of the cylinder on which the near-field measurements are made is large enough to make certain approximations. These approximations make it possible to eliminate the Hankel functions from the probe correction equations to obtain a solution which involves the probe far-field functions themselves and not the cylindrical wave amplitudes in the probe far-field expansions. The simplification is based on a large argument approximation to the probe correction equations that involves an integral definition of the Hankel functions. This solution is presented in this section.

The basic probe correction equations have been given in Equations (3-23) through (3-27). The terms in these equations which involve the probe response are of the form

$$\sum_m \gamma_m(-h)\, H^{(2)}_{n+m}(\Lambda r_o) \qquad (3\text{-}28)$$

where $\gamma_m(h)$ is any one of the four cylindrical wave amplitude functions in the probe field expansion and r_o is the radius of the measurement cylinder. As discussed in Section 2.4, the wavenumber h is related to the elevation angle in the probe far-field pattern by the relation $h = k\cos\theta$, and Λ is given by $\Lambda = \sqrt{k^2-h^2} = k\sin\theta$.

The first step in expressing Equation (3-28) in terms of the probe far-field pattern rather than in terms of the $\gamma_m(-h)$ is to replace the Hankel function by its integral definition. This is [5]

$$H_p^{(2)}(\rho) = \frac{e^{-jp\pi/2}}{\pi} \int_{\frac{\pi}{2}-j\infty}^{3\frac{\pi}{2}+j\infty} e^{j\rho\cos\phi+jp\phi}d\phi \tag{3-29}$$

Before substitution of this into Equation (3-28), it is convenient to change the variable of integration by replacing ϕ with the variable $\phi + \pi$. This transforms the integral definition into one with symmetrical integration limits. The result is

$$H_p^{(2)}(\rho) = e^{jp\frac{\pi}{2}} \int_{\frac{\pi}{2}-j\infty}^{\frac{\pi}{2}+j\infty} e^{-j\rho\cos\phi+jp\phi}d\phi \tag{3-30}$$

When Equation (3-30) is substituted into Equation (3-28), the substitution $-h = k\cos(\pi-\theta)$ is made, and the order of summation and integration in the resulting expression is reversed, the equation becomes

$$\sum_m \gamma_m(-h)\, H_{n+m}^{(2)}(\Lambda r_o)$$

$$= e^{jn\pi/2} \int_{\frac{\pi}{2}-j\infty}^{\frac{\pi}{2}+j\infty} \left[\sum_m j^m \gamma_m\left(k\cos(\pi-\theta)\right) e^{jm\phi}\right]$$

$$\times\, e^{-jkr_o\sin\theta\cos\phi+jn\phi}d\phi \tag{3-31}$$

This integral can be broken into three parts: one over the path from $-\frac{\pi}{2} - j\infty$ to $-\frac{\pi}{2} + j0$, one over the path from $-\frac{\pi}{2}$ to $+\frac{\pi}{2}$, and one over the path from $\frac{\pi}{2} + j0$ to $\frac{\pi}{2} + j\infty$. For kr_o sufficiently large, the first and third integrals are small because the exponent of the complex exponential contains a real and negative part over the respective paths for these integrals that is proportional to kr_o. Thus these two terms will be neglected.

Comparison of the bracketed term in Equation (3-31) to the far-field expressions in Equations (2-62) and 2-63) reveals that this term can be written in terms of the probe far field expressions. For example, if $\gamma_m = c_m$, the bracketed term is $E_\phi^p(\pi-\theta,\phi)/\sin\theta$, where the superscript p implies "probe". If $\gamma_m = d_m$, the bracketed term is $E_\theta^p(\pi-\theta,\phi)/j\sin\theta$. The former choice will be made for illustration in the following. Equation (3-31) then becomes

$$\frac{j^n}{\sin\theta}\int_{-\frac{\pi}{2}}^{\frac{\pi}{2}} E_\phi^p(\pi-\theta,\phi)\, e^{-jkr_o\sin\theta\left[\cos\phi-\frac{n\phi}{kr_o\sin\theta}\right]}\, d\phi \qquad (3\text{-}32)$$

The desired result is obtained from this equation by making a stationary phase approximation to the integral under the assumption of large kr_o. This is done in Appendix D to obtain

$$\frac{j^n}{\sin\theta}\sqrt{\frac{2\pi}{kr_o\sin\theta\cos\phi_n}}\; E_\phi^p(\pi-\theta,\phi_n)$$

$$\times\; e^{-jkr_o\sin\theta\cos\phi_n}\, e^{jn\phi_n} e^{j\pi/4} \qquad (3\text{-}33)$$

where

$$\phi_n = \sin^{-1}\left[\frac{n}{kr_o\sin\theta}\right] \tag{3-34}$$

A similar expression is obtained for $\gamma_m = b_m$ by making the substitution $j^{-1} E_\theta^p(\pi-\theta,\phi)$ for $E_\phi^p(\pi-\theta,\phi)$ in this equation.

Denote the part of Equation (3-33) that does not involve the probe response by $K_p(r_o,\theta,\phi_n)$. The quasi near-field approximation to the coupling equation of Equation (3-22) then becomes

$$K_p(r_o,\theta,\phi_n)\left[a_n(h)E_\phi^p(\pi-\theta,\phi_n) - jb_n(h)E_\theta^p(\pi-\theta,\phi_n)\right]$$

$$= \frac{k^2}{\Lambda^2}\int_{-\infty}^{\infty}\int_{-\pi}^{\pi} v(r_o,\phi_o,z_o)\, e^{-jn\phi_o} e^{jhz_o}\, d\phi_o dz_o \tag{3-35}$$

where as usual $h = k\cos\theta$ and $\Lambda = k\sin\theta$, and ϕ_n is given by Equation (3-34). This equation can be solved for $a_n(h)$ and $b_n(h)$ provided two independent measurements of $v(r_o,\phi_o,z_o)$ are made.

Let $v'(r_o,\phi_o,z_o)$ represent the voltage output of the probe when it is rotated 90^o about its longitudinal axis. Similar to the procedure described in the previous section, a second coupling equation can be written with the exception that E_ϕ^p and E_θ^p must be replaced by the fields of the rotated probe. If these are denoted by $E_\phi^{p'}$ and $E_\theta^{p'}$, then this equation and Equation (3-35) can be solved simulaneously for $a_n(h)$ and $b_n(h)$ to obtain

$$a_n(h) = \frac{1}{K_p(r_o,\theta,\phi_n)\sin^2\theta}$$

$$\times \frac{-E_\theta^{p'}(\pi-\theta,\phi_n)I_n(h)+E_\theta^{p}(\pi-\theta,\phi_n)I_n'(h)}{E_\theta^{p}(\pi-\theta,\phi_n)E_\phi^{p'}(\pi-\theta,\phi_n)-E_\theta^{p'}(\pi-\theta,\phi_n)E_\phi^{p}(\pi-\theta,\phi_n)} \qquad (3\text{-}36)$$

$$b_n(h) = \frac{1}{K_p(r_o,\theta,\phi_n)\sin^2\theta}$$

$$\times \frac{jE_\phi^{p'}(\pi-\theta,\phi_n)I_n(h)-jE_\phi^{p}(\pi-\theta,\phi_n)I_n'(h)}{E_\theta^{p}(\pi-\theta,\phi_n)E_\phi^{p'}(\pi-\theta,\phi_n)-E_\theta^{p'}(\pi-\theta,\phi_n)E_\phi^{p}(\pi-\theta,\phi_n)} \qquad (3\text{-}37)$$

where $I_n(h)$ and $I_n'(h)$ have been defined in Equations (3-25) and (3-26).

Some insight into the probe correction process can be gained by examination of these results. For example, let the probe be vertically polarized so that $E_\phi^p = 0$. When the probe is rotated 90^o, it follows that $E_\theta^{p'} = 0$. Also, for kr_o large, Equation (3-34) shows that $\phi_n \simeq 0$. Thus, under these conditions, Equations (3-36) and (3-37) reduce to

$$a_n(h) = \frac{1}{K_p\sin^2\theta}\ \frac{I_n'(h)}{E_\phi^{p'}(\pi-\theta,0)} \qquad (3\text{-}38)$$

$$b_n(h) = \frac{1}{K_p\sin^2\theta}\ \frac{I_n(h)}{E_\theta^{p}(\pi-\theta,\phi)} \qquad (3\text{-}39)$$

Aside from the factor K_p, it can be seen from these that the cylindrical wave amplitude functions corresponding to a particular elevation angle

θ (or wavenumber $h = k\cos\theta$) are obtained from the probe response at an elevation angle of $\pi-\theta$. This could have been predicted from the geometry of the measurement system because, for example, if the elevation angle of the probe with respect to the antenna is θ, the elevation of the antenna with respect to the probe is $\pi-\theta$.

Although the approximations made in this section are useful for gaining an insight into the probe correction, it can be seen by comparing Equations (3-36) and (3-37) to the exact solutions in Equations (3-23) and (3-24) that, with the exception of the Hankel functions in the exact solution, there is little difference in the computational requirements between the two solutions. Because the Hankel functions can be evaluated numerically by means of very efficient recursion relations, the exact solution can be implemented almost as efficiently as the approximate solution. In particular, if the summations in the exact solutions that involve the probe functions are evaluated in advance and stored in a computer file, there is no advantage to be gained with the approximate solution.

3.5 The Response of an Ideal Probe

Because the solution of Equations (3-23) through (3-27) for the cylindrical wave amplitude functions for the field radiated by an arbitrary antenna require a knowledge of the cylindrical wave amplitude functions for the measuring probe response, the question of the response of an ideal measuring probe arises. If the probe is ideal, it requires no correction and Equations (2-48) and (2-49) can be used to determine the cylindrical wave amplitude functions for the test antenna. It will be shown in this section that the ideal probe response is that of a short dipole.

To obtain the desired results, it will be assumed that the probe response is desired to be directly proportional to the z component of the electric field on the cylinder. From Equations (2-41) through (2-44), it is seen that only the vector $\vec{N}$ in the field expansion for the test antenna has a z component. Therefore, the solution for E_z can be written

$$E_z(r,\phi,z) = \sum_{n=-\infty}^{\infty} e^{jn\phi} \int_{-\infty}^{\infty} b_n(h) \frac{\Lambda^2}{k} H_n^{(2)}(\Lambda r)\, e^{-jhz}\, dz \tag{3-40}$$

When this is compared to Equation (3-21), it can be seen that if $v(r,\phi,z)$ is to be directly proportional to E_z, the cylindrical wave amplitude functions for the probe must be given by

$$c_m(h) = 0 \text{ for all } m \tag{3-41}$$

$$d_m(h) = 0 \quad m \neq 0 \tag{3-42}$$

$$d_o(h) = \text{constant} \tag{3-43}$$

The constant in the latter equation will be normalized to the value k in order to simplify the following.

Thus, if the probe is used as a transmitter, its radiated field follows from Equations (2-39) through (2-44) to be

$$\vec{E}(r,\phi,z) = \int_{-\infty}^{\infty} k\vec{N}^{4}_{oh}(r,\phi,z)\,dh$$

$$= -\hat{r}\int_{\infty}^{\infty} jh\Lambda H_o^{(2)'}(\Lambda r)e^{-jhz}dh$$

$$+ \hat{z}\int_{-\infty}^{\infty} \Lambda^2 H_o(\Lambda r)e^{-jhz}dh \qquad (3\text{-}44)$$

Because the integration does not involve either r or z, this equation can be rewritten in the form

$$\vec{E}(r,\phi,z) = \left[\hat{r}\frac{\partial^2}{\partial r\partial z} + \hat{z}\left(k^2 + \frac{\partial^2}{\partial z^2}\right)\right]$$

$$\times \int_{-\infty}^{\infty} H_o^{(2)}(\Lambda r)\, e^{-jhz}dh \qquad (3\text{-}45)$$

where $\Lambda^2 = k^2 - h^2$. The value of the integral in this equation is given in [7]. It is

$$j2\,\frac{e^{-jkR}}{R} \qquad (3\text{-}46)$$

where $R^2 = r^2 + z^2$ and R is the spherical distance from the origin to the field point. To obtain the desired results, Equation (3-46) is first substituted into Equation (3-45) and the required differentiation is performed. Next, the cylindrical coordinates r and z are changed to the spherical coordinates R and θ with the transformations $r = R\sin\theta$ and $z = R\cos\theta$. Finally, the cylindrical unit vectors $\hat{r}$ and $\hat{z}$ are changed to spherical coordinates with the transformations $\hat{r} = \hat{R}\sin\theta + \hat{\theta}\cos\theta$ and $\hat{z} = \hat{R}\cos\theta - \hat{\theta}\sin\theta$. After a lengthy and tedius procedure, the result is

$$\vec{E}(R,\theta,\phi) = j\,2\,k^3\,e^{-jkR}\left[\hat{R}\cos\theta \times \left(\frac{j2}{(kR)^2} + \frac{2}{(kR)^3}\right) - \hat{\theta}\sin\theta \times \left(\frac{1}{kR} - \frac{j}{(kR)^2} - \frac{1}{(kR)^3}\right)\right] \tag{3-47}$$

This is the field radiated by a short dipole.

3.6 Spatial Sampling on the Cylinder

Because the measurement of the near field of any antenna over some surface enclosing the antenna potentially requires the accumulation of a large amount of data, the problem of determining an optimum spatial sampling rate is one of great practical importance. Sampling rates which are too high result in the acquisition of more data than are necessary to characterize a given near field, while rates that are too low result in data which may be meaningless. In this section, the determination of a reasonable sampling rate on a cylinder enclosing the antenna is discussed. Specifically, high-Q antennas, such as supergain antennas, will be excluded from the discussion because no a priori upper bound on the required sampling rate for such antennas can be specified. The exclusion of this class of antennas is not restrictive in most cases because they are rarely if ever encountered in practice.

To establish a sampling criterion for the near field on a cylinder enclosing an antenna, the variation of the field with the coordinates on the cylinder can be studied by examination of the cylindrical wave expansions developed in Section 3.3. It was shown that each component of the field on a cylinder can be written in the form of a Fourier series in the

azimuth angle ϕ and a Fourier integral in the axial distance z. Thus it follows that the results of the sampling theory of Fourier transform analysis can be used to establish a sample spacing criterion on the cylinder if upper bounds on the angular harmonic n and the wavenumber h can be determined. An examination of the antenna quality factor, or Q, is one means of establishing these bounds.

The Q of an antenna is an important parameter which can be related to the effect of the antenna size on gain, bandwidth, and efficiency. A high Q means that a large amount of reactive energy is stored in the near field of the antenna. This implies large currents on the antenna structure, high ohmic losses, a narrow bandwidth, and extreme frequency sensitivity. Although it is difficult in general to relate the antenna Q to the degree to which it is a supergain structure, it has been shown that a supergain antenna is necessarily a high-Q antenna [8]. Thus the exclusion of high-Q antennas from the discussion will also exclude supergain antennas.

The Q of an antenna which has been tuned to resonance by the addition of a reactive element is defined as [9]

$$Q = \frac{2\omega \max\{W^m, W^e\}}{P} \tag{3-48}$$

where W^m and W^e are the time average magnetic and electric energies stored in the near field of the antenna and P is the total power radiated by the antenna. If the Q of a single cylindrical wave with mode indices n and h is defined as

$$Q_{nh} = \frac{2\omega \max\{W_{nh}^{m}, W_{nh}^{e}\}}{P_{nh}} \tag{3-49}$$

it follows from Equation (3-48) that the Q of an antenna which radiates a spectrum of cylindrical waves is given by the linear combination

$$Q = \frac{\sum_{n=-\infty}^{\infty} \int_{-\infty}^{\infty} |C_{nh}|^2 P_{nh} Q_{nh} dh}{\sum_{n=-\infty}^{\infty} \int_{-\infty}^{\infty} |C_{nh}|^2 P_{nh} dh} \tag{3-50}$$

where C_{nh} is the complex amplitude of the cylindrical wave with mode indices n and h. This equation is simply a weighted average of the Q_{nh} over all n and h, where the weighting factors are $|C_{nh}|^2 P_{nh}$.

Collin and Rothschild [9] have evaluated P_{nh} and Q_{nh} for a single cylindrical wave radiated by an ideal, loss-free antenna of radius a. The term "ideal, loss-free antenna of radius a" was originally defined by Chu [10] as one having no energy storage for $R < a$, where R is the spherical radial distance from the center of the smallest sphere of radius a completely enclosing the antenna. In the present case, it is interpreted as an antenna for which there is no energy storage for $r < a$, where a is the radius of the smallest cylinder completely enclosing the antenna. The Q for this ideal antenna must be less than or equal to that for any other loss-free antenna fitting into the cylinder $r = a$, because any field for $r < a$ can only add to the energy storage.

The expressions for P_{nh} and Q_{nh} for $(TE)_z$ and $(TM)_z$ cylindrical waves are identical and are given by [9]

$$P_{nh} = \frac{2(k^2-h^2)}{\omega\mu} \tag{3-51}$$

$$Q_{nh} = \frac{\pi k^2}{4(k^2-h^2)} \left\{ \frac{4\Lambda a}{\pi} + [(n^2+1-\Lambda^2a^2)(J_n^2+Y_n^2)] \right. \tag{3-52}$$

$$\left. - [(n+1)J_n - \Lambda a J_{n+1}]^2 - [(n+1)Y_n - \Lambda a Y_{n+1}]^2 \right\}$$

where $h < k$ and the argument of the Bessel functions is $\Lambda a = (k^2-h^2)\, a$. For $h \geq k$, $P_{nh} = 0$ and Q_{nh} is undefined.

Collin and Rothschild [9] have shown that the quantity $(1-(h/k)^2)Q_{nh} = \frac{1}{2\omega\varepsilon} P_{nh}Q_{nh}$ increases very rapidly when n becomes larger than Λa. Because this term aside from the factor $\frac{1}{2\omega\varepsilon}$, appears in the numerator of the general expression for Q in Equation (3-50), it follows that Q can become large if C_{nh} is not small for $n > \Lambda a$. Because $\Lambda \leq k$ for real h, it follows that the highest significant angular harmonic in the cylindrical wave expansion of the fields of an antenna which is not a high-Q structure is $N = ka$. If a is taken to be the radius of the smallest sphere completely enclosing the antenna, this result agrees with the conclusions reached by Chu [10] and Harrington [8] in studying the physical limitations of antennas using spherical wave expansions. In general, however, the radius of the smallest cylinder completely enclosing an antenna is less than or equal to the radius of the smallest sphere, the two being equal if the antenna is oriented so that its longest dimension is perpendicular to the axis of the cylinder.

A sample spacing criterion for the azimuth angle ϕ on a cylinder enclosing an antenna can be obtained by applying the Nyquist sampling

criterion of Fourier transform theory to the above result. If N is the maximum angular harmonic in the cylindrical wave expansion of a given field, then it follows that the maximum angular separation between adjacent samples is

$$\Delta\phi = \frac{\pi}{N} \quad . \tag{3-53}$$

In this case N must be chosen as the smallest integer greater than ka, where a is the radius of the smallest cylinder completely enclosing the antenna.

The above limit on N has been verified by Ludwig [11] for a particular antenna. He has shown that over 99.9 per cent of the total power radiated by a circular aperture horn is contained in spherical waves with angular harmonics $|n| \leq ka$, where a is the radius of the smallest sphere containing the aperture. Because a is a function of the location of the origin of the sphere with respect to the center of the aperture, he was able to demonstrate the variation of the maximum significant angular harmonic with the radius of the sphere by varying the position of the origin. Because both cylindrical wave and spherical wave expansions are in the form of a Fourier series in the azimuth angle ϕ, it follows that his results are directly applicable to cylindrical wave expansions for this particular antenna for which the radius of the smallest cylinder completely enclosing the antenna is the same as the radius of the smallest sphere.

A z-sample spacing criterion follows in a similar manner. Collin and Rothschild [9] have shown that the term $P_{nh}Q_{nh}$ in Equation (3-50) increases rapidly for $|n| \geq (k^2-h^2)\, a$. Thus it follows that $|C_{nh}|$ must be small for $h^2 > k^2 - \frac{n^2}{a^2}$. This implies that the highest significant wavenumber in the cylindrical wave expansion of the field of an antenna which is not a high-Q structure is $|h| \leq k$. It follows that the maximum z-sample spacing on the cylinder is given by the Nyquist spacing

$$\Delta z = \frac{\pi}{k} \tag{3-54}$$

$$= \frac{\lambda}{2}$$

It is interesting to compare the two sample spacing criteria which have been developed. If the measurement cylinder is the smallest cylinder completely enclosing the antenna, then it follows that the arc length on the cylinder separating adjacent sample points when sampling in the azimuth direction is

$$\Delta s = a\Delta\phi \tag{3-55}$$

$$= \frac{\pi}{k}$$

$$= \frac{\lambda}{2}$$

This is the same as the z-sample spacing with the exception that $\Delta s > \Delta z$

when sampling on a cylinder of radius greater than a.

Although the sample spacing criteria defined by Equation (3-53) and (3-54) are useful, they are in no way absolute, for it is impossible to predict a priori an exact cutoff harmonic for n and an exact cutoff wavenumber for h in the cylindrical wave expansion of the fields radiated by a given antenna. In practice, more conservative sample spacings have been used. For example, Collin and Zucker [6] state that the maximum order angular harmonic in the cylindrical wave expansion of the field radiated by an aperture on a cylinder is approximately 2ka, where a is the radius of the cylinder. This would lead to a sample spacing in the ϕ direction of one-half that specified by Equation (3-53). Joy and Paris [12] have obtained excellent results in the calculation of the far-field patterns of reflector antennas using a sample spacing of $\lambda/3$ on a plane located in front of the antenna. This spacing effectively allows for a 50 per cent error in the $\lambda/2$ criterion. In the actual measurement of the near field of an antenna, therefore, the sample spacings specified by Equations (3-53) and (3-54) should be used as guidelines in determining the sample spacing between measurement points. In most instances, the sample spacings chosen can be easily verified experimentally on the near-field antenna range.

CHAPTER IV

THE DETERMINATION OF ANTENNA FOCUS FROM NEAR-FIELD MEASUREMENTS ON A CYLINDER

4.1 Introduction

The verification of proper far-field focus for large ground-based reflector antennas is impractical with conventional techniques once the antenna has been installed in the field. However, because it is not impractical to perform near-field measurements on the antenna with portable near-field probe positioners, near-field techniques may prove to be a powerful method for on-site diagnostics such as determining antenna focus.

This chapter presents a study of the application of cylindrical wave techniques to the determination of focus for planar aperture reflector antennas. A method is developed for the calculation of the reflector aperture fields from the near-field on a cylinder enclosing the antenna. The method involves calculation of the cylindrical wave amplitudes for the field radiated by the antenna, a transformation of the cylindrical wave amplitudes into a plane wave spectrum, and finally the calculation of the aperture fields from the plane wave spectrum.

In order to use the aperture fields to determine correct focus of the reflector, it is necessary to know the reflector geometry. In this chapter, a parabolic reflector geometry is assumed. A technique is described for calculating the position of the feed from the known aperture

fields. Computer simulations of the techniques described in this chapter are presented in the following chapter.

4.2 Transformation of Antenna Near-Fields from a Cylinder to a Plane

Figure 5 shows a planar aperture antenna, such as a parabolic reflector, located inside a measurement cylinder such that the antenna aperture is located in the plane defined by $x = 0$. A method is developed in this section by which the aperture fields of the antenna can be calculated from the near-fields on the measurement cylinder. The method takes into consideration only the radiating fields of the antenna, i.e., the reactive or evanescent fields are neglected. This is a valid assumption for most reflector antennas because they are wide bandwidth, low-Q radiators which have very little reactive near-field power. If this were not the case, the geometrical optics techniques used in their design would not be valid.

The radiation from a planar aperture antenna is most conveniently formulated as a modal expansion in rectangular coordinates. Such an expansion is called a plane wave spectrum expansion. It can be shown that this is the most general solution to the wave equation in rectangular coordinates. The solution for the electric field intensity in a region containing no free charge density is given by [13]

$$\vec{E}(\vec{r}) = \int_{-\infty}^{\infty} \int_{-\infty}^{\infty} \vec{A}(\vec{k})\, e^{-j\vec{k}\cdot\vec{r}}\, dk_y\, dk_z \qquad (4\text{-}1)$$

where

$$\vec{k} = \hat{x}\, k_x + \hat{y}\, k_y + \hat{z}\, k_z \qquad (4\text{-}2)$$

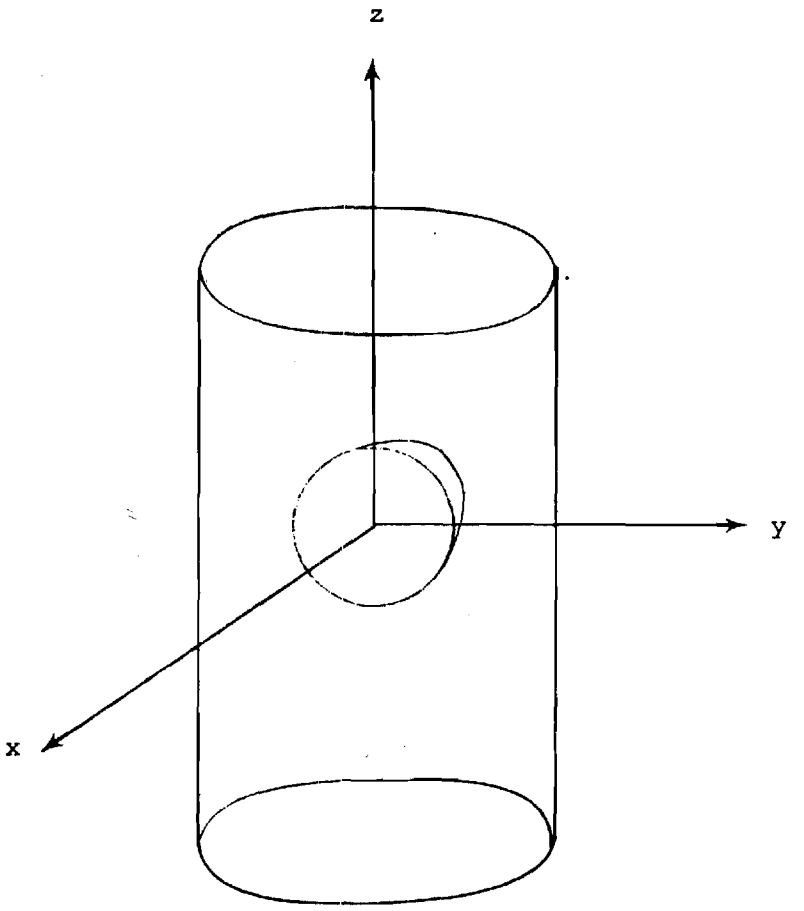

Figure 5. Illustration of a Planar Aperture Antenna Inside a Measurement Cylinder.

$$\vec{r} = \hat{x}\, x + \hat{y}\, y + \hat{z}\, z \tag{4-3}$$

$$\vec{A}(\vec{k}) = \hat{x}\, A_x + \hat{y}\, A_y + \hat{z}\, A_z \tag{4-4}$$

The vector function $\vec{A}(\vec{k})$ is called the plane wave spectrum function. Its argument $\vec{k}$ is called the vector wavenumber.

Although both $\vec{A}$ and $\vec{k}$ have three components, only two are independent. These will be chosen to be the y and z components. It then follows from the condition $\nabla \cdot \vec{E} = 0$ that A_x is given by

$$A_x = - \frac{k_y A_y + k_z A_z}{k_x} \tag{4-5}$$

Also, it follows from the wave equation $\nabla^2 \vec{E} + k^2 \vec{E} = 0$ that k_x is given by

$$\begin{aligned} k_x &= \sqrt{k^2 - k_y^2 - k_z^2} \quad , \quad k_y^2 + k_z^2 \leq k^2 \\ &= -j \sqrt{k_y^2 + k_z^2 - k^2} \quad , \quad k_y^2 + k_z^2 \geq k^2 \end{aligned} \tag{4-6}$$

The latter choice for the algebraic sign of k_x is necessary for a bounded solution as $x \to \infty$. The imaginary values of k_x are associated with evanescent or reactive power storage in the near-field of the antenna.

It is desired to use Equation (4-1) to calculate the aperture field at $x = 0$ from the known fields on a cylinder around the antenna. To do this, the plane wave spectrum function $\vec{A}(\vec{k})$ must be related to the fields on the cylinder. One way to do this is to use the cylindrical wave expansion to calculate the antenna far-field from the near-field on

the cylinder. Then, by equating this to the far field expression for Equation (4-1), the plane wave spectrum function $\vec{A}(\vec{k})$ can be determined. However, the technique cannot be used to determine $\vec{A}$ for $k_y^2 + k_z^2 \geq k^2$ because evanescent waves do not appear in the far-field expressions. As has been discussed, this is not a disadvantage with the reflector antennas concerned by this report.

The far-field expression for Equation (4-1) is obtained by evaluating the double integral by the method of stationary phase. The result is [13]

$$\vec{E} = \frac{j2\pi k e^{-jkR}}{R} \left[\hat{\phi} \left(A_y \sin\theta + A_z \cos\theta \sin\phi \right) - \hat{\theta} A_z \cos\phi \right] \tag{4-7}$$

where A_y and A_z are functions of the wavenumbers at the stationary phase point of the integral. These are

$$k_x = k \sin\theta\cos\phi \tag{4-8}$$

$$k_y = k \sin\theta\sin\phi \tag{4-9}$$

$$k_z = k \cos\theta \tag{4-10}$$

When Equation (4-7) is equated to the far-field expressions developed from the cylindrical wave expansions given in Equations (2-60) through (2-63), the following relations are obtained:

$$A_y \sin\theta + A_z \cos\theta \sin\phi = \sin\theta \sum_{n=-\infty}^{\infty} j^n a_n(k\cos\theta) e^{jn\phi} \qquad (4\text{-}11)$$

$$A_z \cos\phi = -j\sin\theta \sum_{n=-\infty}^{\infty} j^n b_n(k\cos\theta) e^{jn\phi} \qquad (4\text{-}12)$$

where the constant factor $j\pi$ has been absorbed into both A_y and A_z to simplify the equations.

For a given or measured electric field intensity distribution on the measurement cylinder, it is a straightforward process to calculate the cylindrical wave amplitude functions and evaluate the right side of Equations (4-11) and (4-12). These two equations can then be solved simultaneously for A_y and A_z as a function of the arguments given by Equations (4-8) through (4-10). Over the plane $x = 0$, it then follows from Equation (4-1) that the tangential aperture fields E_y and E_z are given by

$$E_y(o,y,z) = \iint_D A_y(k_x,k_y,k_z) e^{-jk_y y} e^{-jk_z z} dk_y dk_z \qquad (4\text{-}13)$$

$$E_z(o,y,z) = \iint_D A_z(k_x,k_y,k_z) e^{-jk_y y} e^{-jk_z z} dk_y dk_z \qquad (4\text{-}14)$$

where D is the domain of integration defined by the condition $k_y^2+k_z^2 \leq k^2$. This is the condition for only radiating waves to be included in the formulation.

The numerical implementation of the techniques described in this section will be presented in the next chapter.

4.3 Calculation of Antenna Focus from Aperture Phase Distributions

Reflector antennas are usually designed by the familiar ray tracing techniques of geometrical optics. The antenna feed is assumed to be a point source radiator, and the aperture field distribution is calculated by tracing rays from this source to the reflector surface and then into the aperture. At the reflector surface, Snell's first law is used to determine the direction of the reflected rays. By tracing rays to each point in the aperture, the aperture phase distribution can be calculated as the phase delay experienced by each ray as it propagates from the feed to the aperture.

Parabolic reflector antennas are normally designed so that the aperture phase distribution is a constant. This is the condition that the reflector be focused for optimum gain in the far-field or at infinity. If the feed is not properly positioned, the antenna focus will be degraded, and the gain will decrease. In addition, the direction in which the antenna is focused can change. Therefore, correct focus is an operational consideration for reflector antenna installations.

This section is devoted to the problem of determining the feed position of a parabolic reflector antenna if its aperture phase distribution is known. Thus this is the inverse of the design problem in which the aperture phase distribution is to be determined from the feed position. The technique is general in that it can be applied to any reflector geometry if the correct aperture phase distribution is known for that geometry. However, the specific derivations in this section will be for the parabolic reflector focused at infinity. The technique is based on a method described

by Kelleher [14] for calculating the phase distribution over the aperture of a reflector antenna.

Let the phase distribution over an aperture located in the plane defined by the relation $x = 0$ be denoted by $\psi(y,z)$. If the reflector which illuminates the aperture is illuminated by a feed which can be considered to be a point source, then Keheller has shown that the phase distribution function over the aperture is given approximately by

$$\psi(y,z) = \hat{kx} \cdot (\vec{U}(y,z) - \vec{V}(y,z)) \tag{4-15}$$

where $k = 2\pi/\lambda$ is the free-space wavenumber, $\vec{U}(y,z)$ is the vector equation of the image wavefront of the point source feed behind the reflector, and $\vec{V}(y,z)$ is the vector equation of some reference equiphase plane.

To obtain the function $\vec{U}(y,z)$, consider the geometry shown in Figure 6. Let $\vec{R}(y,z)$ be the vector equation describing the reflector surface and $\hat{n}(y,z)$ the vector unit normal to the reflector. For a point source feed located at the point Q in the figure, the ray reflected from the reflector at P appears to originate from behind the reflector at Q'. The vector from the origin to this image source can be written

$$\vec{U} = \overrightarrow{OQ} + \overrightarrow{QQ'}$$

$$= \overrightarrow{OQ} + \hat{n}\left[\hat{n} \cdot (\vec{R} - \overrightarrow{OQ}) + \hat{n} \cdot \overrightarrow{PQ'}\right] \tag{4-16}$$

Because the angle of incidence at P must equal the angle of reflection, it follows that

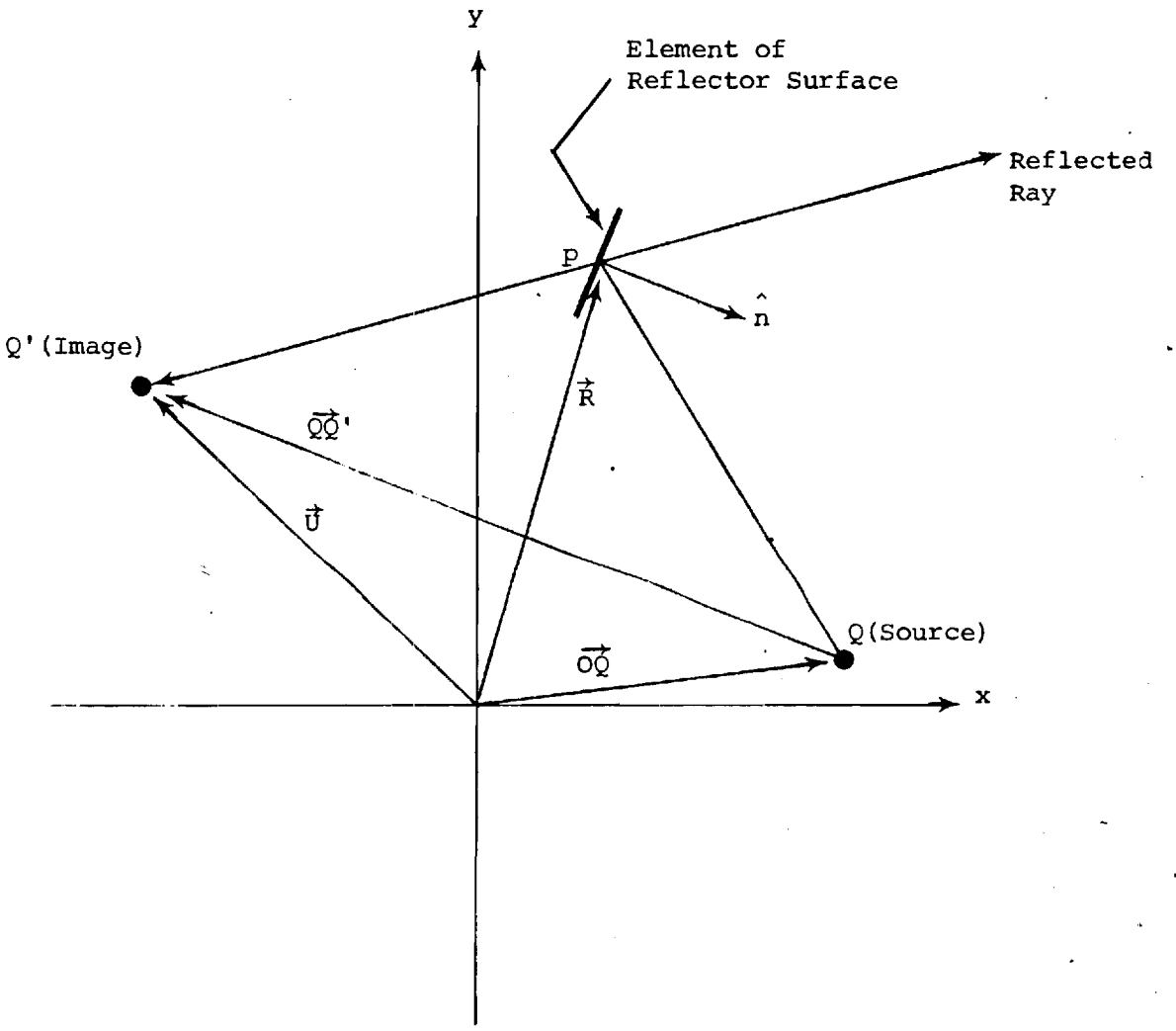

Figure 6. Geometry for the Derivation of the Image Wavefront Equation.

$$\hat{n}\cdot\overrightarrow{PQ'} = \hat{n}\cdot(\vec{R}-\overrightarrow{OQ}) \tag{4-17}$$

Therefore, Equation (4-16) simplifies to

$$\vec{U} = \overrightarrow{OQ} + 2\hat{n}\left[\hat{n}\cdot(\vec{R}-\overrightarrow{OQ})\right] \tag{4-18}$$

The equation for a parabolic reflector with vertex cutting the x axis at the point $x = x_o$ is

$$f(x,y,z) = 4p(x-x_o) - y^2 - z^2 = 0 \tag{4-19}$$

where p is the focal length of the reflector. Thus it follows that $\vec{R}$ and $\hat{n}$ for the parabolic reflector are given by

$$\vec{R} = \hat{x}\left(\frac{4px_o+y^2+z^2}{4p}\right) + \hat{y}\,y + \hat{z}\,z \tag{4-20}$$

$$\hat{n} = \frac{\nabla f}{|\nabla f|}$$

$$= \frac{\hat{x}2p - \hat{y}\,y - \hat{z}\,z}{\sqrt{4p^2 + y^2 + z^2}} \tag{4-21}$$

For a focused reflector, the feed is located at the point $x = x_o + p$ and $y = z = 0$. Let the feed be defocused from this point by an amount a in the x direction, b in the y direction, and c in the z direction. The vector $\overrightarrow{OQ}$ for the defocused reflector is

$$\vec{OQ} = \hat{x}(a + x_o + p) + \hat{y}b + \hat{z}c \tag{4-22}$$

Substitution of these into the equation for $\vec{U}$ yields

$$\vec{U} = \hat{x}(a+x_o+p(1-2B)) + \hat{y}(b+bB) + \hat{z}(c+Bz) \tag{4-23}$$

where

$$B = 1 + 2\frac{2pa - yb - zc}{4p^2 + y^2 + z^2} \tag{4-24}$$

It is convenient to choose the reference plane $\vec{V}(y,z)$ so that $\psi(y,z) = 0$ where $a = b = c = 0$. This will be true if $\vec{V} = \hat{x}(x_o-p)$. Thus Equation (4-15) becomes

$$\psi(y,z) = k[a + 2p(1-B)]$$

$$= k\left[a - 4p\frac{2pa - yb - zc}{4p^2 + y^2 + z^2}\right] \tag{4-25}$$

This is the desired relation. It gives the aperture phase as a function of aperture coordinates and the position of the reflector feed. It is valid for defocus distances which are small compared to the dimensions of the reflector. It is the subject of the balance of this section to determine a, b, and c given the measured distribution for $\psi(y,z)$.

Let the function $\psi(y,z)$ be specified at a discrete set of points in the reflector aperture denoted by (y_i,z_j), where $1 \le i \le M$ and $1 \le j \le N$, and M and N are positive integers. If ψ is known exactly (i.e., with no

measurement error), it follows that Equation (4-25) can be solved for a, b, and c from the known values of ψ at only three points. However, in the presence of measurement error, a statistical approach for obtaining a, b, and c will yield the least uncertainty or error. The method which will be described in the following is based on the minimum mean squared error criterior of statistical estimation theory.

It is convenient to rewrite Equation (4-25) in the form

$$\alpha_{ij}\, a + \beta_{ij}\, b + \gamma_{ij}\, c = \psi_{ij} \tag{4-26}$$

where

$$\alpha_{ij} = k\left[1 - \frac{8p^2}{4p^2 + y_i^2 + z_j^2}\right] \tag{4-27}$$

$$\beta_{ij} = k\,\frac{4py_i}{4p^2 + y_i^2 + z_j^2} \tag{4-28}$$

$$\gamma_{ij} = k\,\frac{4pz_j}{4p^2 + y_i^2 + z_j^2} \tag{4-29}$$

$$\psi_{ij} = (y_i, z_j) \tag{4-30}$$

Let $\overline{\psi}_{ij}$ represent the <u>measured</u> value of the phase at the point (y_i, z_j) in the presence of noise. The square of the rms error between the measured and calculated values of ψ can then be written

$$\varepsilon^2 = \sum_i \sum_j (\psi_{ij} - \bar{\psi}_{ij})^2$$

$$= \sum_i \sum_j (\alpha_{ij}a + \beta_{ij}b + \gamma_{ij}c - \bar{\psi}_{ij})^2 \qquad (4\text{-}31)$$

This equation represents the sum of the squared errors at each measurement point in the aperture. Because each term in the sum is positive, it follows that the minimum value of ε^2 is zero and that the only way this can be achieved is to have zero error between $\bar{\psi}_{ij}$ and ψ_{ij} at every point in the aperture.

For a measured phase distribution $\bar{\psi}_{ij}$, it is desired to find the values of a, b, and c which minimize ε^2 in Equation (4-31). This solution represents the best estimate of the reflector feed coordinates in the minimum mean squared error sense. The solution is obtained by setting equal to zero the partial derivatives of ε^2 with respect to each of the parameters a, b, and c. The three simultaneous equations which are obtained can then be solved for a, b, and c. These equations are

$$\frac{\partial \varepsilon^2}{\partial a} = a \sum_i \sum_j 2\alpha_{ij}^2 + b \sum_i \sum_j 2\alpha_{ij}\beta_{ij}$$

$$+ c \sum_i \sum_j 2\alpha_{ij}\gamma_{ij} - \sum_i \sum_j 2\alpha_{ij}\bar{\psi}_{ij}$$

$$= 0 \qquad (4\text{-}32)$$

$$\frac{\partial \varepsilon^2}{\partial b} = a \sum_i \sum_j 2\alpha_{ij}\beta_{ij} + b \sum_i \sum_j 2\beta_{ij}^2$$

$$+ c \sum_i \sum_j 2\beta_{ij}\gamma_{ij} - \sum_i \sum_j 2\beta_{ij}\bar{\psi}_{ij}$$

$$= 0 \qquad (4\text{-}33)$$

$$\frac{\partial \varepsilon^2}{\partial c} = a \sum_i \sum_j 2\alpha_{ij}\gamma_{ij} + b \sum_i \sum_j 2\beta_{ij}\gamma_{ij}$$

$$+ c \sum_i \sum_j 2\gamma_{ij}^2 - \sum_i \sum_j 2\gamma_{ij}\bar{\psi}_{ij}$$

$$= 0 \qquad (4\text{-}34)$$

For convenience of notation, these three equations will be written in the form

$$A_1 a + B_1 b + C_1 c = D_1 \qquad (4\text{-}35)$$

$$A_2 a + B_2 b + C_2 c = D_2 \qquad (4\text{-}36)$$

$$A_3 a + B_3 b + C_3 c = D_3 \qquad (4\text{-}37)$$

where the coefficients of a, b, and c are defined in Equations (4-32) through (4-34). Simultaneous solution for the defocused feed coordinates yields

$$a = \frac{1}{\Delta}\left[D_1(B_2C_3 - B_3C_2)\right.$$

$$\left. + D_2(B_3C_1 - B_1C_3) + D_3(B_1C_2 - B_2C_1)\right] \tag{4-38}$$

$$b = \frac{1}{\Delta}\left[D_1(A_3C_2 - A_2C_3)\right.$$

$$\left. + D_2(A_1C_3 - A_3C_1) + D_3(A_1C_2 - A_2C_1)\right] \tag{4-39}$$

$$c = \frac{1}{\Delta}\left[D_1([_2C_3 - A_3C_2)\right.$$

$$\left. + D_2(A_3C_1 - A_1C_3) + D_3(A_1B_2 - A_2B_1)\right] \tag{4-40}$$

when Δ is the determinant of the system of equations which is given by

$$\Delta = A_1(B_2C_3 - B_3C_2) + A_2(B_3C_1 - B_1C_3)$$

$$+ A_3(B_1C_2 - B_2C_1) \tag{4-41}$$

In the following chapter, a computer solution for a, b, and c is described that is based on these equations. The solution uses simulated phase data that is obtained by calculating the phase function for a defocused aperture from Equation (4-25) and adding random noise to the data to simulate measurement noise.

CHAPTER V

NUMERICAL CONSIDERATIONS

5.1 Introduction

The application of near-field measurement techniques can require detailed and tedious numerical methods. This chapter is devoted to a discussion of the major numerical considerations that are involved in the application of cylindrical wave techniques to near-field measurements. In order to correct for the probe response, it is necessary to know the cylindrical wave amplitudes for the field radiated by the probe when used as a transmitter. The following section describes how these can be obtained from the measured probe far-field. Next, the techniques for calculating antenna far fields from near fields on a cylinder are discussed. Finally, a numerical solution is presented for calculating the feed position of a parabolic reflector antenna from the near field on a cylinder around the antenna. In each case, numerical examples are presented which have been performed with simulated near field data. The computer programs which have been used in the examples are presented in the appendix.

5.2 Determination of the Probe Correction Coefficients

To evaluate Equations (3-23) and (3-24) for the amplitude functions in the cylindrical wave expansion of the far field radiated by the test antenna, it is necessary to know the amplitude functions in the expansion

of the field radiated by the probe. Because it is necessary to know these functions only for wavenumbers such that $|h| \leq k$, it is possible to obtain them from a knowledge of the far field radiated by the probe when it is connected to a signal source. In this section, a numerical procedure is described for obtaining the necessary probe information from the measured far field of the probe.

To calibrate the probe, it is first necessary to measure both polarization components of its far field when it is used as a transmitter over the surface of a sphere with the probe at the center. It is preferable, but not necessary, for the phase center of the probe to be located at the center of this sphere. If this is true, the number of cylindrical wave harmonics that are necessary to represent the field radiated by the probe will be a minimum. In any subsequent near-field measurements with the probe, the radius of the measurement cylinder is taken to be cylindrical radius out to that point on the probe which was aligned with the center of the sphere when the probe far field was measured. The measurement of the probe far field is most conveniently performed with a gantry positioner such as that shown in Figure 7. In this figure, rotation in the elevation angle θ is provided by the gantry while rotation in the azimuth angle ϕ is provided by the base positioner.

Because it is necessary to resolve the measured probe data into Fourier series in the azimuth angle ϕ, some upper limit on the maximum angular harmonic for the probe must be established. This can be done by using the criterion established by Harrington [8] that the maximum angular harmonic is $N = ka$, where in this case a is the radius of the smallest sphere completely enclosing the probe or its aperture. As an

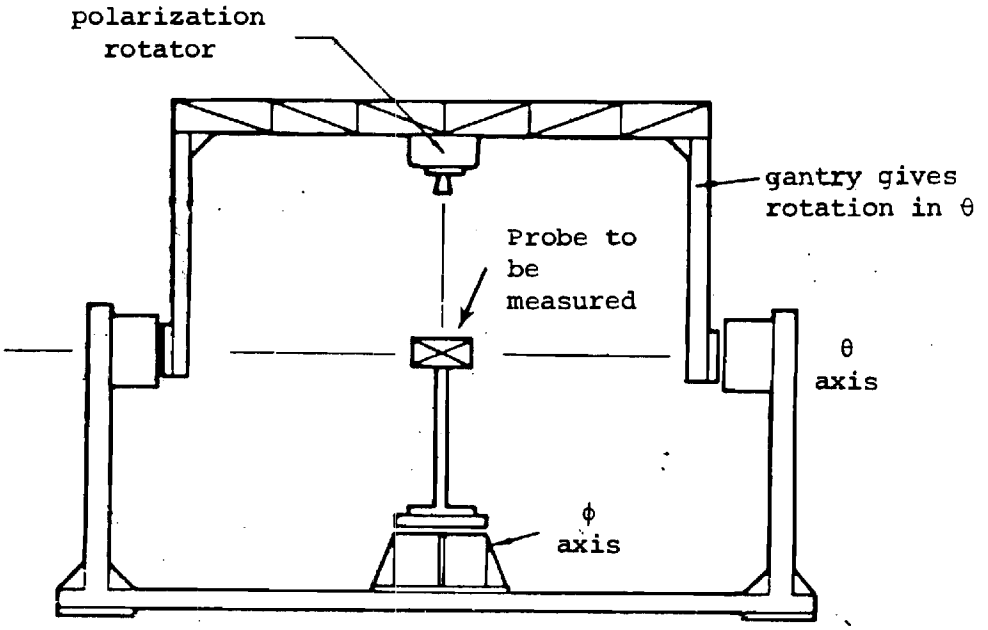

Figure 7. Gantry Positioner for Measuring the Probe Far Field.

example, the aperture of an open-ended WR-90 waveguide can be enclosed by a sphere of radius 1.4 cm. At an operating frequency of 9.375 GHz, it follows that $N \geq (2 \times \pi \times 9.375 \times 10^9/3 \times 10^{10}) \times 1.4 = 2.75$. Thus the choice $N = 3$ would be made for this probe.

Let the probe antenna coordinates be defined as shown in Figure 8. The far-field electric field intensity radiated by the probe can be expressed as

$$E_\theta(\theta,\phi) = j\sin\theta \sum_{n=-N}^{N} j^n d_n(k\cos\theta) e^{jn\phi} \tag{5-1}$$

$$E_\phi(\theta,\phi) = \sin\theta \sum_{n=-N}^{N} j^n c_n(k\cos\theta) e^{jn\phi} \tag{5-2}$$

where $c_n(h)$ and $d_n(h)$, with $h = k\cos\theta$, are the amplitude functions for the cylindrical wave vectors $\vec{M}$ and $\vec{N}$, respectively, in the expansion of the field radiated by the probe. If the probe is rotated 90° in the right-hand sense about the x-axis, the far-field electric field intensity radiated by the rotated probe can be expressed as

$$E'_\theta(\theta,\phi) = j\sin\theta \sum_{n=-N}^{N} j^n d'_n(k\cos\theta) e^{jn\phi} \tag{5-3}$$

$$E'_\phi(\theta,\phi) = \sin\theta \sum_{n=-N}^{N} j^n c'_n(k\cos\theta) e^{jn\phi} \tag{5-4}$$

where $c'_n(h)$ and $d'_n(h)$ are defined similarly. In order to correct for the effects of the probe in calculating the cylindrical wave amplitude functions for the test antenna, it is necessary to know $c_n(h)$, $d_n(h)$, $c'_n(h)$, and $d'_n(h)$ with the argument $h = -k\cos\theta = k\cos(\pi-\theta)$, where θ is the

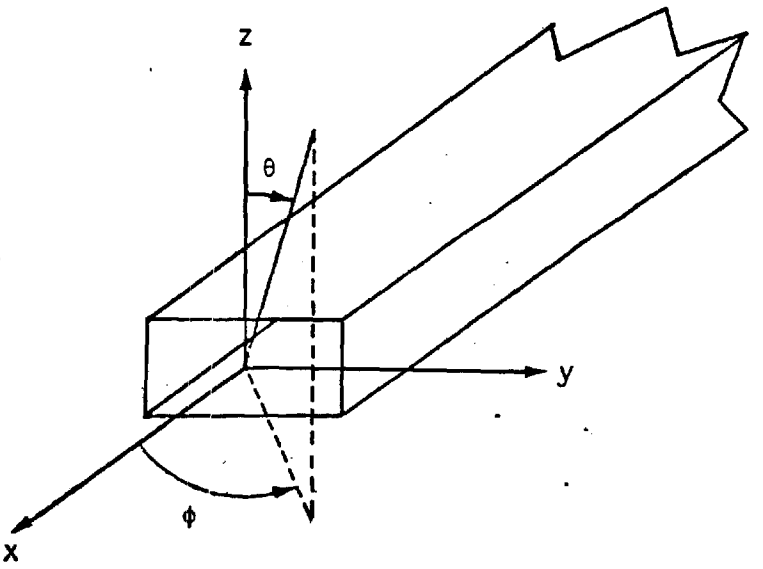

Figure 8. Coordinate System Definitions for the Measuring Probe.

elevation angle for the far field of the test antenna. That is, the elevation angle for the probe is in the direction opposite from that of the test antenna.

Because Equations (5-1) through (5-4) are in the form of a Fourier series in ϕ, the amplitude functions for a particular value of θ can be obtained by numerically evaluating the Fourier inversion integral from the measured fields. For example, the solution for $d_n(k\cos\theta)$ is

$$d_n(k\cos\theta) = \frac{1}{2\pi j^{n+1}\sin\theta} \int_{-\pi}^{\pi} E_\theta(\theta,\phi) e^{-jn\phi} d\phi \qquad (5\text{-}5)$$

This equation requires knowledge of the probe pattern over a full 360° azimuth angle. However, in use, the probe is always pointed to the center of the cylinder. Thus, a better fit of the fields over the front hemisphere of the probe can be obtained if only this portion of its field is used to evaluate $d_n(k\cos\theta)$.

Let the probe fields be specified over the azimuth interval defined by $-\phi_1 \le \phi \le \phi_1$. It is straightforward to show that Equation (5-1) approximates the measured $E_\theta(\theta,\phi)$ over this interval with a minimum mean square error if the $d_n(k\cos\theta)$ satisfy the system of 2N+1 equations

$$\sum_{n=-N}^{N} d_n(k\cos\theta) \frac{\sin(m-n)\phi_1}{(m-n)\phi_1} = \frac{1}{2j^{m+1}\sin\theta} \int_{-\phi_1}^{\phi_1} E_\theta(\theta,\phi) e^{-jm\phi} d\phi \qquad (5\text{-}6)$$

where the integer m is varied from -N to +N to generate the 2N+1 equations. The $d_n(k\cos\theta)$ for the probe can be obtained by solving this system of

equations with a technique such as the Gauss-Jordan method for solving simultaneous equations. The integral on the right of Equation (5-6) is most conveniently evaluated from measured data by the trapezoidal rule for numerical integration [15].

Solutions for $c_n(k\cos\theta)$, $d_n'(k\cos\theta)$, and $c_n'(k\cos\theta)$ can be obtained for the probe in the same way. However, for the case of the rotated probe functions, it is possible to solve for $E_\theta'(\theta,\phi)$ and $E_\phi'(\theta,\phi)$ from the measured $E_\theta(\theta,\phi)$ and $E_\phi(\theta,\phi)$, thus making it unnecessary to perform measurements on the far field of the rotated probe. The necessary transformations are

$$E_\theta'(\theta,\phi) = \frac{E_\theta(\xi,\zeta)\cos\theta\ \sin\phi - E_\phi(\xi,\zeta)\cos\phi}{\sqrt{1 - \sin^2\theta\sin^2\phi}} \tag{5-7}$$

$$E_\phi'(\theta,\phi) = \frac{E_\theta(\xi,\zeta)\cos\theta + E_\phi(\xi,\zeta)\cos\theta\ \sin\phi}{\sqrt{1 - \sin^2\theta\ \sin^2\phi}} \tag{5-8}$$

where

$$\tan\xi = \frac{\sqrt{1 - \sin^2\theta\ \sin^2\phi}}{-\sin\theta\ \sin\phi} \tag{5-9}$$

$$\tan\zeta = \frac{\cos\theta}{\sin\theta\ \cos\phi} \tag{5-10}$$

In using these equations, $E_\theta(\xi,\zeta)$ and $E_\phi(\xi,\zeta)$ can be obtained by numerical interpolation between the measured values.

The amplitude functions for the probe enter into the solutions for $a_n(h)$ and $b_n(h)$ given by Equations (3-23) and (3-24) in the form of summations over the angular harmonics of the probe. The coefficients in the summations are the Hankel functions $H^{(2)}_{n+m}(\Lambda r_o)$ where $\Lambda = \sqrt{k^2-h^2}$ and m is the angular harmonic of the probe. In the calculation of the cylindrical wave functions for the test antenna, it is necessary to evaluate $a_n(h)$ and $b_n(h)$ at $h = k\cos\theta$. Thus the argument of the Hankel function is $\Lambda r_o = kr_o\sin\theta$.

5.3 Method of Far-Field Pattern Calculation

In Section 2.4, it was shown that the far-field electric field intensity over the surface of a sphere surrounding an antenna can be written in the form

$$E_\theta(\theta,\phi) = j\sin\theta \sum_{n=-\infty}^{\infty} j^n b_n(k\cos\theta) e^{jn\phi} \tag{5-11}$$

$$E_\phi(\theta,\phi) = \sin\theta \sum_{n=-\infty}^{\infty} j^n a_n(k\cos\theta) e^{jn\phi} \tag{5-12}$$

These equations are in the form of a Fourier series summation in the azimuth angle ϕ where the Fourier coefficients are functions of the elevation angle θ. A mathematical solution for $a_n(h)$ and $b_n(h)$, where $h = k\cos\theta$, has been presented in Equations (3-23) and (3-24) as a function of the measured response of a probe antenna when the probe is used to measure the near fields of the antenna over some cylinder enclosing it. The numerical implementation of this solution to obtain the far field summations of Equations (5-11) and (5-12) is given in this section.

The numerical solution can be broken down into the flow diagram given in Figure 9. The calculations in that part of the diagram concerned with evaluating the cylindrical wave functions for the field radiated by the probe when it is used as a transmitter have been described in the preceding section and will not be covered here. The basic numerical tool in the calculations is the fast Fourier transform (FFT) algorithm which is used to evaluate the Fourier integrals and perform the Fourier series summations.

Aside from the factors involving the cylindrical wave amplitude functions of the probe when it is used as a transmitter, it was shown in Section 3.3 that the solution for $a_n(h)$ and $b_n(h)$ requires the evaluation of the integrals

$$I_n(h) = \int_{-\infty}^{\infty} \int_{-\pi}^{\pi} v(r_o,\phi_o,z_o) e^{-jn\phi_o} e^{jhz_o} d_o dz_o \qquad (5\text{-}13)$$

$$I_n'(h) = \int_{-\infty}^{\infty} \int_{-\pi}^{\pi} v'(r_o,\phi_o,z_o) e^{-jn\phi_o} e^{jhz_o} d\phi_o dz_o \qquad (5\text{-}14)$$

where $v(r_o,\phi_o,z_o)$ and $v'(r_o,\phi_o,z_o)$ represent the output voltage of the probe on the measurement cylinder of radius r_o. The primed function is used to denote the probe output after it is rotated 90^o about its longitudinal axis.

Let the measurement cylinder be divided into a lattite of points with coordinates $(r_o, n\Delta\phi, m\Delta z)$ where $0 \le n \le N-1$, $0 \le m \le M-1$, and M and N are positive integers. To exactly evaluate Equations (5-13) and (5-14) from the output voltages of the probe at these points, two conditions must be satisfied. First, v and v' must be zero when $z < 0$ or $z > (M-1)\Delta z$.

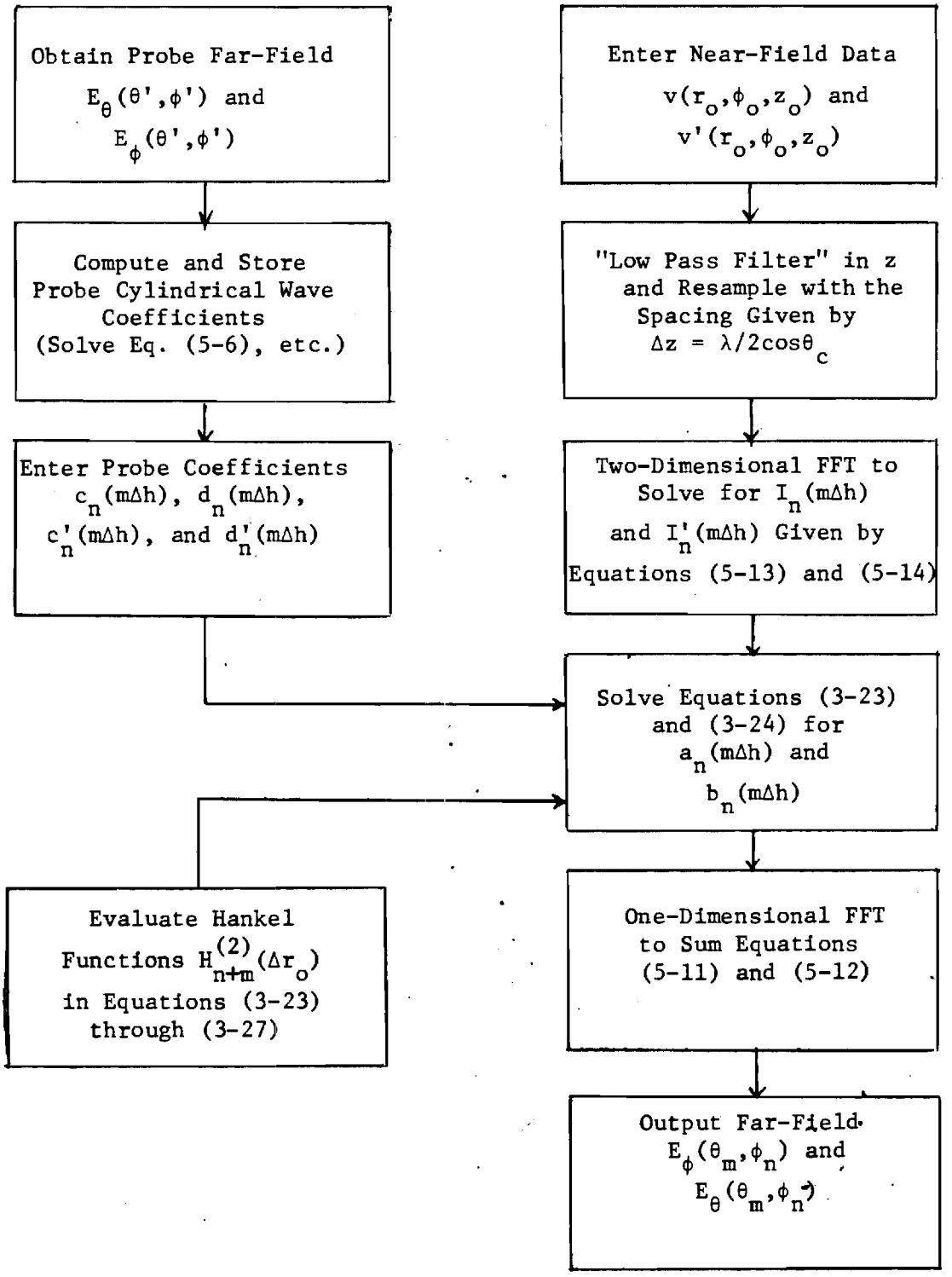

Figure 9. Flow-Diagram for the Far Field Evaluation.

Second, v and v' must have no angular harmonic n greater than $\pi/\Delta\phi$ and must be wavenumber limited in h to a maximum wavenumber less than or equal to $\pi/\Delta z$. The first condition cannot be met with any radiating structure. However, if the test antenna is aligned in the cylinder so that it does not radiate appreciably in the $\pm z$ direction, it can be met approximately if M is chosen large enough. The second condition can be met if the test antenna is not a high-Q structure and the sample intervals $\Delta\phi$ and Δz are chosen in accordance with the sampling criteria discussed in Section 3.5. If these conditions are met, the integrals for $I_n(h)$ and $I_n'(h)$ can be evaluated most efficiently with a two-dimensional Fast Fourier Transform (or FFT) algorithm [16].

The FFT is an algorithm in which the computations are performed "in place," i.e., the two-dimensional input data arrays $v(r_o, n\Delta\phi, m\Delta z)$ and $v'(r_o, n\Delta\phi, m\Delta z)$ are replaced by the output arrays $I_n(m\Delta h)$ and $I_n'(m\Delta h)$ after the calculations are completed. As described by Cochran [16] the output values of the integers m and n are

$$-\frac{M}{2} \le m \le \frac{M}{2} - 1 \qquad (5\text{-}15)$$

$$-\frac{N}{2} \le n \le \frac{N}{2} - 1 \qquad (5\text{-}16)$$

and Δh is given by

$$\Delta h = \frac{2\pi}{M\Delta z} \qquad (5\text{-}17)$$

Because the far-field expressions for $E_\theta(\theta,\phi)$ and $E_\phi(\theta,\phi)$ are evaluated for $h = k\cos\theta$, the values of θ corresponding to $h = m\Delta h$ are given by

$$\theta_m = \cos^{-1}\left(\frac{m\lambda}{M\Delta z}\right) \tag{5-18}$$

Because it is impossible to measure the near field over a complete cylinder enclosing an antenna, the present method for determining the cylindrical wave functions for the test antenna is most suitable when applied to antennas which radiate predominantly in the angular region about $\theta = \frac{\pi}{2}$ defined by $\theta_c < \theta \leq \pi - \theta_c$. In order for all θ_m defined by Equation (5-18) to lie in this interval, it follows that Δz must satisfy

$$\Delta z = \frac{\lambda}{2\cos\theta_c} \tag{5-19}$$

However, for $\theta_c \neq 0$, this condition violates the z-sample spacing criterion discussed in Section 3.5. One solution to this problem is to choose z smaller than that specified by Equation (5-19) and to ignore the calculations for $\theta \leq \theta_c$ and $\theta > \pi - \theta_c$. This is not a very efficient solution because it reduces the resolution of the calculated fields for $\theta_c < \theta \leq \pi - \theta_c$. The decrease in resolution can be overcome by augmenting the near-field data arrays with zeros thereby increasing M. Although this is an acceptable solution, it is inefficient for it increases computer storage requirements, increases computation time, and does not make full use of the FFT computations.

An alternate solution to the above problem is to first "smooth" or "low-pass filter" the near-field data in such a way that it can be resampled by numerical interpolation with the sample spacing specified by Equation (5-19). The "smoothing" operation can be accomplished efficiently with the FFT algorithm. First, the near-field data arrays

are transformed in z so that on output the wavenumber spacing is that specified by Equation (5-17). Second, all elements in the transformed arrays are set equal to zero for all m such that

$$|m| > \frac{M\Delta z}{\lambda} \cos\theta_c \tag{5-20}$$

Finally, the data arrays are inverse transformed to create the "smoothed" arrays. This operation is equivalent to that of filtering the data with an ideal "low-pass filter" with a cutoff wavenumber given by

$$h_c = \frac{2\pi}{\lambda} \cos\theta_c \tag{5-21}$$

After the "smoothing" operation, the near-field data arrays are wavenumber limited in z such that the Nyquist sample spacing is that given by Equation (5-19). Thus the arrays can be resampled in z using numerical interpolation with the sample spacing specified by Equation (5-19). In order to preserve "in place" calculations, the interpolated arrays can directly replace the original arrays during the computations. Because the interpolation process will extract fewer than M samples in z, it is necessary to set equal to zero some of the elements of the original arrays after the interpolation. It can be shown that these zeroes will not affect the accuracy of the subsequent FFT operations. Instead, the resolution will be improved on output since all M values of θ_m will lie in the interval $\theta_c < \theta \leq \pi - \theta_c$.

After the evaluation of $I_n(m\Delta h)$ and $I_n'(m\Delta h)$, the cylindrical wave amplitude functions $a_n(m\Delta h)$ and $b_n(m\Delta h)$ can be solved for using Equations

(3-23) and (3-24). The evaluation of the coefficients in these equations which are determined by the probe was discussed in the preceding section. Because $a_n(m\Delta h)$ and $b_n(m\Delta h)$ are both linear combinations of $I_n(m\Delta h)$ and $I_n'(m\Delta h)$, the computations can again be performed "in place." Thus on output, the original data arrays will contain the set of cylindrical wave amplitude functions from which the far field of the test antenna can be evaluated.

The calculation of the far-field electric field intensity radiated by the test antenna can be achieved by performing the summations indicated by Equations (5-1) and (5-2). Again, this can be done most efficiently with the FFT algorithm. However, each $a_n(m\Delta h)$ and $b_n(m\Delta h)$ must be multiplied by the factors $j^n \sin\theta_m$ and $j^{n+1}\sin\theta_m$, respectively, before the FFT can be used to perform the summations. Because the calculations are performed "in place" the output arrays will be the far-field components $E_\theta(\theta_m,\phi_n)$ and $E_\phi(\theta_m,\phi_n)$ where

$$\phi_n = \frac{2n\pi}{N}, \qquad 0 \le n \le N-1 \tag{5-22}$$

$$\theta_m = \cos^{-1}\left[\frac{m\cos\theta_c}{(M/2)}\right], \quad -\frac{M}{2} \le m \le \frac{M}{2} - 1 \tag{5-23}$$

The complete calculations are summarized in the flow-diagram of Figure 9.

The computer program listed in Appendix E has been written to perform far-field calculations from the near field on a cylinder. The program implements the solution for $a_n(h)$ and $b_n(h)$ given in Equations (2-48) and (2-49). It is easily modified to implement the probe correction theory with the change of only two subroutines. These subroutines

are KOREK and KOEF. An example run of this program will be described in the following which illustrates the program operation. The example calculations are for the far field radiated by a thin half wavelength circumferential slot on a cylinder with a wavenumber radius product of kr = 12. This calculation was first published by Bailin [17] in 1955. Because his calculations were not performed on the computer, he did not present a complete two-dimensional pattern but only selected cuts.

The first step in the program is to initialize all constants and form the near field data arrays. In this example, both the ϕ and z components of $\vec{E}$ on the cylinder are set up as 64 x 64 complex arrays labeled EPHI (64,64) and EZ (64,64), KR = 12 is the cylinder wavenumber radius product, NR is an integer input to the plot routines which is 4 greater than the array dimension 64, NIB is the dimension of the plotter buffer IBUF, and DBM is the maximum number of decibels below 0 dB for which the plots are made. DZ is the specified z sample spacing on the cylinder which is calculated as $\Delta z/\lambda$ from Equation (5-19) with $\theta_c = 30^o$. No z filtering was used in this example because the slot on the cylinder represents an impulse field along the z direction and the sample spacing off the slot is meaningless.

The program first sets $E_\phi = E_z = 0$ on the cylinder. Next, it computes E_z over the slot according to the formula

$$E_z = \cos(\pi\phi/2\phi_o) \qquad (5\text{-}24)$$

where $2\phi_o = 15^o$ which makes the slot width one-half a wavelength for kr = 12. The FFT operations in the program require careful choice of the origin in

the data arrays. The top half of the arrays are the near fields on the bottom of the cylinder, and vice versa. That is, the data is folded in the z direction. This is accomplished by forming the slot field in the first row of the EZ array. The first row in the arrays corresponds to the center of the cylinder.

The program first performs a two-dimensional Fourier transform to evaluate Equations (5-13) and (5-14). Because the E_ϕ array contains all zeroes, the initial FFT operation on it has been ommitted. The first FFT call forward transforms the E_z array by the rows, i.e., in the ϕ coordinate. The second FFT call reverse transforms the E_z array by the columns, i.e., in the z coordinate. After the two FFT operations the first M/2 rows contain the transform values for $0 \leq h \leq h_c$, the last M/2 rows contain the transform values for $-h_c \leq h \leq 0$, where h_c is defined by Equation (5-21). The first N/2 columns contain the transform values for $0 \leq n \leq N/2-1$, the last N/2 columns contain the transform values for $-N/2 \leq n \leq -1$.

Next the program evaluates $a_n(h)$ and $b_n(h)$ according to the solutions given by Equation (2-48) and (2-49). This is performed by subroutines KOREK which calls on subroutine KOEF to form the coefficients of I_ϕ and I_z in these equations. These coefficients involve Hankel functions which are evaluated by subroutine HANKEL.

After $a_n(h)$ and $b_n(h)$ are evaluated by subroutine KOREK, the final step in the far-field calculation is to sum the azimuth Fourier series according to Equations (5-11) and (5-12). The factors $j^{n+1}\sin\theta$ and $j^n\sin\theta$ in these respective equations have been included in $a_n(h)$ and $b_n(h)$ computed by subroutine KOREK. The azimuth series are summed

by a final call to the FFT subroutine for both the E_ϕ and E_z arrays. The two FFT transforms are both inverse row transforms.

Before plotting, the output arrays are converted to decibels and folded in the z direction. The latter step is necessary in order for the 1 + M/2 row to correspond to a 90° elevation angle. Because the E_θ far field component (now contained in the E_z array) is the predominant polarization component, subroutine DB is called first for this array with the last input variable to the subroutine equal to +1. This normalizes the peak value of E_θ to 0 dB. The second call of DB for the E_ϕ far field component uses the last input variable equal to -1. This normalizes the peak value of E_ϕ relative to the peak value of E_θ. The final step in the program is to normalize both output arrays to the range from 0 to 1 by calls to subroutine BNORM and then to call the three-dimensional plotting subroutine PLT.

The example output patterns for the slotted cylinder are given in Figure 10. These patterns agree with the results published by Bailin for this particular example. Because θ_c was set equal to 30° in calculating $\Delta z/\lambda$ from Equation (5-19), the patterns in Figure 10 cover the elevation angles defined by $30^\circ \leq \theta < 150^\circ$. The azimuth angle range covers the complete range of $-180^\circ \leq \phi < 180^\circ$.

A subroutine has been written to perform the z coordinate filtering described for the far field flow diagram of Figure 9. This subroutine is listed in Appendix F. In this subroutine, the complex array P(M,N) is the input near field array, DELI is the z sample spacing to wavelength ratio $\Delta z/\lambda$ in the input data, and THETA is θ_c in Equation (5-23). The variable GAMMA is an angle greater than or equal to THETA which can be

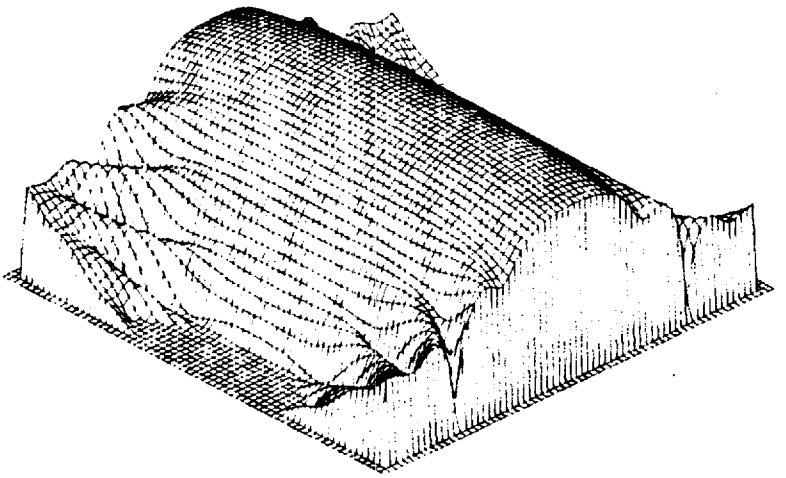

a) Elevation Component

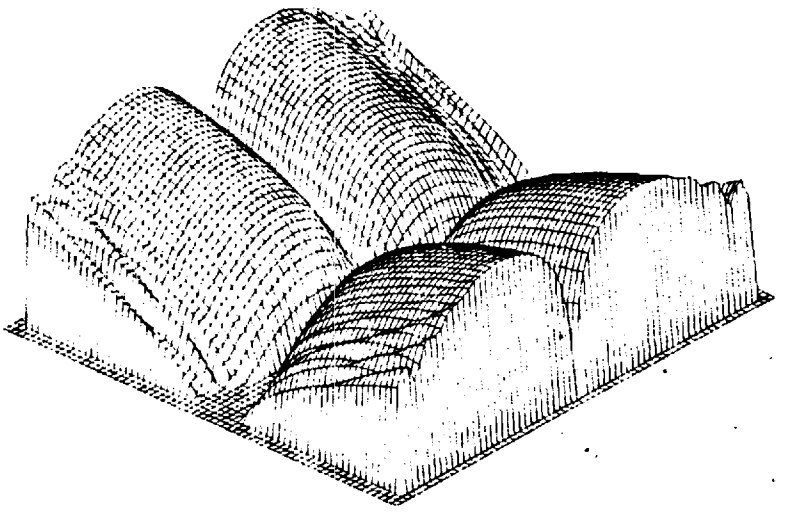

b) Azimuth Component

Figure 10. Far-Field Pattern Radiated by a Half-Wave Circumferential Slot on a Conducting Cylinder.

used to vary the cutoff frequency of the low-pass filter according to the equation $h_c = \frac{2\pi}{\lambda} \cos(\text{GAMMA})$. Normally, GAMMA would be set equal to THETA. However, as an example, if THETA = 45° and GAMMA = 60°, the elevation pattern would be calculated for $45^\circ \leq \theta \leq 135^\circ$ but would be equal to zero for $45^\circ \leq \theta \leq 60^\circ$ and $120^\circ \leq \theta \leq 135^\circ$. In this way, the far side-lobes in a pattern can be selectively deleted by varying GAMMA.

5.4 Method of Antenna Focus Calculation

The flow diagram for calculation of the feed position of a parabolic reflector antenna from near-field measurements on a cylinder is given in Figure 11. The flow diagram is identical to that for the far field pattern calculation of Figure 9 through the block for calculation of the cylindrical wave amplitude functions.

A computer program has been written to calculate the amplitude and phase of the tangential electric field over the plane defined by x = 0 from the near field on a cylinder enclosing the aperture. This program is listed in Appendix G. This program implements the flow diagram of Figure 11 through the block to output the aperture fields E_y and E_z. A separate program to calculate the feed coordinate positions a, b, and c has been written which will be described in the following.

The program listing in Appendix G includes an example of the use of the subroutines to calculate the electric fields over a uniformly illuminated rectangular aperture in the plane x = 0 from the near field on a cylinder around the aperture. In the example, the aperture was assumed to illuminate a 45° sector on the cylinder. The height of the aperture was 7 wavelengths. The fields on the cylinder were assumed

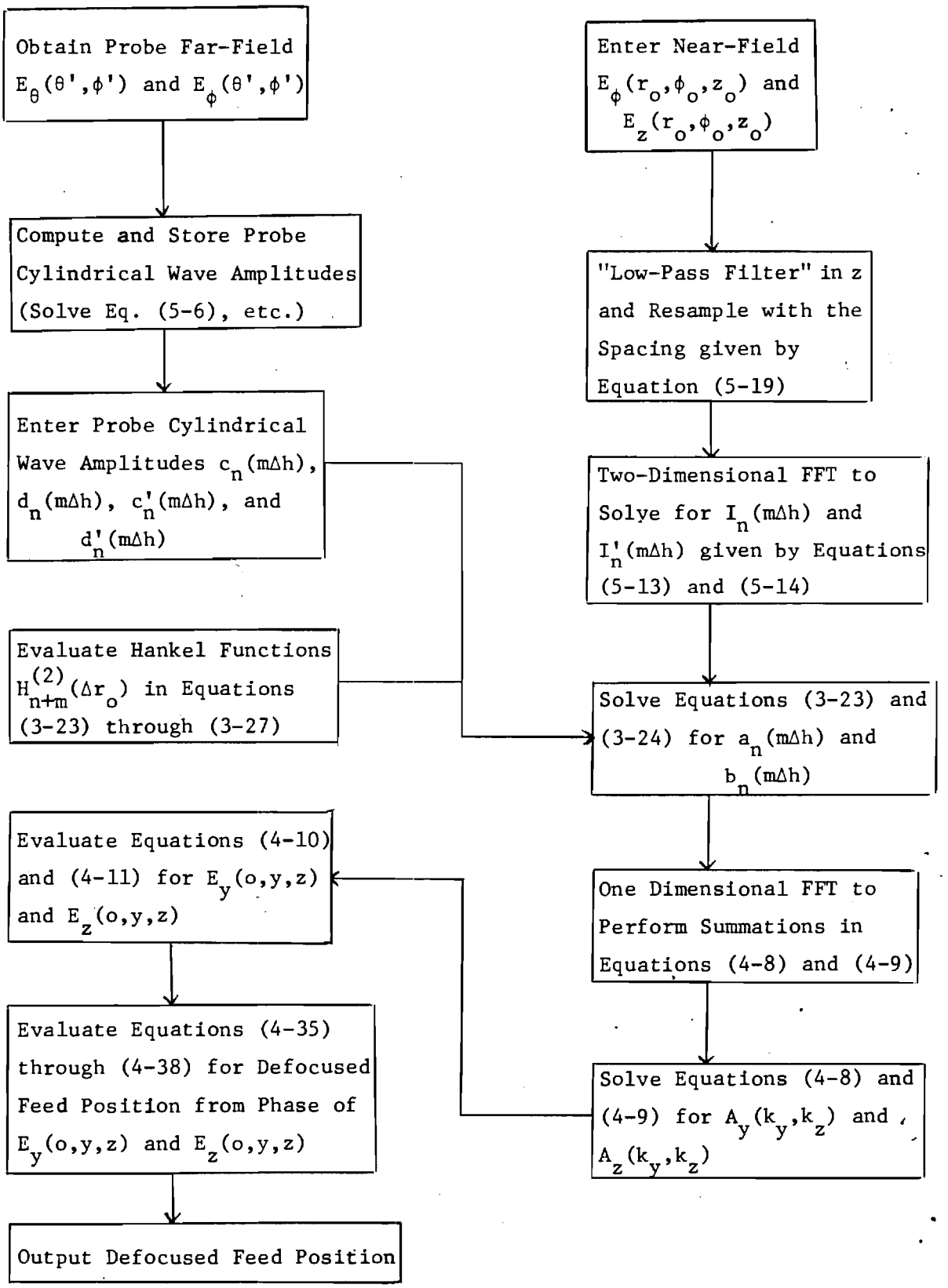

Figure 11. Flow-Diagram for the Feed Position Evaluation

to be those which would exist if geometrical optics were used to calculate the phase delay associated with ray propagation from the aperture to the cylinder. The amplitude distribution on the part of the cylinder illuminated by the aperture was assumed to be a constant.

In the program, the first step is to initialize all constants and form the near field arrays. In this example, the only non-zero field component on the cylinder is E_z. The distribution for E_z is computed as the phase delay from the aperture to the cylinder over that portion of the cylinder which is illuminated by the aperture. KR is the wavenumber radius product for the cylinder which is taken to be 12 in this example. DZ is the ratio of the z sample spacing to wavelength on the cylinder. It is taken to be 0.5. DZ2 is the ratio of the desired z sample spacing to the wavelength in the calculated aperture fields. It is taken to be 7/31 in this example in order for all computed samples to lie in the aperture. DY is the desired y-sample spacing to wavelength ratio in the aperture. It is taken to be the width of the aperture in wavelengths (i.e., $2 \times \sin(45^\circ/2) \times 2\pi/KR$) divided by the number of computed y intervals across the aperture (i.e., 32 - 1 = 31).

Through subroutine KOREK, the program operation is identical to that for the far-field calculation described in the preceding. After KOREK, the EPHI and EZ arrays, respectively, contain the values of the terms $j^n \sin\theta\ a_n(k\cos\theta)$ and $j^{n+1} \sin\theta\ b_n(k\cos\theta)$, respectively in Equations (4-11) and (4-12). The next step is to perform the azimuth series summations in these equations. The FFT could be used. However, it would do this for $-180^\circ \leq \phi < 180^\circ$, and it is desired that the values, of ϕ be those in front of the aperture only. Subroutine CWPW performs

these summations. It does this only for the values of θ and ϕ for which k_x is real in Equation (4-8).

After the two calls to subroutine CWPW, the EPHI and EZ arrays, respectively, contain the values of the right hand side of Equations (4-11) and (4-12), respectively. The next step is to solve these equations simultaneously for A_y and A_z. This is performed by subroutine SIMUL. After this subroutine, subroutine APERTY is used to perform the integration in k_y in Equations (4-13) and (4-14) while APERTZ is used to perform the integration in k_z. Although the FFT would be more efficient for this integration, it does not provide the capability of controlling the sample spacing in the aperture. the FOLDY and FOLDZ subroutines in the program are necessary in order for the center elements of the arrays EPHI and EZ to correspond to the center of the aperture.

The final operations in the program are to convert the aperture fields to amplitude in decibels and phase in degrees. This is accomplished by subroutine DB. Normalization for the plotting subroutine PLT is accomplished by subroutines BNORM and PNORM.

Figure 12 shows the output of the aperture field program for the example discussed. Both the amplitude and phase are relatively constant over the aperture as would be expected for this example. However, no absolute interpretation can be made of the figure because the true aperture field for the assumed field on the cylinder is not known. The increase in the computed phase at the top of the aperture in this example has not been explained. It is felt that this row in the graph represents a scan that is off the aperture because of an oversight in the use of the computer programs. Examination of the amplitude function seems to

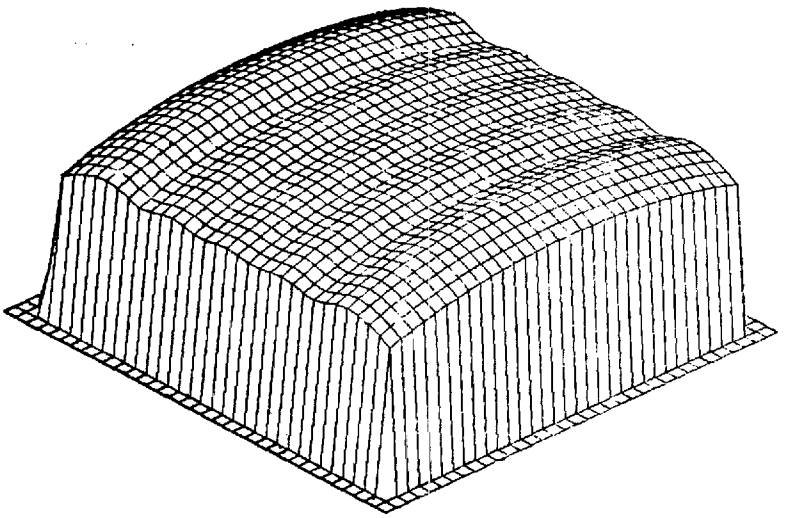

Amplitude

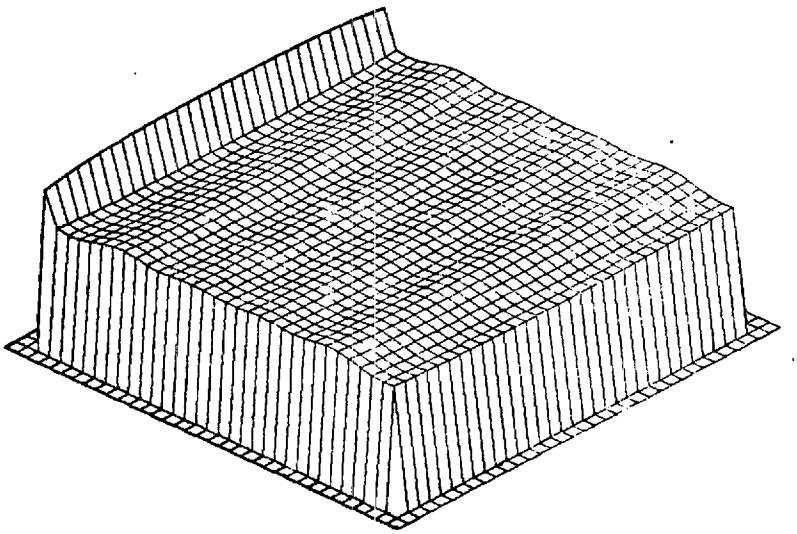

Phase

Figure 12. Amplitude and Phase of E_z in the Aperture for the Example Calculation.

bear this out, for the amplitude of the first row is very small compared to the second row. The program needs further "debugging" and should be run with measured data in order to effectively test it. Figure 12 does not display E_y in the aperture because it was so small (as was expected) that it could not be interpreted.

The far-field pattern radiated by the assumed near-field distribution on the cylinder has been computed with the program described in the preceding section. The elevation component, i.e., E_θ, of this pattern is shown in Figure 13. This pattern exhibits the expected form of that which would be radiated from a rectangular aperture. The azimuth component was so small that it has not been plotted.

A numerical test of the minimum mean-square error solution presented in Section 4.3 for the feed position coordinates of a parabolic reflector has been performed on the computer. For the test, a parabolic reflector with an aperture diameter of 20 wavelengths and a focal length to diameter ratio of 0.375 was assumed. The theoretical phase distribution over the aperture was calculated from Equation (4-25) for four cases. These were as follows: a feed defocus of $\frac{\lambda}{8}$ in the +x direction, a feed defocus of $\frac{\lambda}{8}$ in only the +y direction, a feed defocus of $\frac{\lambda}{8}$ in only the +z direction, and a feed defocus of $\frac{\lambda}{8}$ in all three directions simultaneously. The calculated aperture phase functions for these four cases are displayed in Figures 14 through 17.

To test the minimum mean-square error solutions for the defocused feed position, the calculated phase distribution of Figure 17 was corrupted with random Gaussian noise in order to simulate a measured phase distribution in the presence of measurement noise. The noise was added

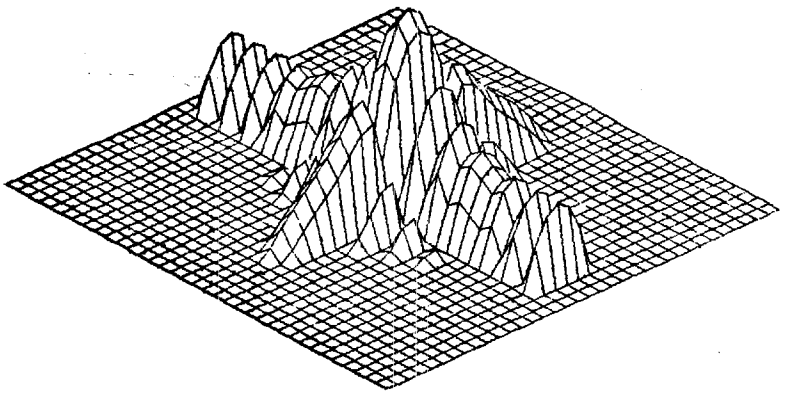

Figure 13. Far-Field Elevation Component Radiated by the Near-Field Distribution on the Cylinder.

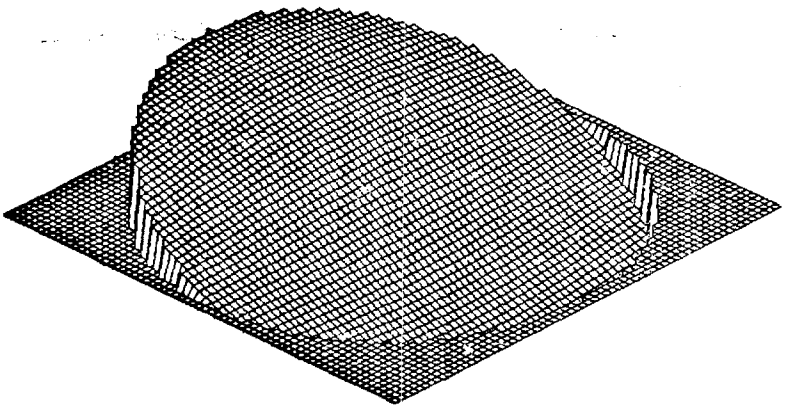

Figure 14. Aperture Phase Distribution for an X Defocus Distance of $\lambda/8$.

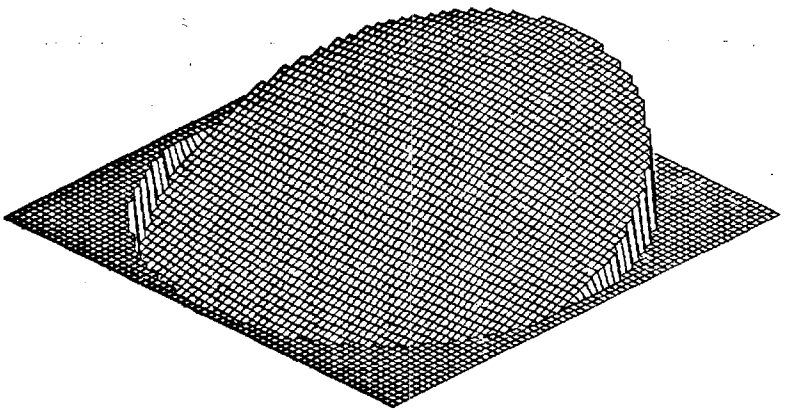

Figure 15. Aperture Phase Distribution for a Y Defocus Distance of $\lambda/8$.

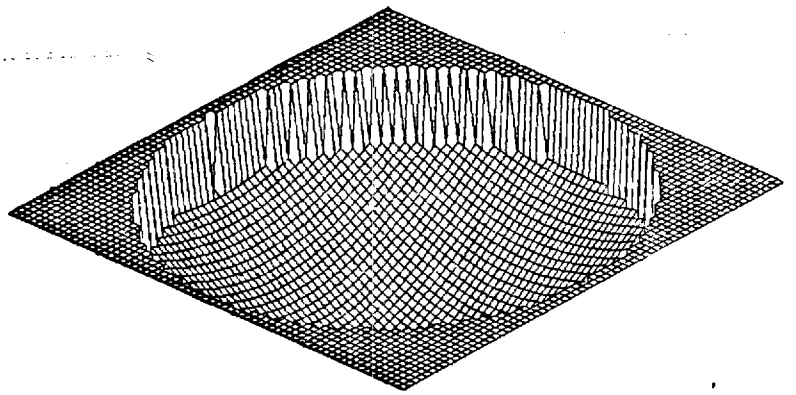

Figure 16. Aperture Phase Distribution for a Z Defocus Distance of $\lambda/8$.

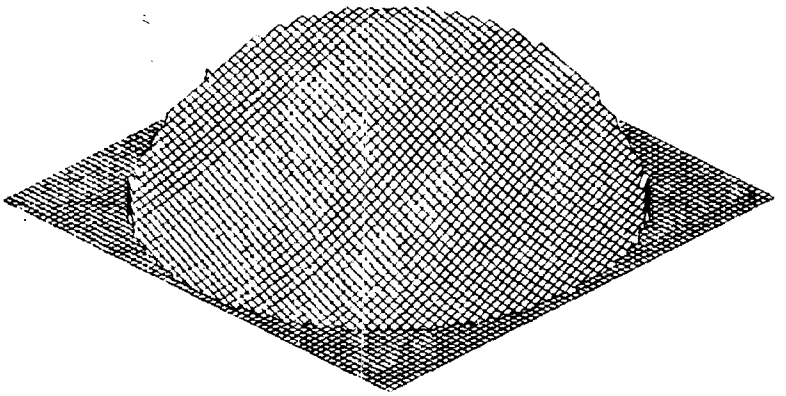

Figure 17. Aperture Phase Distribution for Simultaneous X, Y, and Z Defocus Distances of $\lambda/8$.

to the phase distribution in an amount to make the rms signal to noise ratio be 20 dB. It is felt that this is far worse than that which would exist in a measurement situation. The noise corrupted phase distribution is shown in Figure 18. A computer program was written to calculate the defocus distances for this distribution by the minimum mean-square error solutions given in Equations (4-38) through (4-40). The results were

$$a = \frac{\lambda}{8.014} \qquad \text{(x direction)} \tag{5-25}$$

$$b = \frac{\lambda}{8.014} \qquad \text{(y direction)} \tag{5-26}$$

$$c = \frac{\lambda}{8.004} \qquad \text{(z direction)} \tag{5-27}$$

These represent very small errors, less than 0.2%. However, the error in these solutions is a function of the number of data points in the phase distribution. In this case, that number was approximately 3000. In general, the fewer the number of points used, the greater the uncertainty in the computed values of a, b, and c. This follows because the minimum mean-square error solution represents a statistical average that improves when the number of data points are increased. The computer program which was written to generate the data in Figures 14 through 18 and calculate the defocused feed position is given in Appendix H.

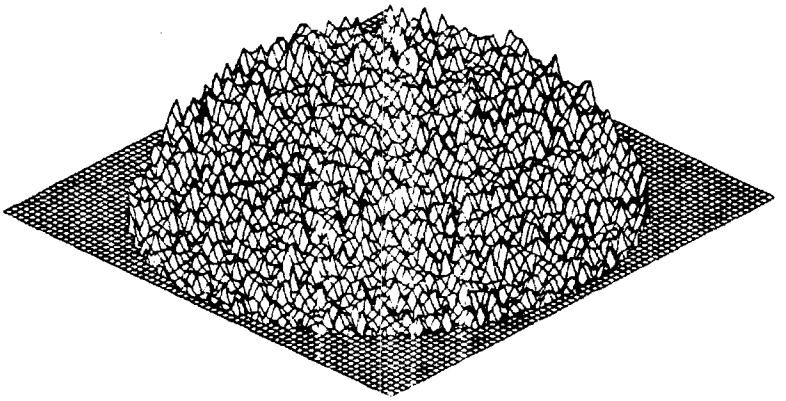

Figure 18. Aperture Phase Distribution of Figure 17 After Addition of Gaussian Random Noise.

CHAPTER VI

CONCLUSIONS AND RECOMMENDATIONS

The basic mathematical theory of probe corrected near-field measurements has been presented in this report. Also, the major numerical considerations in the implementation of this theory have been discussed. A technique for the application of the theory to the determination of the correct focus of planar aperture parabolic reflectors has been given. Although the technique has not been experimentally verified, it has been demonstrated by numerical simulation that the required calculations can be performed by the computer. The major uncertainty is the accuracy of the Kelleher wavefront technique [14] for calculating the theoretical phase distribution in the aperture of a defocused parabolic reflector and the effect of systematic (as opposed to random) errors in the measurement system.

It is felt that a considerable simplification in the implementation of the theory could result if advantage is taken of the symmetry of antennas to which it is applied. For example, a parabolic reflector with a circular aperture may exhibit circular symmetry in the near field of its aperture. If the near field in the aperture is known over any two perpendicular diameter lines, it would then be possible to calculate the feed position by the minimum mean square error method that has been developed. This would greatly reduce the number of points in the aperture at which the phase must be calculated. If such a reduction in the amount of near field data that must be taken could also be achieved, the technique

becomes much more practical. This might be achieved by taking two scans on the cylinder, a longitudinal scan in a plane containing the vertical diameter line of the aperture and an azimuthal scan in a plane containing the horizontal diameter line of the aperture. Whether such circular symmetry in the aperture fields could be exploited to obtain a reduction in the amount of near field data that must be taken is not known. However, the circular field symmetry may lead to such a simplification.

The feed position derivations have been based on equating the far-field approximations derived from cylindrical wave techniques to the far-field approximations derived from plane wave spectrum techniques. However, the plane wave spectrum formulation is valid for only one hemisphere of space, while the cylindrical wave formulation is valid for almost full space, i.e., for a 360° azimuth angle. Thus a problem of theoretical interest is to examine the mathematics of the cylindrical wave solutions to determine if they can be reformulated for only one hemisphere of space. The resulting theory would then be better suited for application to high gain, narrow beam antennas which radiate predominately in one direction. Whether this is possible is not known. If it is, however, it would eliminate the requirement for measuring the near fields on the cylinder behind a directive antenna, thus reducing the amount of near field data which must be recorded in a measurement.

Although the theoretical basis for transforming the near fields on a cylinder into the aperture of an antenna is straightforward, it has not been verified experimentally. Although such an experimental verification is desirable, further numerical simulation may be worthwhile before an experimental effort is made. Specifically, modal expansion

techniques should be used to first calculate the near field on a cylinder from an assumed planar aperture field distribution. The techniques developed in this report could then be used to translate the field on the cylinder back into the aperture. In this way, some bounds could be obtained on the errors introduced by neglecting the evanescent part of the near field in making the transformations from the cylinder to the aperture, or vice versa. Although it is felt that these errors are of little significance for large reflector antennas, such a numerical study should be performed before an experimental verification is attempted.

To this time, there have been no error simulation studies made to determine the effects of random and systematic measurement errors on calculations made from near-field measurements on a cylinder. Error simulation studies for the planar near field measurement surface have been performed [20,21]. No such error studies have been made for the cylindrical surface. This information is necessary if design requirement data are to be available for the mechanical and electrical design of cylindrical near-field ranges. Both random and systematic positional errors should be studied to determine the effects of not only errors in the probe position but also such errors as would occur if the longitudinal axis along which the probe travels is not parallel to the axis of the cylinder.

Finally, the application of plane wave spectrum techniques and spherical wave techniques to the focus problem addressed in this report should be studied. If the test antenna has two degrees of angular rotation freedom, spherical wave techniques may be applicable. In this

case, the near field probe would be held stationary while the test antenna is rotated in front of it. In cases where it is impractical to move the test antenna, the probe may be rotated by a boom to cover the near field of the antenna on concentric circles in a plane parallel to the antenna aperture. In this case, plane wave spectrum techniques could be used to determine correct focus of the antenna.

APPENDIX A

EVALUATION OF EQUATION (2-59)

Each scalar component of the integral in Equation (2-59) is of the form

$$I = \int_C f(\alpha) e^{Rg(\alpha)} \, d\alpha \qquad \text{(A-1)}$$

This integral can be evaluated for large R using the method of steepest descent. This method consists of first finding the point α_o on C at which $g'(\alpha) = 0$. The contour C is then deformed into the path S which passes through α_o and on which $\mathrm{Re}[g(\alpha)] \leq \mathrm{Re}[g(\alpha_o)]$ and $\mathrm{Im}[g(\alpha)] = \mathrm{Im}[g(\alpha_o)]$. The point α_o is called the saddle point of the integral and S the steepest descent path. If this path exists, the change in variables

$$g(\alpha) = g(\alpha_o) - w^2 \qquad \text{(A-2)}$$

can be made where w is real and α lies on S. Thus the integral can be transformed into

$$I = e^{Rg(\alpha_o)} \int_{-\infty}^{\infty} f(\alpha) \, e^{-Rw^2} \frac{d\alpha}{dw} \, dw \qquad \text{(A-3)}$$

where α is a function of w defined implicitly by Equation (A-2).

The method of steepest descent refers to the first term in the asymptotic expansion about $R = \infty$ of the integral in Equation (A-3). This is shown by Clemmow [18] to be

$$I = \pm \sqrt{\frac{-2\pi}{Rg''(\alpha_o)}}\, e^{Rg(\alpha_o)}\, f(\alpha_o) \qquad \text{(A-4)}$$

where the ambiguity in sign must be resolved by examining

$$\left[\frac{d\alpha}{dw}\right]_{\alpha=\alpha_o} = \pm \sqrt{\frac{-2}{g''(\alpha_o)}} \qquad \text{(A-5)}$$

at the saddle point. The sign in Equation (A-5) must be chosen to make $d\alpha$ tangent to S at $\alpha = \alpha_o$. The corresponding sign is then used in Equation (A-4).

The function $g(\alpha)$ in the integral to be evaluated is

$$g(\alpha) = -jk\sin(\alpha+\theta) \qquad \text{(A-6)}$$

The saddle point is found by setting $g'(\alpha_o) = 0$.

$$g'(\alpha_o) = -jk\cos(\alpha_o+\theta) = 0 \qquad \text{(A-7)}$$

The only solution to this equation which lies on C is

$$\alpha_o = \frac{\pi}{2} - \theta \qquad \text{(A-8)}$$

At α_o, it follows that $g(\alpha_o) = -jk$.

The region of the complex α-plane for which $\mathrm{Re}[g(\alpha)] \leq \mathrm{Re}[g(\alpha_o)]$ is defined by the equation

$$\cos(\alpha_r+\theta)\sinh \alpha_i \leq 0 \qquad \text{(A-9)}$$

where $\alpha = \alpha_r + j\alpha_i$. This region is the shaded region in Figure 19. The steepest descent path must lie in this region to insure convergence of the integral. On this path $\mathrm{Im}[g(\alpha)] = \mathrm{Im}[g(\alpha_o)]$. Thus the equation for the path is

$$\sin(\alpha_r+\theta)\cosh \alpha_i = 1 \qquad \text{(A-10)}$$

This path is sketched in Figure 19.

To resolve the sign ambiguity in Equation (A-5), $d\alpha/dw$ must be calculated at the saddle point. At this point $g''(\alpha_o) = jk$. Thus, using Equation (A-5), $d\alpha/dw$ is given by

$$[d\alpha/dw]_{\alpha=\alpha_o} = \pm \sqrt{\frac{-2}{jk}} \qquad \text{(A-11)}$$

$$= \pm (1+j)\sqrt{1/k}$$

Examination of Figure 19 at $\alpha = \alpha_o$ shows that

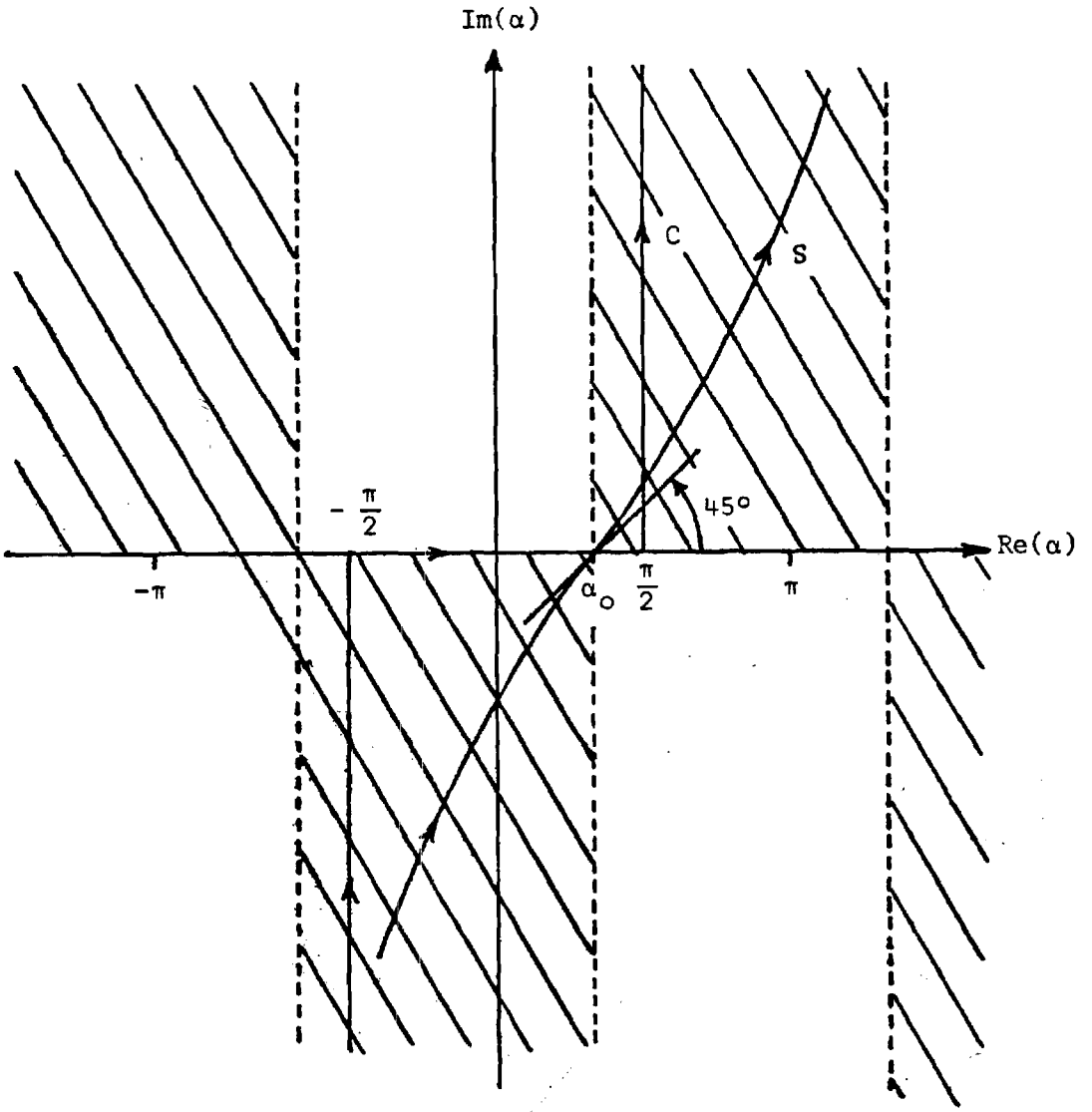

Figure 19. The Path of Steepest Descent

$$\frac{d\alpha}{dw} = \left(1 + j\frac{\partial \alpha_i}{\partial \alpha_r}\right) \frac{d\alpha_r}{dw} \qquad \text{(A-12)}$$

$$= (1 + j) \frac{d\alpha_r}{dw}$$

Since a positive increment in w corresponds to moving along S in the positive direction, it follows from Figure 19 that $d\alpha_r/dw > 0$ at every point on S. Therefore, the positive sign in Equation (A-11) must be chosen in order for this equation to agree with Equation (A-12). Thus, for the problem at hand, Equation (A-4) becomes

$$I = + \sqrt{\frac{-2\pi}{Rg''(\alpha_o)}}\, e^{Rg(\alpha_o)}\, f(\alpha_o) \qquad \text{(A-13)}$$

With the substitution of the above result into Equation (2-40), the far-field electric field intensity becomes

$$\vec{E} = \frac{-2k\sin\theta}{R}\, e^{-jkR} \sum_{n=-\infty}^{\infty} j^n\, e^{jn\phi} [\hat{\phi} a_n(k\cos\theta) \qquad \text{(A-14)}$$

$$+ j(\hat{r}\cos\theta - \hat{z}\sin\theta) b_n(k\cos\theta)]$$

This is the desired expression.

APPENDIX B

VECTOR TRANSLATION THEOREMS FOR CYLINDRICAL VECTOR WAVE FUNCTIONS

In the derivation of the response of a probe used to measure the near field of an antenna on a cylinder, it is necessary to be able to translate the reference coordinate of the probe to that of the antenna being tested. The following is a derivation of the necessary theorems.

Let the coordinates (r_o,ϕ_o,z_o) be the location of the origin of the coordinate system (r',ϕ',z') in the coordinate system (r,ϕ,z) as shown in Figure 20. It is desired to express the cylindrical vector wave functions $\vec{M}^{(4)}_{nh}(r',\phi',z')$ and $\vec{N}^{(4)}_{nh}(r',\phi',z')$ as functions of the coordinates (r,ϕ,z). These vectors have been defined previously in Section 2.3.

In the system (r',ϕ',z') the generating function ψ is given by

$$\psi(r',\phi',z') = H_n^{(2)}(\Lambda r')e^{jn\phi'}\, e^{-jhz'} \tag{B-1}$$

This can be expressed as a function of (r,ϕ,z) by using Graf's addition theorem [19] for the Hankel function, which states

$$H_n^{(2)}(\Lambda r') = e^{-jn\phi'} \sum_{m=-\infty}^{\infty} H_{n+m}^{(2)}(\Lambda r_o)J_m(\Lambda r)e^{jm(\phi_o-\phi)} \tag{B-2}$$

When this is substituted into Equation (B-1), the generating function

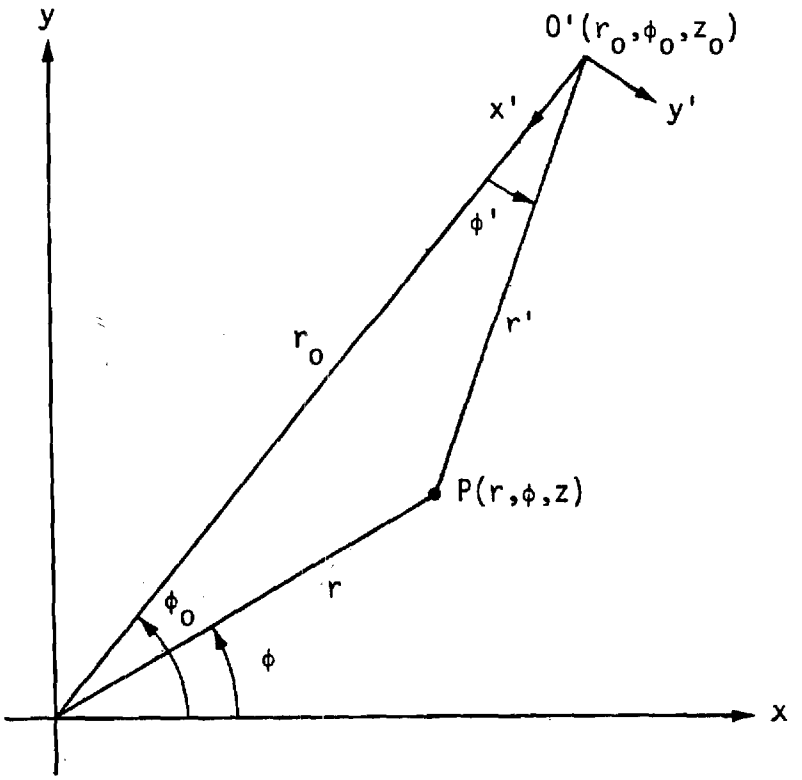

Figure 20. Coordinate System for the Cylindrical Wave Addition.

is transformed into

$$\psi = \sum_{m=-\infty}^{\infty} \left[H_{n+m}^{(2)}(\Lambda r_o) e^{jm\phi_o} e^{jhz_o} \right] J_m(\Lambda r) e^{-jm\phi} e^{-jhz} \qquad \text{(B-3)}$$

The vectors $\vec{M}_{nh}^{4}$ and $\vec{N}_{nh}^{4}$ are obtained by the following operations on ψ:

$$\vec{M}_{nh}^{4} = \nabla' \times \hat{z}\psi \qquad \text{(B-4)}$$

$$\vec{N}_{nh}^{4} = \frac{1}{k_o} \nabla' \times \vec{M}_{nh}^{4} \qquad \text{(B-5)}$$

where the primes denote operations on the primed coordinates (r',ϕ',z'). Since the gradient operation is invariant to a coordinate transformation, these become

$$\vec{M}_{nh}^{4} = \sum_{m=-\infty}^{\infty} \left[H_{n+m}^{(2)}(\Lambda r_o) e^{jm\phi_o} e^{jhz_o} \right] \nabla \times \left[\hat{z} J_m(\Lambda r) e^{-jm\phi} e^{-jhz} \right] \qquad \text{(B-6)}$$

$$\vec{N}_{nh}^{4} = \frac{1}{k_o} \sum_{m=-\infty}^{\infty} \left[H_{n+m}^{(2)}(\Lambda r_o) e^{jm\phi_o} e^{jhz_o} \right] \nabla \times \nabla \times \left[\hat{z} J_m(\Lambda r) e^{-jm\phi} e^{-jhz} \right] \qquad \text{(B-7)}$$

With the definitions of $\vec{M}_{nh}^{1}$ and $\vec{N}_{nh}^{1}$ from Section 2.3, these expressions reduce to

$$\vec{M}_{nh}^{4}(r',\phi',z') = \sum_{m=-\infty}^{\infty} (-1)^m H_{n+m}^{(2)}(\Lambda r_o) e^{jm\phi_o} e^{jhz_o} \vec{M}_{-mh}^{1}(r,\phi,z) \qquad \text{(B-8)}$$

$$\vec{N}^{4}_{nh}(r',\phi',z') = \sum_{m=-\infty}^{\infty} (-1)^m H^{(2)}_{n+m}(\Lambda r_o) e^{jm\phi_o} e^{jhz_o} \vec{N}^{1}_{-mh}(r,\phi,z) \qquad \text{(B-9)}$$

These are the desired translation theorems. They are valid for all $r \leq r_o$.

APPENDIX C

ORTHOGONALITY PROPERTIES OF THE CYLINDRICAL WAVE VECTORS

There are four orthogonality properties of the cylindrical wave vectors $\vec{M}$ and $\vec{N}$ over a cylinder of constant radius which are useful in the evaluation of the Lorentz reciprocity integral in Section 3.3. These properties are developed below.

Property A

$$\int_{-\infty}^{\infty}\int_{-\pi}^{\pi} \vec{M}^{i}_{nh} \times \vec{M}^{j}_{m\eta} \cdot \hat{r} d\phi dz = 0 \qquad \text{for all m, n, } \eta\text{, and h} \qquad \text{(C-1)}$$

This property follows from the fact that the vector $\vec{M}$ contains no z-component. Thus the product $\vec{M}^{i}_{nh} \times \vec{M}^{j}_{m\eta}$ has only a z-component which is zero when scalar-multiplied by the unit vector $\hat{r}$.

Property B

$$\int_{-\infty}^{\infty}\int_{-\pi}^{\pi} \vec{N}^{i}_{nh} \times \vec{N}^{j}_{m\eta} \cdot \hat{r} d\phi dz = 0 \qquad \text{for all m, n, } \eta \text{ and h} \qquad \text{(C-2)}$$

The integrand in Equation (C-2) can be simplified as follows:

$$\vec{N}^{i}_{nh} \times \vec{N}^{j}_{m\eta} \cdot \hat{r} = \vec{N}^{j}_{m\eta} \cdot (\hat{r} \times \vec{N}^{i}_{nh})$$

$$= \left(\frac{nh\lambda^2}{k^2 r} Z_n^i(\Lambda r)\ Z_m^j(\lambda r) - \frac{m\eta\Lambda^2}{k^2 r} Z_n^i(\Lambda r)\ Z_m^j(\lambda r) \right) e^{j(m+n)\phi}\ e^{-j(\eta+h)z}$$

This is identically zero when integrated with respect to ϕ and z unless $m = -n$ and $\eta = -h$. However, under these conditions, the term in brackets is identically zero since $\lambda = \Lambda$ when $\eta = -h$. Thus property B follows immediately.

Property C

$$\int_{-\infty}^{\infty} \int_{-\pi}^{\pi} \vec{N}_{nh}^i \times \vec{M}_{m\eta}^j \cdot \hat{r} d\phi dz = \frac{4\pi^2\Lambda^3}{k} Z_n^i(\Lambda r) Z_{-n}^{'j}(\Lambda r)\delta(\eta+h) \qquad \text{for } m = -n \quad \text{(C-3)}$$

$$= 0 \qquad \text{otherwise}$$

The integrand of the above integral can be simplified as follows:

$$\vec{N}_{nh}^i \times \vec{M}_{m\eta}^j \cdot \hat{r} = -\vec{N}_{nh}^i \cdot (\hat{r} \times \vec{M}_{m\eta}^j)$$

$$= \frac{\lambda\Lambda^2}{k} Z_n^i(\Lambda r) Z_m^{'j}(\lambda r) e^{j(m+n)\phi}\ e^{j(\eta+h)z}$$

This is zero when integrated with respect to ϕ unless $m = -n$. In this case the integral of the exponential term involving ϕ is 2π. The integral of the exponential term involving z results in the factor $2\pi\delta(\eta+h)$. Since this is zero for $\eta + h \neq 0$, it follows that the substitution $\eta = -h$ can be made in the rest of the expression. Thus property C follows immediately.

Property D

$$\int_{-\infty}^{\infty}\int_{-\pi}^{\pi} \vec{M}^{i}_{nh} \times \vec{N}^{j}_{m\eta} \cdot \hat{r}\,d\phi\,dz = -\frac{4\pi^2\Lambda^3}{k} Z_n'^{i}(\Lambda r) Z^{j}_{-n}(\Lambda r)\delta(\eta+h) \text{ for } m=-n \qquad (C\text{-}4)$$

$$= 0 \quad \text{otherwise}$$

This property follows immediately from property C.

APPENDIX D

STATIONARY PHASE EVALUATION OF EQUATION (3-32)

Equation (3-32) is of the form

$$I = \int_a^b A(\phi) e^{jkr_o \mu(\phi)} d\phi \tag{D-1}$$

It is shown in [3] that for kr_o sufficiently large, the asymptotic value of the integral is given by

$$I = A(\phi_o) \sqrt{\frac{2\pi}{kr_o |\mu''(\phi_o)|}} \; e^{j[kr_o \mu(\phi_o) \pm \pi/4]} \tag{D-2}$$

where the + or minus sign in the exponent is chosen to correspond to the sign of $\mu''(\phi_o)$. The stationary phase point of the integral is ϕ_o which is obtained by equating the first derivative of $\mu(\phi)$ to zero.

$$\mu'(\phi_o) = 0 \tag{D-3}$$

In Equation (3-32), $\mu(\phi)$ is given by

$$\mu(\phi) = -\sin\theta \left[\cos\phi - \frac{n\phi}{kr_o \sin\theta} \right] \tag{D-4}$$

The derivative of this with respect to ϕ is

$$\mu'(\phi) = -\sin\theta \left[-\sin\phi - \frac{n}{kr_o \sin\theta} \right] \tag{D-5}$$

This is zero for

$$\phi_o = \sin^{-1} \left[\frac{-n}{kr_o \sin\theta} \right] \tag{D-6}$$

The second derivative of $\mu(\phi)$ is

$$\mu''(\phi) = \sin\theta\cos\phi \tag{D-7}$$

It follows from Equation (D-6) that $\mu''(\phi_o)$ is positive for large kr_o. Thus from Equation (D-1), the value of the integral of interest is

$$I = \frac{j^n}{\sin\theta} E_\phi^p (\pi - \theta, \phi_n) \times \sqrt{\frac{2\pi}{kr_o \sin\theta\cos\phi_n}} e^{-jkr_o \sin\theta\cos\phi_n} \times e^{jn\phi_n} e^{j\pi/4} \tag{D-8}$$

This is the desired result.

APPENDIX E

COMPUTER PROGRAMS FOR THE FAR FIELD EVALUATION

```
      PROGRAM FARFLD(INPUT,OUTPUT,TAPE5=INPUT,TAPE6=OUTPUT)
C CALCULATES FAR FIELD PATTERN
C FROM NEAR FIELD ON A CYLINDER.
C
      REAL KR
      COMPLEX EPHI(64,64),EZ(64,64)
      DIMENSION EZB(68,68)
      DIMENSION A(64),B(64)
      DIMENSION IBUF(512)
      COMMON BUF(6000)
      DATA PI/3.141592654/
      M=64
      N=64
      KR=12.
      NR=68
      NIB=512
      DBM=40.
      DZ=+1./(2.*COS(30.*PI/180.))
      DEL=45./8.
      PHI=0.
      M2=1
      DO 2 I=1,64
      DO 2 J=1,64
      EPHI(I,J)=CMPLX(0.,0.)
2     EZ(I,J)=CMPLX(0.,0.)
      DO 4 J=1,64
      IF(PHI.GE.172.5.AND.PHI.LE.187.5)
     +EZ(M2,J)=CMPLX(COS((PHI-180.)*PI/15.0),0.)
4     PHI=PHI+DEL
      CALL FFT(EZ,M,N,-1,-1)
      CALL FFT(EZ,M,N,1,1)
      CALL KOREK(EPHI,EZ,M,N,KR,DZ)
      CALL FFT(EPHI,M,N,1,-1)
      CALL FFT(EZ,M,N,1,-1)
      CALL DB(EZ,M,N,1)
      CALL DB(EPHI,M,N,-1)
      CALL FOLDZ(EZ,M,N)
      CALL FOLDZ(EPHI,M,N)
      CALL BNORM(EZ,M,N,DBM)
      CALL BNORM(EPHI,M,N,DBM)
      CALL PLT(EPHI,EZ,M,N,EZB,NR,IBUF,NIB)
40    STOP
      END
C*************************************************************
      SUBROUTINE KOREK(EPHI,EZ,M,N,KR,DELZF)
      REAL KR
      COMPLEX EPHI(M,N),EZ(M,N),HANK,C2,C3,Z
      COMMON HANK(400),C1(256),C2(256),C3(256)
      Z=CMPLX(0.,1.)
      M2=M/2
      CALL KOEF(1,DELZF,KR,M,N)
      DO 10 J=1,N
      EPHI(1,J)=(C1(J)*EZ(1,J)-EPHI(1,J))*C2(J)
10    EZ(1,J)=Z*EZ(1,J)*C3(J)
      DO 20 I=2,M2
      I1=M-I+2
      CALL KOEF(I,DELZF,KR,M,N)
      DO 20 J=1,N
      EPHI(I,J)=(C1(J)*EZ(I,J)-EPHI(I,J))*C2(J)
      EPHI(I1,J)=(-C1(J)*EZ(I1,J)-EPHI(I1,J))*C2(J)
      EZ(I,J)=Z*EZ(I,J)*C3(J)
20    EZ(I1,J)=Z*EZ(I1,J)*C3(J)
      I1=M2+1
      CALL KOEF(I1,DELZF,KR,M,N)
```

```
     +2.17138671875,-.4140625,.25/
      DATA (C(I,2),I=1,5)/177.015765666961 67,-10.319938659667 9687,
     +1.07373046875,-.2578125,.25/
      DATA (D(I,1),I=1,5)/93.900510999891 4929,-6.552185058593 7499,
     +.8382812499999999,-.2604166666666666667,.5/
      DATA (D(I,2),I=1,5)/40.832015991210 9374,-3.161315917968 75,
     +.49453125,-.21875,.5/
      L=2*L
      L1=L+2
      DO 20 I=1,800
20    BJ(I)=0.
      X=Z
      CX=2./Z
      XXX=1./X
      XX=XXX*XXX
      T=SQRT(PI2*X)
      DO 5 J=1,2
      A=J-1.25
      P=C(1,J)
      DO 3 I=2,5
3     P=P*XX+C(I,J)
      BT=(A*P*XX+1.)/T
      P=D(1,J)
      DO 4 I=2,5
4     P=P*XX+D(I,J)
      PHI=X+A*P*XXX-(A+.75)*PI2
      BJ(J)=BT*COS(PHI)
5     BY(J)=BT*SIN(PHI)
      BY(2)=-BY(1)
      BY(4)=-BY(2)
      TT=0.
      DO 6 I=6,L1,2
      TT=TT+1.
      BY(I)=CX*TT*BY(I-2)-BY(I-4)
      IF(LEGVAR(BY(I)).NE.0)GO TO 10
6     CONTINUE
      R=ABS(BY(L1))
      L1=L1+2
      DO 8 I=L1,800,2
      TT=TT+1.
      BY(I)=CX*TT*BY(I-2)-BY(I-4)
      IF(LEGVAR(BY(I)).NE.0)GO TO 10
7     IF(1.E-9*ABS(BY(I)).GE.R)GO TO 9
8     CONTINUE
      GO TO 11
9     M=I
      GO TO 15
10    M=I-2
      GO TO 12
11    M=800
12    R=1.E-9*ABS(BY(M))
      MP2=M+2
      DO 13 IK=2,M,2
      I=MP2-IK
      IF(ABS(BY(I)).LE.R)GO TO 14
13    CONTINUE
14    L=I-2
      L1=I
15    BJ(M-1)=0.
      BJ(M-3)=1.E-37
      M1=M-5
      TT=M/2-1
      MF1=M1+1
      DO 16 IK=1,M1,2
```

```
      INCR=(J-1)*NEL
      SC =0.0
      CO =1.0
      DO 17 II=1,NEL2
      J1=II+INCR
      J2=J1+NEL2
      IF(IOPT)12,14,14
12    DO 13 L=1,M
      T1=A(L,J1)
      T2=A(L,J2)*CMPLX(CO,SO*ISN)
      A(L,J1)=T1+T2
13    A(L,J2)=T1-T2
      GO TO 16
14    DO 15 L=1,N
      T1=A(J1,L)
      T2=A(J2,L)*CMPLX(CC,SO*ISN)
      A(J1,L)=T1+T2
15    A(J2,L)=T1-T2
16    SN=SO*CI+CO*SI
      CS=CO*CI-SO*SI
      CC=CS
      SC=SN
17    CONTINUE
      IF(ISN.GE.0)GO TO 19
      DO 18 K=1,M
      DO 18 L=1,N
18    A(K,L)=A(K,L)/MM
19    RETURN
      END
C*************************************************************
      SUBROUTINE DB(E,M,N,IOPT)
      COMPLEX E(M,N)
      PIDEG=180./3.14159265
      R=1.E-20
      DO 1 I=1,M
      DO 1 J=1,N
      Z=REAL(E(I,J))**2+AIMAG(E(I,J))**2
      IF(Z.GT.R)R=Z
      IF(Z.GE.1.E-20) E(I,J)=CMPLX(2,PIDEG*ATAN2(AIMAG(E(I,J)),
     +REAL(E(I,J))))
1     IF(Z.LT.1.E-20)E(I,J)=CMPLX(0.,0.)
      IF(IOPT.GE.0) RNORM=R
      R=RNORM*1.E-20
      DO 2 I=1,M
      DO 2 J=1,N
      Z=REAL(E(I,J))
      IF(Z.LE.R) E(I,J)=CMPLX(-200.,0.)
2     IF(Z.GT.R) E(I,J)=CMPLX(10.*ALOG10(Z/RNORM),AIMAG(E(I,J)))
      RETURN
      END
C*************************************************************
      SUBROUTINE FOLDZ(E,M,N)
      COMPLEX E,TEMP
      DIMENSION E(M,N)
      M1=M/2
      DO 10 I=1,M1
      I1=M1+I
      DO 10 J=1,N
      TEMP=E(I,J)
      E(I,J)=E(I1,J)
10    E(I1,J)=TEMP
      RETURN
      END
C*************************************************************
```

```
      GO TO 4
3     CALL PLTT(XPAGE,YPAGE,IPEN)
      IPEN=2
4     HID(I+J)=YPAGE
      GO TO 7
5     IF(I.EQ.1) IPEN=3
      IF(IPEN.EQ.3)GO TO 6
      X1N=LASTX*HID(I+J)-LASTH*XPAGE-LASTX*YPAGE+XPAGE*LASTY
      X1D=HID(I+J)-LASTH-YPAGE+LASTY
      X1=X1N/X1D
      Y1=(X1*(HID(I+J)-LASTH)+LASTH*XPAGE-LASTX*HID(I+J))/(XPAGE
     +-LASTX)
      CALL PLTT(X1,Y1,2)
      IPEN=3
6     CALL PLTT(XPAGE,YPAGE,IPEN)
7     CONTINUE
      DO 8 I=1,NIJ
8     HID(I)=-.5
      DO 16 K=1,IMAX
      I=IMAX-K+1
      AI=I-1.
      DO 16 J=1,JMAX
      AJ=J-1.
      LASTX=XPAGE
      XPAGE=(AJ+AI)*XSIZE/(RI+RJ)
      LASTY=YPAGE
      YPAGE=(AJ*RI/RJ-AI*RJ/RI+PJ)*YSIZE/(RJ+RI)+HEIGHT*
     +E(I,J)
      LASTH=LASTHM
      LASTHM=HID(I+J)
      IF(YPAGE-HID(I+J))13,14,9
9     IF(J.NE.1) GO TO 10
      CALL PLTT(XPAGE,YPAGE,3)
      IPEN=2
      GO TO 12
10    IF(IPEN.EQ.2)GO TO 11
      X1N=LASTX*YPAGE-LASTY*XPAGE-LASTX*HID(I+J)+XPAGE*
     +HID(I+J-1)
      X1D=YPAGE-LASTY-HID(I+J)+HID(I+J-1)
      X1=X1N/X1D
      Y1=(X1*(YPAGE-LASTY)+LASTY*XPAGE-LASTX*YPAGE)/(XPAGE-
     +LASTX)
      CALL PLTT(X1,Y1,3)
      IPEN=2
11    CALL PLTT(XPAGE,YPAGE,IPEN)
12    HID(I+J)=YPAGE
      GO TO 16
13    IPEN=3
      GO TO 15
14    IF(J.EQ.1) IPEN=3
15    CALL PLTT(XPAGE,YPAGE,IPEN)
16    CONTINUE
      CALL PLTT(XSIZE+4.,-1.,-3)
      RETURN
      END
C*************************************************************
      SUBROUTINE PLTT(X,Y,IPN)
      XLST=XN
      YLST=YN
      ILST=IN
      XN=X
      YN=Y
      IN=IPN
      IF(IPN.EQ.2.AND.ILST.EQ.3)GO TO 2
```

APPENDIX F

LOW PASS FILTER SUBROUTINE

```
      SUBROUTINE FIL(P,M,N,DELI,THETA,GAMMA)
      COMPLEX P(M,N),CONV(128)
      DIMENSION R(65),K(65)
      DATA PI/3.14159265/
      PID=PI/180.
      MAXM=1+INT(M*DELI*SIN(THETA*PID))
      MAXN=1+INT(N*DELI*SIN(THETA*PID))
      CALL FFT(P,M,N,-1,-1)
      CALL FFT(P,M,N,-1,1)
      CALL FOLD(P,M,N)
      M1=M/2+1
      N1=N/2+1
      DO 1 I=1,M
      DO 1 J=1,N
      Z=SQRT((FLOAT(I-M1)/FLOAT(MAXM))**2+(FLOAT(J-N1)/FLOAT(MAXN))**2)
    1 IF(Z.GT.1.) P(I,J)=CMPLX(0.,0.)
      CALL FOLD(P,M,N)
      CALL FFT(P,M,N,1,-1)
      CALL FFT(P,M,N,1,1)
      Z=1./(2.*SIN(GAMMA*PID)*DELI)
      N1=M/2-2
      N2=N1+1
      N3=N2+1
      N4=N3+1
      N5=N4+1
      CALL KARR(R,K,Z,N2,L)
      DO 5 J=1,N
      DO 4 I=1,M
      CONV(I)=P(I,J)
    4 P(I,J)=CMPLX(0.,0.)
      DO 5 I=1,L
      I1=K(I)
      P(N4-I,J)=CONV(N3-I1)*(1.-R(I))+CONV(N2-I1)*R(I)
    5 P(N3+I,J)=CONV(N4+I1)*(1.-R(I))+CONV(N5+I1)*R(I)
      N1=N/2-2
      N2=N1+1
      N3=N2+1
      N4=N3+1
      N5=N4+1
      CALL KARR(R,K,Z,N2,L)
      DO 6 I=1,M
      DO 7 J=1,N
      CONV(J)=P(I,J)
    7 P(I,J)=CMPLX(0.,0.)
      DO 6 J=1,L
      I1=K(J)
      P(I,N4-J)=CONV(N3-I1)*(1.-R(J))+CONV(N2-I1)*R(J)
    6 P(I,N3+J)=CONV(N4+I1)*(1.-R(J))+CONV(N5+I1)*R(J)
      RETURN
      END
```

APPENDIX G

COMPUTER PROGRAMS FOR THE APERTURE FIELD CALCULATIONS

```
      PROGRAM APERT(INPUT,OUTPUT,TAPE5=INPUT,TAPE6=OUTPUT)
C
      REAL KR
      COMPLEX EPHI(32,32),EZ(32,32)
      DIMENSION EZB(36,36)
      DIMENSION A(32),B(32)
      DIMENSION IBUF(512)
      COMMON BUF(3000)
      DATA PI/3.141592654/
      NIB=512
      M=32
      N=32
      DBM=40.
      NR=36
      KR=12.
      DZ=.5
      DZ2=7./31.
      DY=2.*SIN(22.5*PI/180.)*KR/(2.*PI*31.)
      DO 2 I=10,24
      DO 2 J=1,32
      EPHI(I,J)=CMPLX(0.,0.)
      EZ(I,J)=CMPLX(0.,0.)
      PHI=(J-16.)*2.*PI/32.
      IF(J.GE.14.OR.J.LE.18)EZ(I,J)
     +=CEXP(CMPLX(0.,-12.*COS(PHI)))
2     CONTINUE
      CALL FOLDZ(EZ,M,N)
      CALL FFT(EZ,M,N,-1,-1)
      CALL FFT(EZ,M,N,1,1)
      CALL KOREK(EPHI,EZ,M,N,KR,DZ)
      CALL CWPW(EZ,M,N,DY,DZ)
      CALL CWPW(EPHI,M,N,DY,DZ)
      CALL SIMUL(EPHI,EZ,M,N,DY,DZ)
      CALL APERTY(EPHI,M,N,DY)
      CALL APERTY(EZ,M,N,DY)
      CALL FOLDY(EZ,M,N)
      CALL FOLDY(EPHI,M,N)
      CALL APERTZ(EPHI,M,N,DZ2)
      CALL APERTZ(EZ,M,N,DZ2)
      CALL DB(EZ,M,N,1)
      CALL FOLDZ(EZ,M,N)
      CALL DB(EPHI,M,N,-1)
      CALL FOLDZ(EPHI,M,N)
      CALL BNORM(EZ,M,N,DBM)
      CALL BNORM(EPHI,M,N,DBM)
      CALL PNORM(EZ,M,N)
      CALL PNORM(EPHI,M,N)
      CALL PLOTS(IBUF(1),512,9,00)
      CALL PLT(EZ,M,N,EZB,NR,IBUF,NIB)
      CALL PLT(EPHI,M,N,EZB,NR,IBUF,NIB)
      CALL PLOT(0.0,0.0,999)
      STOP
      END
C*****************************************************************
      SUBROUTINE KOREK(EPHI,EZ,M,N,KR,DELZF)
      REAL KR
      COMPLEX EPHI(M,N),EZ(M,N),HANK,C2,C3,Z
      COMMON HANK(400),C1(256),C2(256),C3(256)
      Z=CMPLX(0.,1.)
      M2=M/2
      CALL KOEF(1,DELZF,KR,M,N)
      DO 10 J=1,N
      EPHI(1,J)=(C1(J)*EZ(1,J)-EPHI(1,J))*C2(J)
10    EZ(1,J)=Z*EZ(1,J)*C3(J)
```

```
      SUBROUTINE HANKEL(Z,L)
C THIS PROGRAM IS WRITTEN FOR Z GREATER THAN OR
C EQUAL TO 8. FOR SMALLER ARGUMENTS, ACCURACY DECREASES.
      DIMENSION BJ(800),BY(800)
      DIMENSION DJ(2),DY(2)
      DIMENSION C(5,2),D(5,2)
      COMMON BJ
      EQUIVALENCE (BJ(1),BY(1))
C
      DATA PI2/1.5707963267948966/
      DATA(C(I,1),I=1,5)/427.54717584246826,-23.3947982788085937,
     +2.17138571875,-.4140625,.25/
      DATA (C(I,2),I=1,5)/177.01576566696167,-10.3199386596679687,
     +1.07373046875,-.2578125,.25/
      DATA (D(I,1),I=1,5)/93.900510998914929,-6.552185085937499,
     +.838281249999999999,-.260416666666666667,.5/
      DATA (D(I,2),I=1,5)/40.832015991210937 4,-3.16131591796875,
     +.49453125,-.21875,.5/
      L=2*L
      L1=L+2
      DO 20 I=1,800
20    BJ(I)=0.
      GO TO 2
      WRITE(6,1)Z
1     FORMAT(1H ,4HZ = ,E14.8,*IS AN INCORRECT ARGUMENT IN
     +SUBROUTINE HANKEL*,/)
      STOP
2     X=Z
      CX=2./Z
      XXX=1./X
      XX=XXX*XXX
      T=SQRT(PI2*X)
      DO 5 J=1,2
      A=J-1.25
      P=C(1,J)
      DO 3 I=2,5
3     P=P*XX+C(I,J)
      BT=(A*P*XX+1.)/T
      P=D(1,J)
      DO 4 I=2,5
4     P=P*XX+D(I,J)
      PHI=X+A*P*XXX-(A+.75)*PI2
      DJ(J)=BT*COS(PHI)
5     DY(J)=BT*SIN(PHI)
      BY(2)=-DY(1)
      BY(4)=-DY(2)
      TT=0.
      DO 6 I=6,L1,2
      TT=TT+1.
      BY(I)=CX*TT*BY(I-2)-BY(I-4)
      IF(LEGVAR(BY(I)).NE.0)GO TO 10
6     CONTINUE
      R=ABS(BY(L1))
      L1=L1+2
      DO 8 I=L1,800,2
      TT=TT+1.
      BY(I)=CX*TT*BY(I-2)-BY(I-4)
      IF(LEGVAR(BY(I)).NE.0)GO TO 10
7     IF(1.E-9*ABS(BY(I)).GE.R)GO TO 9
8     CONTINUE
      GO TO 11
9     M=I
      GO TO 15
10    M=I-2
```

```
      GO TO 11
9     DO 10 L=1,N
      T1=A(I2,L)
      A(I2,L)=A(I1,L)
10    A(I1,L)=T1
11    CONTINUE
      DO 17 I=1,IEXP
      NEL=2**I
      NEL2=NEL/2
      NSET=MM/NEL
      SI=SIN(PI2/NEL)
      CI=COS(PI2/NEL)
      DO 17 J=1,NSET
      INCR=(J-1)*NEL
      SO =0.0
      CC =1.0
      DO 17 II=1,NEL2
      J1=II+INCR
      J2=J1+NEL2
      IF(IOPT)12,14,14
12    DO 13 L=1,M
      T1=A(L,J1)
      T2=A(L,J2)*CMPLX(CO,SO*ISN)
      A(L,J1)=T1+T2
13    A(L,J2)=T1-T2
      GO TO 16
14    DO 15 L=1,N
      T1=A(J1,L)
      T2=A(J2,L)*CMPLX(CC,SO*ISN)
      A(J1,L)=T1+T2
15    A(J2,L)=T1-T2
16    SN=SO*CI+CO*SI
      CS=CO*CI-SO*SI
      CO=CS
      SO=SN
17    CONTINUE
      IF(ISN.GE.0)GO TO 19
      DO 18 K=1,M
      DO 18 L=1,N
18    A(K,L)=A(K,L)/FM
19    RETURN
      END
C*************************************************************
      SUBROUTINE DB(E,M,N,IOPT)
      COMPLEX E(M,N)
      PIDEG=180./3.14159265
      R=1.E-20
      DO 1 I=1,M
      DO 1 J=1,N
      Z=REAL(E(I,J))**2+AIMAG(E(I,J))**2
      IF(Z.GT.R)R=Z
      IF(Z.GE.1.E-20) E(I,J)=CMPLX(Z,PIDEG*ATAN2(AIMAG(E(I,J)),
     +REAL(E(I,J))))
1     IF(Z.LT.1.E-20)E(I,J)=CMPLX(0.,0.)
      IF(IOPT.GE.0) RNORM=R
      R=RNORM*1.E-20
      DO 2 I=1,M
      DO 2 J=1,N
      Z=REAL(E(I,J))
      IF(Z.LE.R) E(I,J)=CMPLX(-200.,0.)
2     IF(Z.GT.R) E(I,J)=CMPLX(10.*ALOG10(Z/RNORM),AIMAG(E(I,J)))
      RETURN
      END
C*************************************************************
```

```
      RETURN
40    DO 50 J=1,N
50    A(I,J)=CMPLX(0.,0.)
      RETURN
      END
C*************************************************************
      SUBROUTINE SIMUL(EPHI,EZ,M,N,DY,DZ)
      COMPLEX EPHI(M,N),EZ(M,N),ZERO
      ZERO=CMPLX(0.,0.)
      N2=N/2
      M2=M/2
      MM=INT(FLOAT(M)*DZ-1.E-20)
      IF(MM.GT.M2)MM=M2
      EZ(1,1)=-EZ(1,1)
      DO 10 J=2,N2
      J1=N-J+2
      CP=SQRT(1.-(FLOAT(J-1)/FLOAT(N2))**2)
      EZ(1,J)=-EZ(1,J)/CP
10    EZ(1,J1)=-EZ(1,J1)/CP
      J1=N2+1
      EZ(1,J1)=ZERO
      DO 20 I=2,MM
      I1=M-I+2
      CT=FLOAT(I-1)/(M*DZ)
      ST=SQRT(1.-CT**2)
      EZ(I,1)=-EZ(I,1)
      EPHI(I,1)=EPHI(I,1)/ST
      NN=INT(FLOAT(N2)*ST-1.E-20)
      IF(NN.GT.N2)NN=N2
      DO 20 J=2,NN
      SP=FLOAT(J-1)/(N2*ST)
      CP=SQRT(1.-SP**2)
      J1=N-J+2
      EZ(I,J)=-EZ(I,J)/CP
      EZ(I,J1)=-EZ(I,J1)/CP
      EZ(I1,J)=-EZ(I1,J)/CP
      EZ(I1,J1)=-EZ(I1,J1)/CP
      EPHI(I,J)=(EPHI(I,J)-EZ(I,J)*CT*SP)/ST
      EPHI(I,J1)=(EPHI(I,J1)+EZ(I,J1)*CT*SP)/ST
      EPHI(I1,J)=(EPHI(I1,J)+EZ(I1,J)*CT*SP)/ST
20    EPHI(I1,J1)=(EPHI(I1,J1)-EZ(I1,J1)*CT*SP)/ST
      I1=MM+1
      I2=M-MM+1
      J1=NN+1
      J2=N-NN+1
      IF(I1.GT.M2)GO TO 40
      DO 30 I=I1,I2
      DO 30 J=1,N
      EPHI(I,J)=ZERO
30    EZ(I,J)=ZERO
40    IF(J1.GT.N2)RETURN
      DO 50 J=J1,J2
      DO 50 I=1,M
      EPHI(I,J)=ZERO
50    EZ(I,J)=ZERO
      RETURN
      END
C*************************************************************
      SUBROUTINE APERTZ(A,M,N,DZ)
      COMPLEX A(M,N),ARS,AIS,Z
      COMMON AR(128),AI(128)
      REAL KZ
      DATA PI/3.1415926545/
      Z=CMPLX(0.,1.)
```

```
      A(I,J+1)=ARS+Z*AIS
10    A(I,N-J+1)=CONJG(ARS-Z*AIS)
      KY=N2*DY2
      ARS=FS(AR,N,KY)
      AIS=FS(AI,N,KY)
      A(I,N2+1)=ARS+Z*AIS
20    CONTINUE
      RETURN
      END
C*************************************************************
      COMPLEX FUNCTION FS(B,N,PHI)
      DIMENSION B(N)
      COMPLEX Z
      FS=CMPLX(0.,0.)
      Z=CEXP(CMPLX(0.,PHI))
      N2=N/2
      DO 10 I=1,N2
10    FS=FS*Z+B(N2-I+1)
      DO 20 I=1,N2
20    FS=FS*Z+B(N-I+1)
      FS=FS*CEXP(CMPLX(0.,-N2*PHI))
      RETURN
      END
C*************************************************************
      SUBROUTINE PLT(EZA,M,N,EZB,NR,IBUF,NIB)
C
      COMPLEX EZA(M,N)
      DIMENSION EZB(NR,NR)
      DIMENSION IBUF(NIB)
      MN=NR-2
      DO 10 I=3,MN
      DO 10 J=3,MN
10    EZB(I,J)=REAL(EZA(I-2,J-2))
      CALL PLOTMX(15.0)
      HEIGHT=1.0
      XSIZE=4.
      YSIZE=2.
      CALL PLOT3D(EZB,NR,NR,XSIZE,YSIZE,HEIGHT,IBUF,NIB)
      CALL PLOT(5.0,0.0,-3)
      DO 20 I=3,MN
      DO 20 J=3,MN
20    EZB(I,J)=AIMAG(EZA(I-2,J-2))
      CALL PLOT3D(EZB,NR,NR,XSIZE,YSIZE,HEIGHT,IBUF,NIB)
      CALL PLOT(5.0,0.0,-3)
      RETURN
      END
C*************************************************************
      SUBROUTINE BNORM(E,M,N,DBMAX)
      COMPLEX E(M,N)
      DO 10 I=1,M
      DO 10 J=1,N
      X=REAL(E(I,J))/DBMAX+1.
      IF(X.LT.0.)X=0.
10    E(I,J)=CMPLX(X,AIMAG(E(I,J)))
      RETURN
      END
C*************************************************************
      SUBROUTINE PNORM(E,M,N,DBMAX)
      COMPLEX E(M,N)
      DO 10 I=1,M
      DO 10 J=1,N
      X=(AIMAG(E(I,J))+180.)/360.
10    E(I,J)=CMPLX(REAL(E(I,J)),X)
      RETURN
```

```
      CALL PLTT(XPAGE,YPAGE,3)
      IPEN=2
      GO TO 12
10    IF(IPEN.EQ.2)GO TO 11
      X1N=LASTX*YPAGE-LASTY*XPAGE-LASTX*HID(I+J)+XPAGE*
     +HID(I+J-1)
      X1D=YPAGE-LASTY-HID(I+J)+HID(I+J-1)
      X1=X1N/X1D
      Y1=(X1*(YPAGE-LASTY)+LASTY*XPAGE-LASTX*YPAGE)/(XPAGE-
     +LASTX)
      CALL PLTT(X1,Y1,3)
      IPEN=2
11    CALL PLTT(XPAGE,YPAGE,IPEN)
12    HID(I+J)=YPAGE
      GO TO 16
13    IPEN=3
      GO TO 15
14    IF(J.EQ.1) IPEN=3
15    CALL PLTT(XPAGE,YPAGE,IPEN)
16    CONTINUE
      CALL PLTT(XSIZE+4.,-1.,-3)
      RETURN
      END
C*************************************************************
      SUBROUTINE PLTT(X,Y,IPN)
      XLST=XN
      YLST=YN
      ILST=IN
      XN=X
      YN=Y
      IN=IPN
      IF(IPN.EQ.2.AND.ILST.EQ.3)GO TO 2
      IF(IPN.EQ.3)RETURN
      CALL PLOT(X,Y,IPN)
      X1=X
      RETURN
2     CALL PLOT(X1,YLST,3)
      CALL PLOT(XLST,YLST,3)
      CALL PLOT(X,Y,2)
      X1=X
      RETURN
      END
C*************************************************************
      SUBROUTINE FOLDY(E,M,N)
C
      COMPLEX E,TEMP
      DIMENSION E(M,N)
C
      N1=N/2
      DO 10 J=1,N1
      J1=N1+J
      DO 10 I=1,M
      TEMP=E(I,J)
      E(I,J)=E(I,J1)
10    E(I,J1)=TEMP
C
      RETURN
      END
```

APPENDIX H

COMPUTER PROGRAMS FOR THE APERTURE PHASE AND FEED DEFOCUS CALCULATIONS

```
      PROGRAM APRT3(INPUT,OUTPUT,TAPE5=INPUT,TAPE6=OUTPUT)
C
C TEST OF PHASE FUNCTION.
C AX,BX,CX EQUAL 1. OR 0. DEPENDING WHETHER THE ERRORS ON X,Y,
C OR Z ARE WANTED OR NOT.
C
      COMPLEX AXY(5000)
C
      DIMENSION X(65),Y(65)
      DIMENSION MXL(65),MXR(65)
      DIMENSION NSI(65),NSF(65)
      DIMENSION PHI(5000),PNO(5000)
      DIMENSION XNC(50000)
      DIMENSION EPHI(69,69),IBUF(512)
      DIMENSION APA(65,65)
C
      COMMON/A1/RE,DXY,KSI
C
      DATA NR,NXP,NP,NO,NIB/65,69,5000,50000,512/
      DATA PI/3.14159264/
C
      READ(5,*)AX,BX,CX,NER
      READ(5,*)NI,DB,HEIGHT
C
      A=AX*PI/4.
      B=BX*PI/4.
      C=CX*PI/4.
      RE=20.*PI
      PC=.375*2.*RE
C
      WRITE(6,10)
      WRITE(6,15)A,B,C
      WRITE(6,20)RE,NI
C
      CALL DSIO(NI,X,Y,MXL,MXR,NSI,NSF,NR,NXY,N1)
      WRITE(6,25)
      WRITE(6,30)
      NF=NSF(KSI)
      CALL APHI(X,Y,MXL,MXR,NSI,NSF,NXY,PHI,A,B,C,N1,NP,
     +DXY,KSI,AXY,PC)
C
      NXP=NXY+4
      IF(NER.GE.1)GO TO 5
      CALL PLT(HEIGHT,PHI,EPHI,MXL,MXR,NSI,NSF,NXY,NP,IBUF,NIB,
     +APA,NXP)
      GO TO 40
C
5     CALL EQ3(PHI,AXY,NP,PC,AR,BR,CR)
      NC=10*NP
      CALL PPN(PHI,PNO,XNO,NP,NC,MXL,MXR,NSI,NSF,NXY,KSI,DB)
      CALL EQ3(PHI,AXY,NP,PC,AR,BR,CR)
      CALL PLT(HEIGHT,PHI,EPHI,MXL,MXR,NSI,NSF,NXY,NP,IBUF,
     +NIB,APA,NXP)
C
10    FORMAT(15X,*PHASE ERROR EFFECT*,//)
15    FORMAT(2X,*VALUE OF A*,10X,1F10.3/
     +       2X,*VALUE OF B*,10X,1F10.3/
     +       2X,*VALUE OF C*,10X,1F10.3)
20    FORMAT(2X,*VALUE OF THE RADIUS OF THE APERTURE*,1F10.3/
     +       2X,*NUMBER OF DIVISIONS                *,I10)
25    FORMAT(1X,*C*,//)
30    FORMAT(15X,*VALUES OF THE PHASE FUNCTION.*,/)
C
40    STOP
```

```
20    KP=KP+1
      GO TO 10
25    KP=NXY
30    KM=KP-1
      CALL DST(AD,KM,KP,KXY,X,NXY)
      GO TO 50
40    KXY=KP
C
50    RETURN
      END
C*************************************************************
      SUBROUTINE DST(AD,KM,KP,KXY,X,NXY)
C
C SELECTS ONE MARK.
C
      DIMENSION X(NXY)
C
      D1=AD-X(KM)
      D2=AD-X(KP)
      IF(ABS(D1).GE.ABS(D2))GO TO 10
      KXY=KM
      GO TO 20
10    KXY=KP
C
20    RETURN
      END
C*************************************************************
      SUBROUTINE ANPT(KSI,MXL,MXR,NSI,NSF,NXY)
C
C STARTING AND FINAL POINTS FOR EACH LINE.
C
      DIMENSION MXL(NXY),MXR(NXY)
      DIMENSION NSI(NXY),NSF(NXY)
C
      NI=1
      NF=1
      NSI(1)=1
      NSF(1)=1
      DO 10 KM=2,KSI
      NIA=MXR(KM-1)-MXL(KM-1)+1
      NIB=MXR(KM)-MXL(KM)+1
      NI=NI+NIA
      NF=NF+NIB
      NSI(KM)=NI
      NSF(KM)=NF
10    CONTINUE
C
      RETURN
      END
C*************************************************************
      SUBROUTINE APHI(X,Y,MXL,MXR,NSI,NSF,NXY,PHI,A,B,
     +C,N1,NP,DXY,KSI,AXY,P)
C
C PHASE FUNCTIONS.
C
      COMPLEX AXY(NP)
C
      DIMENSION X(NXY),Y(NXY)
      DIMENSION MXL(NXY),MXR(NXY)
      DIMENSION NSI(NXY),NSF(NXY)
      DIMENSION PHI(NP)
C
      DO 20 KM=1,KSI
      NI=NSI(KM)
```

```
      M=10
      I=1
      XM=0.
      SIG=1.
      IU=3
      IP=0
C
      CALL NRAND(NP,M,I,XM,SIG,IU,XNO,IP)
C
      DO 2 IX=1,NP
      IQ=I+M*(IX-1)
      PNO(IX)=XNO(IQ)
2     CONTINUE
C
      DO 5 I=1,NF
      PNO(I)=(1./NF)*PNC(I)
5     CONTINUE
C
      WRITE(6,10)
      WRITE(6,25)DB
      GO TO 40
C
      WRITE(6,20)
C
      CALL WRTE(PNC,NF,MXL,MXR,NSI,NSF,NXY,KSI)
C
10    FORMAT(1X,*C*,//)
20    FORMAT(10X,*VALUES OF NORMALLY DISTRIBUTED NOISE.*,/)
25    FORMAT(5X,*RATIO SIGNAL TO NOISE.*,1F10.3,2X,*DB*,//)
C
40    RETURN
      END
C*************************************************************
      SUBROUTINE WRTE(Z,NP,MXL,MXR,NSI,NSF,NXY,KSI)
C
C WRITE STATEMENTS.
C
      DIMENSION Z(NP)
      DIMENSION MXL(NXY),MXR(NXY)
      DIMENSION NSI(NXY),NSF(NXY)
C
      DO 10 KM=1,KSI
      NIA=MXR(KM)-MXL(KM)+1
      LX=6*(MXL(KM)-1)
      NI=NSI(KM)
      NF=NSF(KM)
      WRITE(6,20)LX,NIA,(Z(I),I=NI,NF)
10    CONTINUE
C
20    FORMAT(=X,=F6.3,///)
C
      RETURN
      END
C*************************************************************
      SUBROUTINE EQ3(PHI,AXY,NF,PC,AR,BR,CR)
C
C COEFFICIENTS FOR THE SYSTEM OF EQUATIONS.
C
      COMPLEX AXY(NP)
C
      DIMENSION PHI(NP)
C
      B1=4.*PC
      B2=B1*PC
```

```
      Y3=0.
      Z3=0.
      C3=0.
C
      RETURN
      END
C*************************************************************
      SUBROUTINE COEF(B1,B2,XA,YA,TX,TY,TZ,ZNM,TPZ)
C
C CALCULATIONS OF TERMS.
C
      ZNX=B1*XA
      ZNY=B1*YA
      SQ=XA**2+YA**2
      ZNM=SQ-B2
      ZNP=SQ+B2
      TX=ZNX/ZNP
      TY=ZNY/ZNP
      TZ=ZNM/ZNP
      TPZ=1.-2.*B2/ZNP
C
      RETURN
      END
C*************************************************************
      SUBROUTINE DET(F1,F2,F3,G1,G2,G3,H1,H2,H3,D)
C
C DETERMINANT.
C
      A=F1*(G2*H3-G3*H2)
      B=F2*(G1*H3-G3*H1)
      C=F3*(G1*H2-G2*H1)
      D=A-B+C
C
      RETURN
      END
C*************************************************************
      SUBROUTINE PLT(HEIGHT,PHI,EPHI,MXL,MXR,NSI,NSF,NXY,NP,IBUF,
     +NI8,APA,NXP)
C
C PLOT OF THE PHASE FUNCTION.
C
      DIMENSION PHI(NP),EPHI(NXP,NXP)
      DIMENSION APA(NXY,NXY)
      DIMENSION MXL(NXY),MXR(NXY)
      DIMENSION NSI(NXY),NSF(NXY)
      DIMENSION IBUF(NI8)
C
      DO 20 I=1,NXY
      DO 10 J=1,NXY
      IF(J.GE.MXL(I).AND.J.LE.MXR(I)) GO TO 5
      APA(I,J)=0.
      GO TO 10
5     K=J-MXL(I)
      APA(I,J)=PHI(NSI(I)+K)
10    CONTINUE
20    CONTINUE
C
      N2=NXY+2
      DO 22 I=3,N2
      DO 22 J=3,N2
      EPHI(I,J)=APA(I-2,J-2)
22    CONTINUE
C
      CALL ANORM(EPHI,NXP,NXP)
```

```
      LASTX=XPAGE
      XPAGE=(AJ+AI)*XSIZE/(RI+RJ)
      LASTY=YPAGE
      YPAGE=(AJ*RI/RJ-AI*RJ/RI+RJ)*YSIZE/(RJ+RI)+HEIGHT*E(I,J)
      LASTH=LASTHM
      LASTHM=HID(I+J)
      IF(YPAGE-HID(I+J))5,5,2
2     IF(I.NE.1)GO TO 3
      CALL PLTT(XPAGE,YPAGE,3)
      IPEN=2
      GO TO 4
3     CALL PLTT(XPAGE,YPAGE,IPEN)
      IPEN=2
4     HID(I+J)=YPAGE
      GO TO 7
5     IF(I.EQ.1) IPEN=3
      IF(IPEN.EQ.3)GO TO 6
      X1N=LASTX*HID(I+J)-LASTH*XPAGE-LASTX*YPAGE+XPAGE*LASTY
      X1D=HID(I+J)-LASTH-YPAGE+LASTY
      X1=X1N/X1D
      Y1=(X1*(HID(I+J)-LASTH)+LASTH*XPAGE-LASTX*HID(I+J))/(XPAGE
     +-LASTX)
      CALL PLTT(X1,Y1,2)
      IPEN=3
6     CALL PLTT(XPAGE,YPAGE,IPEN)
7     CONTINUE
      DO 8 I=1,NIJ
8     HID(I)=-.5
      DO 16 K=1,IMAX
      I=IMAX-K+1
      AI=I-1.
      DO 16 J=1,JMAX
      AJ=J-1.
      LASTX=XPAGE
      XPAGE=(AJ+AI)*XSIZE/(RI+RJ)
      LASTY=YPAGE
      YPAGE=(AJ*RI/RJ-AI*RJ/RI+RJ)*YSIZE/(RJ+RI)+HEIGHT*
     +E(I,J)
      LASTH=LASTHM
      LASTHM=HID(I+J)
      IF(YPAGE-HID(I+J))13,14,9
9     IF(J.NE.1) GO TO 10
      CALL PLTT(XPAGE,YPAGE,3)
      IPEN=2
      GO TO 12
10    IF(IPEN.EQ.2)GO TO 11
      X1N=LASTX*YPAGE-LASTY*XPAGE-LASTX*HID(I+J)+XPAGE*
     +HID(I+J-1)
      X1D=YPAGE-LASTY-HID(I+J)+HID(I+J-1)
      X1=X1N/X1D
      Y1=(X1*(YPAGE-LASTY)+LASTY*XPAGE-LASTX*YPAGE)/(XPAGE-
     +LASTX)
      CALL PLTT(X1,Y1,3)
      IPEN=2
11    CALL PLTT(XPAGE,YPAGE,IPEN)
12    HID(I+J)=YPAGE
      GO TO 16
13    IPEN=3
      GO TO 15
14    IF(J.EQ.1) IPEN=3
15    CALL PLTT(XPAGE,YPAGE,IPEN)
16    CONTINUE
C
      CALL PLTT(XSIZE+4.,-1.,-3)
```

BIBLIOGRAPHY

1. W. M. Leach, Jr., "Probe Compensated Near-Field Measurements on a Cylinder," Ph.D. Dissertation, Georgia Institute of Technology, School of Electrical Engineering, September 1972.

2. W. M. Leach, Jr. and D. T. Paris, "Probe Compensated Near-Field Measurements on a Cylinder," IEEE Trans. Ant. and Propagt., Vol. AP-21, No. 4, July 1973, pp. 435-445.

3. A. Papoulis, The Fourier Integral and its Applications, McGraw Hill, 1962.

4. Hansen, Phys. Rev., Vol. 47, pp. 139-143, Jan., 1935; Physics, Vol. 7, pp. 460-465, Dec. 1936, J. App. Phys., Vol. 8, pp. 282-286, Apr., 1937.

5. J. A. Stratton, Electromagnetic Theory, McGraw Hill, 1941.

6. R. E. Collin and F. J. Zucker, Antenna Theory Part I, McGraw Hill, 1969.

7. I. S. Gradshteyn and I. M. Ryzhik, Table of Integrals, Series, and Products, Academic Press, 1965, p. 714.

8. R. F. Harrington, "Effect of Antenna Size on Gain, Bandwidth, and Efficiency," Jour. Res. NBS - D. Radio Propagt., Vol. 64D, Jan. - Feb. 1960, pp. 1-12.

9. R. E. Collin and S. Rothschild, "Evaluation of Antenna Q," IEEE Trans. on Ant. and Propagt., Vol. AP-12, Jan., 1964, pp. 23-27.

10. L. F. Chu, "Physical Limitations of Omni-Directional Antennas," Jour. App. Phy., Vol. 19, Dec., 1948, pp. 1163-1175.

11. A. C. Ludwig, "Near-Field Far-Field Transformations Using Spherical Wave Expansions," IEEE Trans. on Ant. and Propagt., Vol. AP-19, May 1971, pp. 214-220.

12. E. B. Joy and D. T. Paris, "Spatial Sampling and Filtering in Near-Field Measurements," IEEE Trans. on Ant. and Propagt., Vol. AP-20, May 1972, pp. 253-261.

13. D. T. Paris, W. M. Leach, Jr., and E. B. Joy, "Basic Theory of Probe Compensated Near-Field Measurements," IEEE Trans. on Ant. and Propagt., Vol. AP- , No. , May 1978, pp.

14. K. S. Kelleher, "Antenna Wavefront Problems," Naval Res. Lab. Report No. 3530, Sept., 1949.

15. M. L. James, et. al., Applied Numerical Methods for Digital Computation, Harper and Row, 1977.

16. W. T. Cochran, et. al., "What is the Fast Fourier Transform?," Proc. IEEE, Vol. 55, October 1967, pp. 1664-1667.

17. L. L. Bailin, "The Radiation Field Produced by a Slot in a Large Circular Cylinder," IRE Trans. on Ant. and Propagt., Vol. AP-3, July 1955, pp. 128-137.

18. P. C. Clemmow, The Plane Wave Spectrum Representation of Electromagnetic Fields, Oxford: Pergamon Press, 1966.

19. M. Abramowitz and I. A. Stegun, Handbook of Mathematical Functions, Dover Publications, 1965.

20. G. P. Rodrigue, E. B. Joy, and C. P. Burns, "An Investigation of the Accuracy of Far-Field Radiation Patterns Determined from Near-Field Measurements," Georgia Institute of Technology Final Report on U. S. Army Missile Command Contract DAAH01-72-C-0950, Aug., 1973.

21. R. C. Baird, A. C. Newell, P. F. Wacker, and D. M. Kerns, "Recent Experimental Results in Near-Field Antenna Measurements," Electronics Letters, Vol. 6, May 1970, pp. 347-349.